Design of Neural Network-based MPPT with Neutral Point Clamped Converter for Grid Connected PV System



By

MD. ENAMUL HAQUE
21MET002F

A thesis submitted in partial fulfillment of the requirements for the degree of

MASTER of SCIENCE in Energy Technology

Institute of Energy Technology (IET)

CHITTAGONG UNIVERSITY OF ENGINEERING AND TECHNOLOGY

May 2025

Declaration

I hereby declare that the work contained in this thesis has not been previously submitted to meet the requirements for an award at this or any other higher education institution. To the best of my knowledge and belief, the thesis contains no material previously published or written by another person except where due reference is cited.

Signature and Date

Md. Enamul Haque

21MET002F

Institute of Energy Technology

Chittagong University of Engineering & Technology (CUET)

(For Postgraduate Students only)

Copyrights about this Thesis

Copyright © Md. Enamul Haque, 2025.

This work may not be copied without the permission of the author or Chittagong University of Engineering & Technology

Dedication

I want to dedicate this thesis to the Almighty Allah, who is the source of life and strength of knowledge and wisdom, for his guidance, mental strength, and support, as well as for providing me with a healthy life that enabled me to carry out this study.

This research, which is proudly and sincerely devoted to the individuals who inspire us, is the result of countless and costly sacrifices. I sincerely dedicate this work to my beloved father Late Shukur Ali and my mother, Mst. Rupia Khatun, who have been my source of strength and inspiration throughout this research. I completed this thesis thanks to their continuous financial, emotional, spiritual and moral support. This thesis is also dedicated to my teachers, who guided me on the right life path. Thanks to my parents, relatives, guardians, classmates and friends who extended their help with challenges along the way. Their support helped me see this adventure through to the end.

List of Publications

Journal Article

- Publication 1: **M. E. Haque** and N. Mohammad, "Design of a Neural Network-based Hybrid MPPT with a Neutral Point Clamped Converter for Grid Connected PV System", [Under Review].

Conference Paper

- Publication 2: **M. E. Haque** and N. Mohammad, "Design and Performance Analysis of Neural Network-Based MPPT in PV System with Energy Storage Management", *6th International Conference on Electrical Engineering and Information & Communication Technology (ICEEICT)*, 02-04 May 2024, Dhaka, Bangladesh, pp. 1378-1383. doi: 10.1109/ICEEICT62016.2024.10534419.
- Publication 3: **M. E. Haque** and N. Mohammad, "Performance Analysis of Levenberg-Marquardt algorithm-based Neural Network MPPT of a Solar PV System", *4th International Conference on Electrical, Computer and Communication Engineering (ECCE), 13-15 February 2025*, Chittagong, Bangladesh, pp. 1-6. doi: 10.1109/ECCE64574.2025.11013780
- Publication 4: S. M. Salam, N. Mohammad, D.K. Chowdhury and **M. E. Haque**, "A Techno-Economic Analysis of an IEEE 39 Sustainable Grid Bus for DSM on Load Flexibility Options", *4th Int. Conf. on Innovations in Science, Engineering and Technology (ICISET), 26-27 October 2024*, Chittagong, Bangladesh, pp. 1-6. doi: 10.1109/ICISET62123.2024.10939135.

Approval by the Supervisor

This is to certify that ***Md. Enamul Haque*** has carried out this work under my supervision, and he has fulfilled the relevant Academic Ordinance of the Chittagong University of Engineering and Technology, so that he is qualified to submit the following thesis in an application for the degree of MASTER of SCIENCE in Energy Technology.

Signature and Date

Nur Mohammad, PhD

Professor

Department of Electrical & Electronic Engineering

Chittagong University of Engineering & Technology

Acknowledgment

Alhamdulillah! In the beginning, Almighty Allah gave me the patience to complete the thesis successfully. It truly gives me great pleasure to convey my sincere appreciation and gratitude to my mentor, philosopher, and supervisor, ***Dr. Nur Mohammad***, Professor of the Department of Electrical and Electronic Engineering, Chittagong University of Engineering and Technology (CUET). Above all, his dedication and keen interest in his overwhelming attitude towards helping his students were solely responsible for completing my work. His timely advice, meticulous scrutiny, scholarly advice and scientific approach have helped me to a very great extent to accomplish this thesis.

I would also like to express my gratitude to the Central Library, Advance Power System Lab (APS), Department of Electrical and Electronic Engineering (EEE) and Institute of Energy Technology (IET) at Chittagong University of Engineering and Technology (CUET), Chattogram-4349, Bangladesh for providing the support to carry out this research work.

Abstract

Energy is now becoming one of the key factors of modern civilization. In our daily lives, it enables comfort and sustainability, despite the electricity demand still facing challenges in generation. Machine learning (ML) techniques are becoming crucial for optimizing the performance of solar energy harvesting systems to overcome this problem. The main purpose is to develop a model for a supervised ML-based maximum power point tracking (MPPT) control system utilizing a neutral point clamped (NPC) converter, ensuring a reliable power supply under varying operational and environmental conditions. This study investigates a neural network (NN) based Levenberg-Marquardt (LM) train algorithm to extract the MPPT power generation in the grid-connected solar photovoltaic (PV) system with the NPC converter model and explore the performance of energy management systems. Utilizing MPPT, we enhance the efficiency of the proposed solar system. It investigates the battery operation strategies under different loading conditions. To evaluate the NPC converter, we suggested a space vector pulse width modulation (SV-PWM) technique of 15% to enable control of the DC link neutral point voltage, thereby adjusting switching states and reducing operational loss. The system performance demonstrates high tracking efficiency, reduces oscillation, facilitates smooth load switching, and improves power quality with an effective energy storage system. The results indicate that the Hybrid (P&O, NN) MPPT is superior (96% efficiency) at energy harvesting, while the outperformed LM-based NN MPPT is better (SOC range ~ 45.0042%) at energy storage. The proposed framework offers a reliable and efficient solution for modern grid-connected PV systems with energy storage.

বিমূর্ত

শক্তি আধুনিক সভ্যতার অন্যতম গুরুত্বপূর্ণ উপাদান হয়ে উঠছে। আমাদের দৈনন্দিন জীবনে, বিদ্যুৎ চাহিদা এখনও উৎপাদন সমস্যার সম্মুখীন হওয়া সত্ত্বেও, এটি আরাম এবং স্থায়িত্ব নিশ্চিত করে। এই সমস্যা কাটিয়ে উঠতে সৌর শক্তি সংগ্রহ ব্যবস্থার কর্মক্ষমতা অপ্টিমাইজ করার জন্য মেশিন লার্নিং (ML) কৌশলগুলি গুরুত্বপূর্ণ হয়ে উঠছে। মূল উদ্দেশ্য হল একটি তত্ত্বাবধানে থাকা ML-ভিত্তিক ম্যাক্সিমাম পাওয়ার পয়েন্ট ট্র্যাকিং টেকনিক (MPPT) কন্ট্রোলারের জন্য একটি মডেল তৈরি করা যার মধ্যে একটি নিউট্রাল পয়েন্ট ক্ল্যাম্পড (NPC) কনভার্টার রয়েছে যাতে বিভিন্ন অপারেশন এবং পরিবেশগত পরিস্থিতিতে নির্ভরযোগ্য বিদ্যুৎ সরবরাহ নিশ্চিত করা যায়। এই গবেষণায় একটি নিউরাল নেটওয়ার্ক (NN) ভিত্তিক লেভেনবার্গ-মার্কোয়ার্ড (LM) ট্রেইন অ্যালগরিদম অনুসন্ধান করা হয়েছে যা NPC কনভার্টার মডেলের সাহায্যে গ্রিড-সংযুক্ত সৌর ফটোভোলটাইক (PV) সিস্টেমে MPPT বিদ্যুৎ উৎপাদন নিষ্কাশন করে এবং শক্তি ব্যবস্থাপনা সিস্টেমের কর্মক্ষমতা অন্বেষণ করে। MPPT ব্যবহার করে, আমরা প্রস্তাবিত সৌর সিস্টেম দক্ষতা বৃদ্ধি করি। এটি বিভিন্ন লোডিং অবস্থার অধীনে ব্যাটারি অপারেশন কৌশলগুলি তদন্ত করে। NPC কনভার্টার মূল্যায়ন করার জন্য, আমরা 15% স্পেস ভেক্টর পালস উইথড মড্যুলেশন (SV-PWM) কৌশল প্রস্তাব করেছি যাতে DC লিঙ্ক নিউট্রাল পয়েন্ট ভোল্টেজ নিয়ন্ত্রণ করা যায়, যার ফলে সুইচিং অবস্থা সামঞ্জস্য করা যায় এবং অপারেশনাল ক্ষতি হ্রাস পায়। সিস্টেমের কর্মক্ষমতা উচ্চ ট্র্যাকিং দক্ষতা প্রদর্শন করে, ওসিলেশন হ্রাস করে, মসৃণ লোড স্যুইচিং সহজতর করে এবং কার্যকর শক্তি সঞ্চয় ব্যবস্থার মাধ্যমে বিদ্যুৎ মান উন্নত করে। ফলাফলগুলি দেখায় যে হাইব্রিড MPPT (96% দক্ষতা) শক্তি সংগ্রহের ক্ষেত্রে উন্নত, যেখানে উন্নতমানের LM-ভিত্তিক NN MPPT শক্তি সঞ্চয়ের ক্ষেত্রে আরও ভাল। প্রস্তাবিত কাঠামোটি শক্তি সঞ্চয় সহ আধুনিক গ্রিড-সংযুক্ত PV সিস্টেমগুলির জন্য একটি নির্ভরযোগ্য এবং দক্ষ সমাধান প্রদান করে।

Table of Contents

Declaration i

Dedication ii

List of Publications iii

Approval by the Supervisor iv

Acknowledgment v

Abstract vi

Table of Contents viii

List of Figures xii

List of Tables xvi

Nomenclature xviii

Chapter 1: Introduction 1

1.1 Background 1

1.2 Photovoltaic Systems 3

1.2.1 Infrastructure of Grid Connected PV Systems 5

1.2.1.1 Generation system: 8

1.2.1.2 Converter System: 8

1.2.1.3 Transmission system: 9

1.2.1.4 Battery Energy Storage System (BESS): 9

1.2.1.5 Distribution system 11

1.2.1.6 End-user System 11

1.3 Challenges in Grid-Connected PV Systems 12

1.4 Maximum Power Point Tracking (MPPT) 13

1.4.1 Challenges and Importance 13

1.5 NPC Converter in Renewable Energy Systems 13

1.6 Problem Statement 15
1.6.1 Hypothesis 15
1.6.2 Research Questions 15
1.7 Research Aims and Objectives 16
1.8 Significance and Scope 16
1.9 Thesis Organisation 17
Outline of Chapter 2 17
Outline of Chapter 3 18
Outline of Chapter 4 18
Outline of Chapter 5 18
2 Literature Review 19
2.1 Current Structure of Power System and Renewable Energy 19
2.2 Energy Harvesting from Solar PV Systems 26
2.3 Review of Existing Research and Identified Gaps 29
2.3.1 MPPT Technique 30
2.3.1.1 Hybrid MPPT Algorithms 32
2.3.2 Neutral Point Clamped (NPC) Converters 34
2.3.3 Neural Networks in Power Electronics & PV Systems 37
2.4 Significance and Contribution 39
2.5 Summary 40
3 Research Methodology 41
3.1 System Overview 41
3.2 Data Collection and Analysis 42
3.3 Simulation Setup and Parameters 43
3.3.1 Modeling of PV cell 44
3.3.2 Boost Converter Design 46
3.4 Energy Storage Management System (ESMS) 48

3.5 Design of Maximum Power Point Tracking 50
3.5.1 MPPT algorithm used in this study 50
3.5.1.1 Perturb and Observe (P&O) MPPT 50
3.5.1.2 Neural Network-based MPPT 53
3.5.1.3 Proposed Hybrid (P&O, Neural Network) MPPT 60
3.6 NPC Converter Topology & Control Design 62
3.6.1 Space Vector Modulation (SVM) 64
3.6.2 Switching Strategy 68
3.6.3 Space Vector PWM (SV-PWM) Algorithm 69
3.7 Integration of the Study System 71
3.7.1 Grid Synchronization: 72
3.7.2 Proposed Control Strategies 75
3.7.3 Voltage Stability Management for Solar PV System 77
3.7.4 Harmonic Distortion 79
3.8 Summary 79
4 Results Analysis and Discussion 81
4.1 Performance Evaluation 81
4.1.1 Solar Irradiance 81
4.1.2 Solar Energy Generation 83
4.1.2.1 Power Production 83
4.2 Performance analysis of MPPT algorithms 83
4.2.1 Simulation Result of MPPT(P&O) Power 83
4.2.2 Simulation Result of MPPT(NN) Power 84
4.2.2.1 Training, Testing & Validation Process 84
4.2.3 Simulation Result of MPPT(Hybrid) Power 89
4.3 Storage Capacity 89
4.4 Battery Operation 90
4.4.1 Simulation Result of Battery (P&O) 90
4.4.2 Simulation Result of Battery (NN) 91
4.4.3 Simulation Result of Battery (Hybrid) 92

4.5 Comparative Analysis 93
4.6 Performance Analysis of NPC Converter 97
4.6.1 Operation Strategy of Voltage 97
4.6.2 NPC Operation 98
4.7 System-level Analysis: Grid connected Performance 99
4.7.1 THD Evaluation 99
4.7.2 Power Quality Assessment 101
4.7.3 Reliability 104
4.8 Summary 104
5 Conclusions and Future Study 105
5.1 Summary 105
5.2 Key Insights 106
5.3 Contribution 107
5.4 Ethical Concerns 108
5.5 Limitations of the Study 108
5.6 Recommendation for further study 109
Bibliography 111
Appendices 123
Appendix A : Specification of System Parameters 123
Appendix B : Pseudocode of this thesis Algorithm 123
Appendix C : Architecture of Grid Connected Model on MATLAB Simulink 126

List of Figures

Figure 1.1 Structure of the Power Grid Topology [6]. 3

Figure 1.2 Solar photovoltaic systems [13]. 5

Figure 1.3 Grid Connected PV system [15]..... 6

Figure 1.4 Main types of grid connected PV power generation systems [16]. 7

Figure 1.5 Diagram of Battery Energy Storage System [17]. 10

Figure 1.6 Structure of the power system [21]. 14

Figure 2.1 Global energy consumption forecast until 2050, by energy source (July 2024). 20

Figure 2.2 Electricity generation in Bangladesh by fuel type (August 2024). 21

Figure 2.3 Power generation capacity of Bangladesh (June 2024) [30]. 24

Figure 2.4 Energy consumption by various sectors of Bangladesh [31]. 24

Figure 2.5 Bangladesh Public and Private sector-based energy generation scenario (June 2024) [30]. 25

Figure 2.6 Potential of solar PV power generation for Bangladesh and major initiatives of different solar projects [44], [45]. 27

Figure 2.7 Solar radiation level at different locations of Bangladesh [50]. ... 28

Figure 2.8 PV array battery charging power transfer Graph [21]..... 30

Figure 2.9 Classification of MPPT techniques [59]..... 31

Figure 2.10 Different DC/AC power converters used for applications. 34

Figure 2.11 Research gap by reviewing a few key papers by comparing and contrasting the objectives, the pros and cons of a neural network-based grid connected MPPT PV system and NPC converter..... 38

Figure 2.12 The working flow of the Research framework. 39

Figure 3.1 The Overall Research Methodological Framework. 41

Figure 3.2 Simplified diagram of the proposed battery-based grid-connected PV system model. 42

Figure 3.3 Operating principle of a PV cell [13]. 43

Figure 3.4 The equivalent electrical circuit model of a solar cell. 44

Figure 3.5 Converter Circuit Design. (a) Switch is ON (S=1). (b) Switch is OFF (S=0). 46

Figure 3.6 dp/dv sign at various points of the curve [130]..... 51

Figure 3.7 P&O algorithm flowchart..... 52

Figure 3.8 Neural Network Model & flowchart of MPP. 53

Figure 3.9 Neural Network's (a) Function block (b) Layer configuration (c) Process layer (d) Final trained neural network. 55

Figure 3.10 Structure of basic neural network model..... 56

Figure 3.11 Development of the ANN flowchart. 57

Figure 3.12 Ten hidden layer nodes (ANN model architecture). 58

Figure 3.13 Proposed Hybrid (P&O, NN) model algorithm flowchart. 60

Figure 3.14 Neutral-point diode clamped Three level inverter. 62

Figure 3.15 Three-level inverter Space Vector Diagram (α, β) frame..... 65

Figure 3.16 Vector map of (Sector I). 66

Figure 3.17 Pattern of SV-PWM duty cycles switching application. 70

Figure 3.18 Solar PV and battery control integration with NPC inverter configuration. 72

Figure 3.19 PV grid configuration; (a) Equivalent circuit diagram, (b) Phasor diagram. 73

Figure 3.20 Control Block diagram of a 3-Level NPC inverter system. 76

Figure 4.1 The measurement of Solar (a) PV maximum power production (b) Temperature data. 83

Figure 4.2 Whole-day Observing P&O MPPT PV power. 84

Figure 4.3 Whole-day Observing NN MPPT PV power. 84

Figure 4.4 Regression plot of the proposed ANN model. 86

Figure 4.5 Error histogram plot of the proposed ANN PV model. 86

Figure 4.6 Training state plot of the proposed ANN MPPT. 87

Figure 4.7 Proposed Neural Network Algorithm Performance Test. 87

Figure 4.8 Whole-day Observing Hybrid MPPT PV power. 89

Figure 4.9 Response of Battery (a) Current, (b) Voltage, (c) Power & (c) SOC (%) with varying irradiance and load conditions for P&O System. .. 91

Figure 4.10 Response of Battery (a) Current, (b) Voltage, (c) Power & (c) SOC (%) with varying irradiance and load conditions for Neural Network System. 92

Figure 4.11 Response of Battery (a) Current, (b) Voltage, (c) Power & (c) SOC (%) with varying irradiance and load conditions for Hybrid system. 92

Figure 4.12 Power response comparison of Pmpp, PP&O, PNN, PHybrid. 93

Figure 4.13 Observing whole-day results of PV Voltage, Current, and Bus Voltage and iboost curve of PV array. 94

Figure 4.14 Observing whole-day results of PV power, Bus voltage, and SOC, Voltage, Current in Battery Stage. 95

Figure 4.15 Generating Voltage, Vpv; DC Bus Voltage, Vdc and DC link voltage +Vdc/2, -Vdc/2..... 97

Figure 4.16 Id and Iq curve of the inverter current regulator. 98

Figure 4.17 (a) Modulation Index; (b) 3-level PWM inverter line-to-line output voltage. 98

Figure 4.18 Duty cycle of the Switches with reference sawtooth waveform of frequency 5 kHz (SVPWM) 99

Figure 4.19 Experimental waveforms of 3-phase grid Voltage (Vabc) and Current (Iabc) a, b, c at rated output. 99

Figure 4.20 Output active and reactive power of the grid, P MW & Q MW. 100

Figure 4.21 Load Flow Analysis Experimental on Proposed PV Model..... 102

Fig. B.01 The proposed MATLAB Simulink model. 126

List of Tables

Table 1.1 Different software tools are used for MPPT Techniques and NPC converter analysis 14

Table 2.1. Current electricity structure of Bangladesh (June 2024) [33], [34], [35]..... 22

Table 2.2 Overview of Power Generation 23

Table 2.3 RE generation sector of Bangladesh (December 2024) [41]..... 25

Table 2.4 Comparative assessment of different hybrid MPPT techniques. 33

Table 2.5 Analysis of grid-connected multilevel inverters..... 36

Table 2.6 Main characteristics of different controllers proposed in scientific articles. 37

Table 3.1 Different parameters of the proposed model..... 47

Table 3.2 Neural Network function 59

Table 3.3. NPC Switching States (ONE LEG) 63

Table 3.4 Different Switching States and Vectors in NPC Converter. 66

Table 3.5 Switching Vector Times of a Three-Level Inverter in Sector I..... 67

Table 3.6 Conventional switching sequence of the three-level inverter SVM. 68

Table 3.7 Grid-synchronization Parameters. 73

Table 3.8 System Parameter 77

Table 4.1 Changing environmental conditions data on a day. 82

Table 4.2 Levenberg-Marquardt ANN Parameters. 85

Table 4.3 Comparative Analysis of Levenberg-Marquardt Train ANN Algorithm. 88

Table 4.4 Response of Simulation MPPT. 94

Table 4.5 Comparison of MPPT methods with various Parameters. 96

Table 4.6 FFT Analysis of THD (SVM) 100

Table 4.7 FFT Analysis of THD (SVPWM) 101

Table 4.8 Load flow converged in 15 iterations 103

Table A.5.1. Specifications of the solar PV modules. 123

Nomenclature

Acronyms and Abbreviations	
ANN	Artificial Neural Network
AC	Alternative Current
AI	Artificial Intelligence
DC	Direct Current
DG	Distributed Generation
DoD	Depth of discharge
DR	Demand Response
DSM	Demand-side Management
BEMS	Battery Energy Management System
BESS	Battery Energy Storage System
ECS	Energy Capacitor Systems
ESS	Energy Storage Systems
ESSM	Energy Storage System Management
FESS	Flywheel Energy Storage Systems
FFT	Fast Fourier Transformation
FOCV	Fractional Open Circuit Voltage
GoB	Government of Bangladesh
GMMP	Global Maximum Power Point
HC	Hill Climb
IDCOL	Infrastructure Development Company Limited
INC	Incremental Conductance
LM	Levenberg Marquardt
LMPP	Local Maximum Power Point
MATLAB	Matrix Laboratory
ML	Machine Learning
MPC	Model Predictive Control

Acronyms and Abbreviations	
MPPT	Maximum Power Point Tracker
NPC	Neutral Point Clamped
NLP	Non-linear Programming
NN	Neural Network
NTV	Nearest Three Vectors
PCC	Point of Common Coupling
PSIM	Physical Security Information Management
PSCAD	Power Systems Computer Aided Design
PLECS	Piecewise Linear Electrical Circuit Simulation
P&O	Perturb and Observe
PV	Photovoltaic
PWM	Pulse with Modulation
RE	Renewable Energy
RES	Renewable Energy Resource
SHS	Solar Home System
SCADA	Supervisory control and data acquisition
SPWM	Sinusoidal pulse width modulation
SVM	Space Vector Modulation
SVD	Space Vector Diagram
SV-PWM	Space Vector Pulse Width Modulation
THD	Total Harmonic Distortion

Symbols	
$E_{PV(AC)}$	Energy generated and injected into grid (kWh)
G	Irradiance
H_T	Total horizontal irradiance on PV array plane (Wh/m^2)
I_{DC}	DC current (A)
$N_{Batt(max)}$	Maximum battery banks required
$N_{Batt(min)}$	Minimum battery banks required
$P_{PV(total)}$	Rated/installed capacity of the integrated solar PV system/plant
P_{in}	Input power
P_{load}	Load or output power (W)
P_{max}	Output maximum Power
$P_{nominal}$	Nominal power at STC
$P_{total\ def}$	Total deferrable load
T	Temperature
V_{DC}	DC or Battery voltage (nominal) (V)

Chapter 1: Introduction

This chapter provides a background study of neural network-based Maximum Power Point Tracking (MPPT) and Neutral Point Clamped Converter (NPC) concepts and their prospects in section 1.1. Section 1.2 describes the overview of grid-connected PV systems. Section 1.3 represents the basic description of MPPT challenges and grid-connected PV systems. Then narrates an overview of the challenges and importance of MPPT and NPC converters in renewable energy systems in sections 1.4 and 1.5. Section 1.6 discusses the research hypothesis formulation of the thesis. Specific research aims, purposes, and objectives are reported in Section 1.7. Section 1.8 relates to the significance and scope of this research and provides definitions of the terms used. Then, discuss the organization of the remaining chapters of the thesis in section 1.9.

1.1 BACKGROUND

Nowadays, most nations are focusing on energy-driven economic and industrial revolutions. A crucial element of this shift is adopting continuous and sustainable energy generation. While increasing power production through traditional fossil fuel methods can boost energy output, it often leads to unsustainable practices. Scientists and politicians must consider the next generation of safer technology for people and the environment. Because of global warming, using too much fossil fuel to produce power is bad for the environment. Therefore, the main considerations for energy safety and security are the harnessing and exploitation of renewable energy (RE) and appropriate economic management. Fossil fuels continue to provide the great majority of the world's energy, notwithstanding the rapid worldwide expansion of renewable sources.

Solar power systems, or photovoltaics, are a rapidly growing renewable energy source. However, operating at the Maximum Power Point (MPP) under various climatic conditions is essential for their efficiency. One of the most important control strategies to ensure the PV system reaches its maximum power output is Maximum Power Point Tracking, or MPPT. Previous MPPT algorithms, such as Perturb and Observe (P&O) and Incremental Conductance (INC), have drawbacks including slow convergence and getting trapped in local maxima. This study proposes a novel method for a grid-connected PV system that combines a Neutral Point Clamped (NPC) converter with a neural network (NN)-based MPPT control. One of the main challenges in integrating renewable energy sources into microgrids is the need for efficient and reliable power conversion systems. In this system, we increase the maximum power output from solar energy. The author [1] reviews 19 methods, categorized into three groups: offline methods (such as short circuit current, open-circuit voltage, look-up table, curve-fitting, and AI algorithms), online methods (such as extremum seeking control, ripple correlation control, hill climbing, incremental conductance, P&O, and modified P&O [2]). NPC converters are power inverters well-suited for application in power conversion systems. They are efficient and capable of handling the high voltages and currents typical in renewable energy applications. One of the key difficulties in incorporating renewable energy sources into microgrids is the need for efficient energy management systems. Battery Energy Management Systems (BEMS) play a vital role in regulating the charging and discharging of batteries within microgrids. BEMS must maximize battery performance while ensuring safety and reliability [3]. An NPC inverter is a multilevel power converter that uses clamping diodes to ensure proper voltage sharing across the power switches [4]. The architecture of a three-level NPC inverter includes three NPC phase-legs, each containing four controllable transistors, resulting in a total of 16 potential states. However, only three of these

states are feasible, since the others would cause DC-link short circuits. These three states produce three distinct output voltages [5].

1.2 PHOTOVOLTAIC SYSTEMS

Photovoltaic systems are becoming increasingly popular in grid applications because they generate clean and renewable energy. However, maximizing the power output of these systems is crucial for efficient operation, which is where MPPT algorithms come into play. By integrating a Neural Network-based MPPT with an NPC Converter, we can optimize the performance of grid-connected PV systems and improve overall energy efficiency.

The overall 14 decades, the power grid network has been built from the late 1880s to accommodate the ever-increasing demand for electricity. The power grid is an essential component of modern civilization, providing uninterrupted and effective power delivery. It is challenging to consider that, due to various losses, the produced power does not equal the power used at the end-user level. Without power, it is much harder to imagine the consequences. The four main parts of the grid network are the different generating systems, transmission lines, distribution systems, and consumer systems (see Figure 1.1).

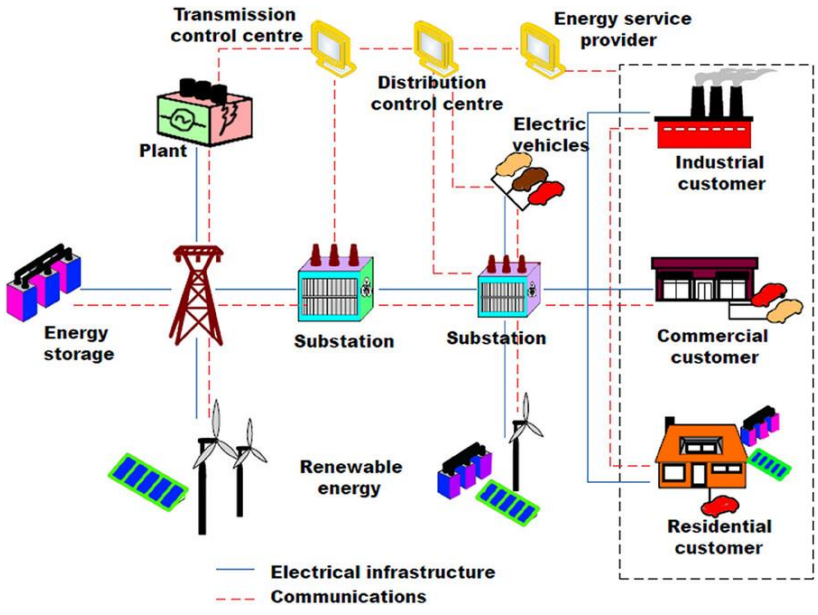


Figure 1.1 Structure of the Power Grid Topology [1].

A typical smart grid system is categorized based on techno-economic criteria. For instance, on-grid and off-grid systems differ by their connection to the master grid. An on-grid system is a dependent grid model in which the grid is connected to the main grid, either for a short or long period, and the grid system is operationally or energetically connected to it [2]. In the case of self-sustaining on-grid systems, they are cut off from the main grid [3]. An on-grid system offers a steady supply, can handle a high load capacity at any time, is simple to manage, operates economically, and allows the producing sources to exchange peak loads [4]. Among the main issues with on-grid systems are high transmission losses, high transient currents, high voltage swings, the inability to satisfy peak demands, and network overload-related blackouts [5]. A grid that is isolated from the main grid can overcome these issues. An off-grid system is disconnected from the main grid to function independently. Because it is semi-isolated, it is less affected by major grid disruptions, and since it has a low voltage level, the controller is easy to use and reasonably priced. Additionally, it offers a more reliable and economical model [6],[7]. Electricity circulates from power plants to homes and businesses via substations, which regulate the voltage used in transmission and distribution. A smart grid uses automation, communication, and information technologies to monitor and control power flows in real time, maintaining a balanced supply and demand.

The integrated grid system is an electrical network that can automatically combine the activities of all users linked to it, power production, distribution, prosumers, and those that do both, to supply efficient, cost-effective, and secure electricity supplies. It employs innovative technologies such as advanced monitoring, DSM, control, and communication. Based on the electricity generation performance from DER, the suggested integrated PV model is used as an off-grid stand-alone system and a grid-connected (integrated) PV system. Basically, a photovoltaic module or array is the primary component that

transforms solar energy into Direct Current (DC) power; however, additional main components (PV module, battery, charge controller, inverter) are needed to create a PV system that stores and delivers the energy to customers.

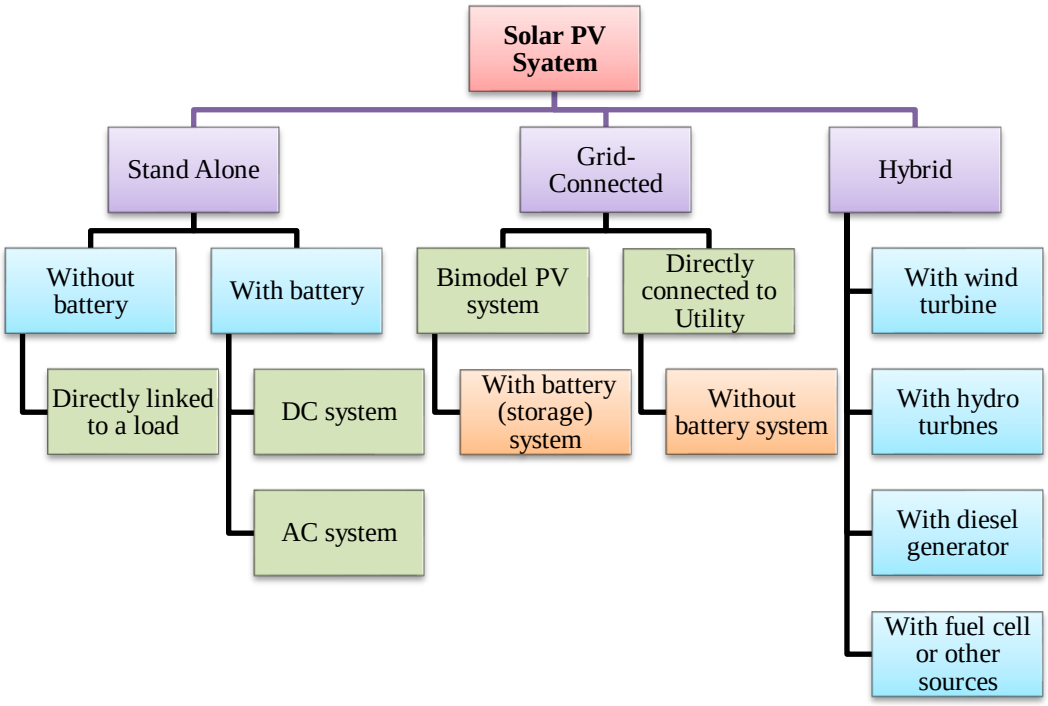


Figure 1.2 Solar photovoltaic systems [8].

Most PV systems used to have battery reserves to work without sunlight. Grid-connected PV systems do not use batteries [9]. Figure. 1.2 represents the classification type of solar photovoltaic systems into stand-alone, grid-connected systems and hybrid. The Converting power can be utilized by a local off-grid network (stand-alone PV system), a commercial power grid (Grid-connected PV system), or both (Bimodal PV System).

1.2.1 Infrastructure of Grid Connected PV Systems

These systems are commonly found in residential and commercial settings and consist of solar panels, inverters, and other power-generating components. Implementing a neural network-based MPPT system, along with a neutral point-clamped converter, can significantly enhance the proficiency of grid-connected photovoltaic (PV) systems in these applications.

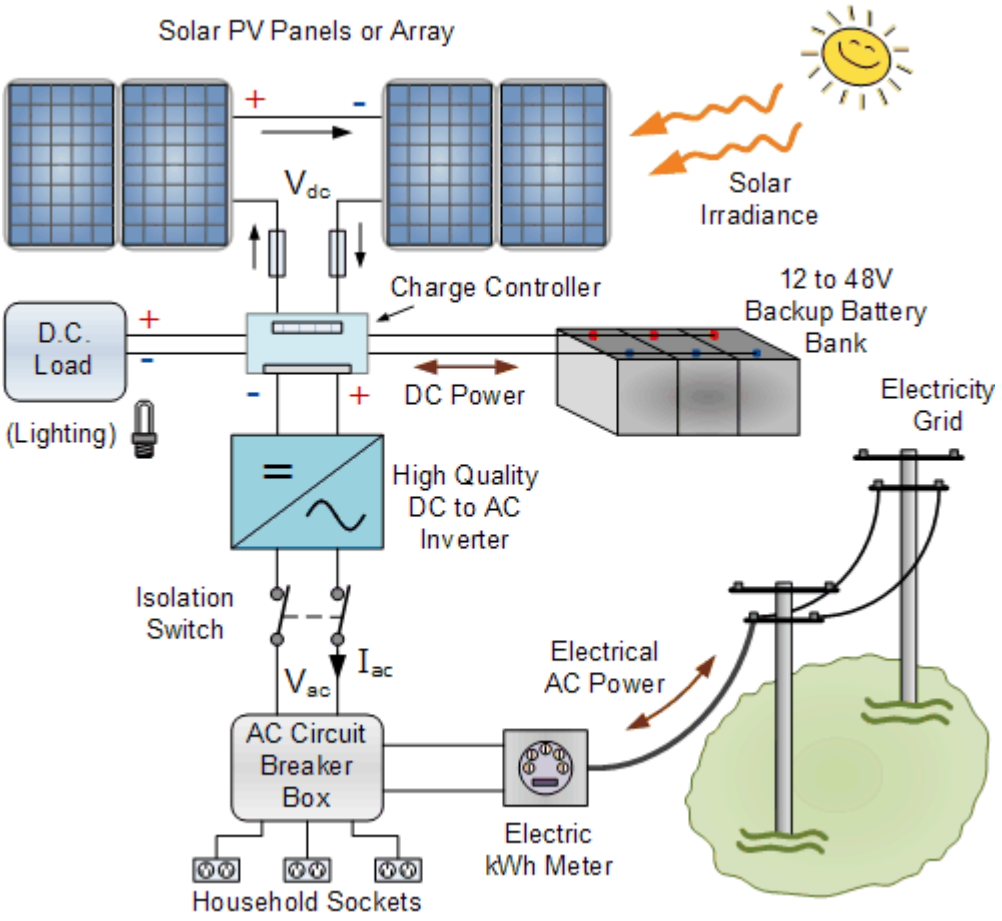


Figure 1.3 Grid Connected PV system [10].

Several components work together in a photovoltaic (PV) system to efficiently capture and use solar energy. Photovoltaic arrays are made up of interconnected solar panels that receive sunlight and convert it into electrical energy. Several parts, including an inverter to convert DC to AC power, power electronics converters (including sophisticated NPC converters) for the best energy management, and a charge controller to keep the battery from overcharging, are used to manage and process this energy. The system also contains a mounting framework to attach solar panels, cabling, circuit breakers, fuses, and a disconnect button to ensure safety and reliability. While a tracking system ensures the panels are oriented for optimal sun exposure, other equipment, including voltage meters, keeps an eye on the system's operation. Grid-integration techniques in grid-tied systems allow for the continuous transmission of energy to the utility grid, which is backed by auxiliary energy sources to

manage variable loads. These components work together to provide a strong infrastructure for generating and utilizing renewable energy.

The main types of grid-connected solar energy systems can be classified according to different compositions and purposes of use.

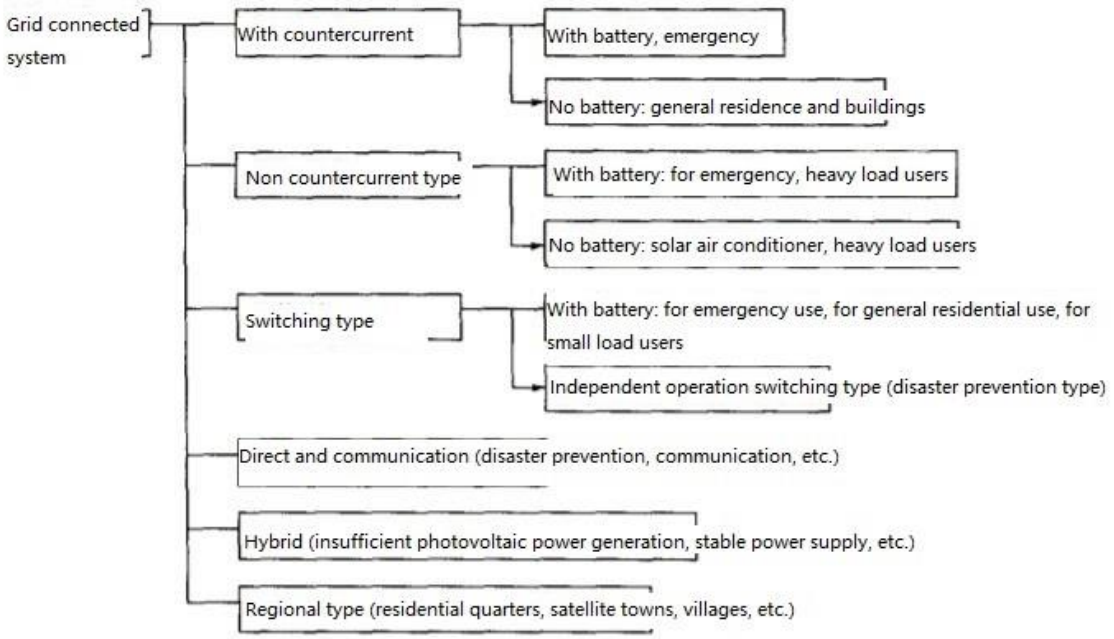


Figure 1.4 Main types of grid connected PV power generation systems [11].

Figure 1.4, power generation systems can be classified based on energy transmission into grid-connected systems with or without reverse current, switched grid-connected systems, direct and AC grid-connected systems, mixed systems, and regional systems. A ***countercurrent grid-connected system*** provides electricity when solar output is poor and delivers excess solar energy to the grid to optimize efficiency. The ***non-countercurrent system*** prevents excess energy from flowing to the grid but draws power when needed. There are two categories of switched grid-connected systems, which are typically used to avert disasters: ***general and self-operating***. Solar systems include solar cells, batteries, inverters, switchers, and loads. They operate independently under normal conditions and automatically switch to grid power under insufficient sunshine or low battery, allowing for smaller, cost-effective batteries. During emergencies, self-operating

systems, which are intended for disaster situations, use stored energy to power vital loads like lights, medical equipment, shelters, and communication systems by connecting to the grid via a grid connection device and disconnecting. ***Direct systems*** deliver DC power to communication equipment; however, AC grid-connected systems power AC loads. ***Hybrid grid-connected systems*** integrate solar, wind, or fuel cells; the wind-solar hybrid system prioritizes renewable energy, while the solar PV and fuel cell system increases efficiency and lowers emissions. The ***regional grid-connected system*** consists of solar cells, power regulators, and loads, with each PV system directly connected to the power grid. Excess energy is sent to the grid, while energy is drawn from the grid when the load's demand exceeds solar generation.

1.2.1.1 Generation system:

Real-time tracking of the MPP is achieved through a neural network-based MPPT algorithm that optimizes energy output. The NPC converter is highly efficient and reliable in converting the generated DC power into AC power for grid connection.

1.2.1.2 Converter System:

Grid power generation units require inverters to manage differing AC power needs for end users. While some renewable energy sources (RESs) produce DC, like solar PV, others generate AC, necessitating power conversion for compatibility with modern appliances or battery systems. Inverters in microgrids perform essential roles such as converting DC to AC for residential use, managing AC-to-DC conversion for battery charging, and ensuring frequency balance.

In AC-coupled setups, energy generation and storage units have independent inverters connected on the AC side, with battery inverters overseeing charge and discharge processes. In DC-coupled configurations, shared inverters between storage and generation systems improve efficiency,

reducing conversion stages and enhancing battery charging performance. These configurations ensure optimal integration of RESs, storage, and utility systems. To ensure the robustness and efficiency of the proposed NPC converter designs, several tests can be conducted. simulation-based evaluations that assess performance parameters including efficiency, harmonic distortion, and voltage balancing under various load and grid situations using programs like MATLAB/Simulink. Experimental validation utilizing a scaled prototype can confirm these findings, with an emphasis on dynamic responsiveness, transient behaviour, and recovery durations. Total harmonic distortion (THD) may be deliberately used by harmonic analysis with FFT across various load profiles, highlighting the converter's harmonic suppression capabilities. Additionally, evaluating neutral-point voltage balancing solutions under both steady-state and dynamic settings helps confirm their effectiveness. Grid compliance tests may guarantee the designs fulfil regulatory criteria for power quality and stability.

1.2.1.3 Transmission system:

When combined, these components ensure efficient delivery of generated power to the grid, reducing losses and enhancing overall system performance. The neural network-based MPPT algorithm can also adjust to shifting environmental circumstances, which increases the system's effectiveness even further.

1.2.1.4 Battery Energy Storage System (BESS):

In grid systems that depend on non-dispatchable renewable energy sources (RESs) like solar and wind, energy storage systems (ESS) like batteries are crucial because they guarantee on-demand electricity by storing energy for usage in times when resources are not accessible. ESS improves system stability by meeting peak use needs, although grid-connected microgrids powered by continuous diesel generators may not require batteries. To maximize performance, lifetime, and cost-effectiveness, choosing the best ESS is essential.

Although conventional lead-acid batteries are widely used, more recent technologies such as lithium-ion and nickel-metal hydride batteries offer increased durability and efficiency at lower costs. However, significant battery systems pose safety issues such as hydrogen gas build-up and electrolyte leakage; therefore, they must be installed in well-ventilated places.

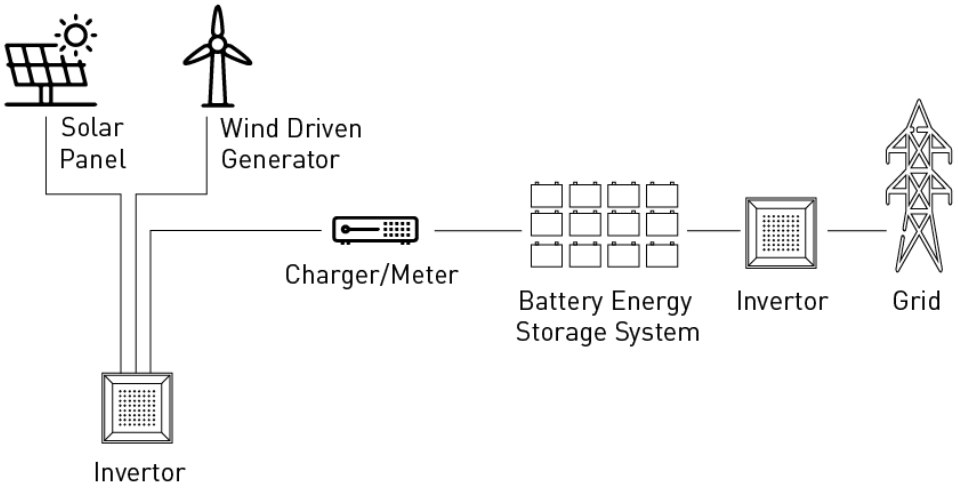


Figure 1.5 Diagram of Battery Energy Storage System [12].

Among the several grid storage technologies, Battery Energy Storage Systems (BESS) stand out due to their special features and applications. Through charging during off-peak demand periods and discharging during peak demand intervals, energy storage systems in grid-connected photovoltaic systems offer several advantages, including flattening load curves and increasing grid efficiency. They make frequency control possible through quick charging and draining, guaranteeing grid stability. They improve grid resilience and facilitate short-term load increases by serving as backup power. They also store and control sporadic variations from renewable energy sources and enhance power quality by regulating voltage and compensating for reactive power.

The integration of intelligent control systems, such as neural networks, is advancing grid-connected photovoltaic systems. By forecasting system behaviour and optimizing power output, these technologies improve grid stability. Additionally, bidirectional power flow makes energy storage

integration easier, allowing the storage of excess solar energy and subsequent discharge to increase grid resilience and curtail the use of fossil fuels.

1.2.1.5 Distribution system

The power distribution system delivers electricity from the power generation station to final users. It includes lines of distribution and transmission, transformers with supporting infrastructure such as poles. Overhead transmission is more commonly used than underground lines because it is less expensive to build. The system can handle various voltages, including AC and DC, as well as single- and three-phase power. In a large microgrid, transformers raise voltage for efficient transmission, while step-down transformers reduce high or medium voltages to about 220 V or 415 V for homes and businesses.

1.2.1.6 End-user System

End-user systems in grids enable safe and efficient energy access for consumers and prosumers by meeting a variety of demands through secure connections, danger mitigation, and exact metering. They provide customers access to real-time consumption data, assist operators in projecting demand, and assist regulators in establishing reasonable rates that balance operational requirements and cost while protecting equipment and boosting system dependability.

- **Metering System**

Traditional electricity metering systems, particularly analog meters, pose challenges in terms of time-consuming billing, bill distribution, and payment processes. Modern metering technologies, such as smart and pre-paid meters, make these chores easier and provide better energy management.

Pre-paid meters: Electricity bills can be paid in advance by consumers using pre-paid meters, also referred to as pay-as-you-go systems. Credits are added to meters by special codes, and payment options include scratch cards and mobile

banking. By giving users instant feedback on their energy use, these devices promote more economical use. In contrast, these meters are advantageous over the benchmark technology in many countries in the 21st century, requiring utility companies to send meter readers and invoices regularly. However, a lack of real-time input frequently leads to increased energy use.

Smart meters: Pre-paid and post-paid smart meters are more convenient and functional than standard meters. They facilitate two-way communication between utilities and customers, allowing for remote monitoring, real-time updates, early problem identification, automated meter reading, and variable pricing. Smart meters improve grid reliability by resolving power quality concerns, minimizing overloads, and facilitating demand-side management (DSM).

All things considered, smart metering systems help consumers and utilities alike by increasing efficiency, enhancing grid management, and raising consumer knowledge of energy costs and consumption.

1.3 CHALLENGES IN GRID-CONNECTED PV SYSTEMS

Renewable energy-to-grid integration involves deploying microgrids with solar, wind, and storage systems for isolated operation or grid islanding during disturbances. It includes the creation of new guidelines and standards (IEEE Std 1547-2018) for connecting increasingly dispersed energy systems and aids in planning for a future that improves energy resilience without requiring significant expenditures for significant infrastructure improvements to the present system, concerns like voltage fluctuations, power quality difficulties, and grid stability. Implementing sophisticated control techniques and communication protocols can assist in addressing these issues while also optimizing the system's performance. Besides, using energy storage devices can lessen the effects of solar power generation's fluctuation and intermittency. Grid-

connected PV systems may satisfy energy demands more reliably and flexibly by integrating these options.

1.4 MAXIMUM POWER POINT TRACKING (MPPT)

1.4.1 Challenges and Importance

The MPPT algorithm is critical in increasing the energy production of solar array by constantly changing the switching point to the MPP. Increasing total system efficiency and guaranteeing optimal energy generation depend on this improvement. The most significant challenge is the dynamic nature of solar radiation, which constantly fluctuates due to factors like cloud cover, shading, and time of day [13]. Implementing an efficient MPPT algorithm can help extend the lifespan of solar panels by keeping them from functioning at suboptimal levels, resulting in a higher return on investment for solar systems.

In solar systems, MPPT is an essential approach that maximizes the amount of energy extracted from PV panels. Through maximizing energy extraction, MPPT dynamically modifies the PV array's operating current and voltage to meet the MPP. This is the key to improving efficiency. However, despite their benefits, standard MPPT approaches have intrinsic drawbacks, such as a slower reaction to abrupt environmental changes, the inability to monitor numerous peaks in partially shadowed situations, and greater complexity in multisource systems. The efficiency of solar energy conversion is greatly improved by this dynamic optimization, which raises energy production and lowers system expenses.

1.5 NPC CONVERTER IN RENEWABLE ENERGY SYSTEMS

The NPC converter's capacity to produce multilevel output waveforms makes it a popular technology in RE systems [14]. This eliminates harmonic distortion, improves power quality, and lowers switching losses when compared to standard two-level converters [15]. For higher power applications such as

wind and solar power generation, where they connect with the grid and enable effective power transmission, NPC converters are especially well-suited.

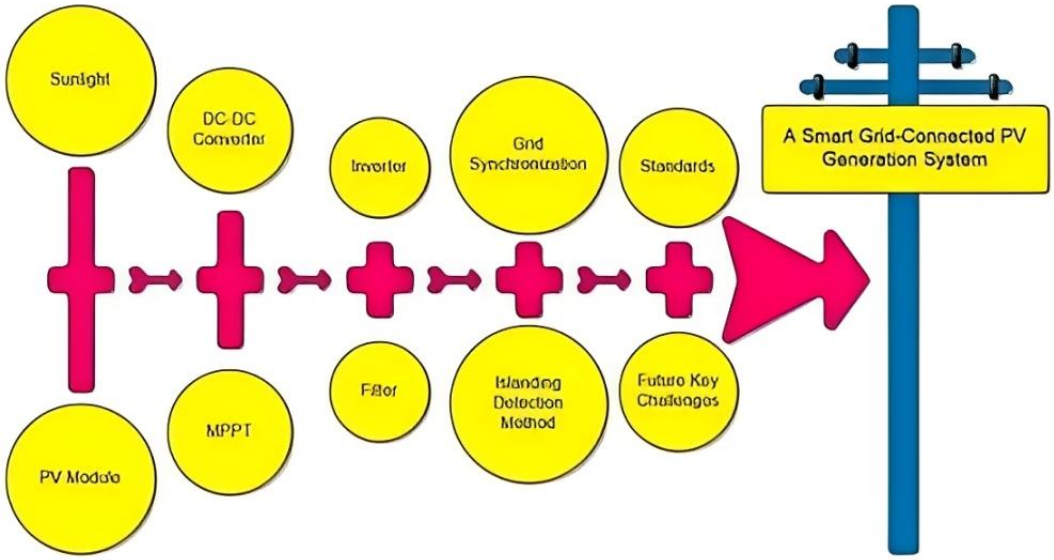


Figure 1.6 Structure of the power system [16].

Additionally, their modular design allows for scalability and improved power capacity, making them an adaptable choice for large-scale RE projects. Figure 1.6 represents the basic structure of the power system, where we collect the data from various generations of sunlight. It then monitors, controls, and applies the data to forecast the best MPPT operation and filters the supply with various modulation techniques.

Table 1.1 Different software tools are used for MPPT Techniques and NPC converter analysis

Name	**Application & Key Features**
PSIM	Focus on power electronics simulation [17],[18].
PLECS or PSCAD/EMTDC	PLECS or PSCAD/EMTDC offer more advanced features and capabilities for complex simulations [19].
MATLAB Simulink Power Systems	ANN Toolbox, a Matrix programming language used by engineers in power systems, electronics and control as among other fields. Other languages (C++, Java, and Fortran) are compatible [20].

1.6 PROBLEM STATEMENT

Based on the discussion in the earlier Section 1.3-1.5, an advanced MPPT technique used for solar harvesting energy, and integrating energy into the grid system is envisioned in this research. The supervised machine learning methods are discussed in depth, which should have the least computational complexity, be easier to implement, analyze, and be user-friendly. Artificial Neural Network (ANN) based MPPT approaches are expected to predict maximum power forecasting, bidirectional DC boost converter for the on-grid battery management system, and NPC inverter to convert DC to AC energy from a grid-connected Demand Side Management (DSM) system. This research also hypothesizes the switching Pulse Width Modulation (PWM) technique for a grid-connected NPC converter.

1.6.1 Hypothesis

A Machine Learning Based MPPT for grid-connected solar PV integrated with energy storage can provide better DSM. The hypothesis is associated with the following research questions.

1.6.2 Research Questions

There are two research questions to be answered. (1) If three different MPPT approaches (P&O, Neural Network and their combined Hybrid) of energy harvesting are investigated, how do we set their performance indices for a PV system? Carrying out these MPPT methods, the Neural Network performs better in high temperature and irradiance conditions. Although P&O performs slightly differently under these conditions, the Hybrid (P&O, Neural Network) approach yields a better response with the same parameter conditions. The other part of the research question concerns the energy supply for grid integration operations. So, (2) Can we apply the Space Vector PWM technique in the NPC converter for better switching operation rather than the SVM technique to slow down the

switching function? Based on the effective response into the grid of NPC gate pulse Switching, the energy conversion mechanism performed is relatively faster than the PWM approach, which reduces the system's operation.

1.7 RESEARCH AIMS AND OBJECTIVES

This research work aims to design a model and analyse around 1,500 kW of battery-based grid-tied solar integration systems. Therefore, an ML-based MPPT approach using an NPC converter for grid-connected systems has been developed to amplify power generation and compare performance under variable conditions. The main objective with specific aims is:

- To develop a machine learning-based MPPT controller with an NPC converter for a Grid-connected PV system under varying irradiance, temperature, and operation conditions.
- To evaluate the effectiveness of a solar PV system having the NPC converter using voltage as a reference point for adjusting the duty cycle.
- To compare the harmonic distortion and other critical parameters generated by NPC converters with the existing literature review.

1.8 SIGNIFICANCE AND SCOPE

The primary purpose of this research study is to track maximum PV power in various environmental conditions. The following are the expected outputs from this suggested model. The proposed model-constrained machine learning-based energy harvesting of the solar PV system increases the PV performance of the hybrid MPPT, optimization the grid-based battery energy storage system, prepares an effective architecture of neural network MPPT, performs better on grid demand-side management, maintains the permissible total harmonic distortion level, and creates a green environmental balance. The control and operational framework is employed to develop the proposed simulation model,

ensuring reliable performance under dynamic loading conditions and facilitating optimal energy storage within a grid-scale battery system.

The simulation results will illustrate the performance of the proposed model and juxtapose with the traditional MPPT approach using either individual or hybrid strategies. The hybrid MPPT algorithm is expected to improve the retention of surplus grid energy by a measurable percentage. The key handout of this research is the development of a neural network-based hybrid MPPT technique for RE and battery-integrated grid energy. To evaluate the performance of the proposed model, a comparison between the suggested MPPT technique with the SV-PWM approach is analyzed and examined. The MATLAB Simulink simulation results demonstrate the cost-effectiveness and superior performance of the proposed MPPT method when compared to machine learning or individual MPPT approaches using a neutral point clamped converter on the grid.

1.9 THESIS ORGANISATION

Including the first stated introduction chapter, this thesis is segmented into four chapters (Chapters 2 through 5), each briefly described below.

Outline of Chapter 2

Chapter 2 reviews the relevant and existing machine learning-based MPPT and NPC converter infrastructure to find the research problem. In the current structure of power systems, renewable energy and energy harvesting from solar PV, the concept of neural network-based hybrid MPPT is present. Review of existing research and identification of gaps in the MPPT technique with a hybrid combination concept. The application of a power converter NPC, analysis of grid-connected multilevel inverters, and SVPWM technique for solution of the operation function. Relevant MPPT and NPC objectives and their strength and

weaknesses are reported. The idea of a novel energy harvesting from solar PV by neural network-based MPPT is analyzed and discussed.

Outline of Chapter 3

Chapter 3 is organized based on the research methodology and design of an advanced three-phase, 3L NPC inverter model to examine the integration of solar PV systems with MPPT and battery storage. The description and performance evaluations of a comparison of solar PV using various MPPT and NPC converters are provided in detail. As a result, we recommend selecting the most superior hybrid MPPT techniques for solar harvesting. The process of data collection (practical data and simulated data) is presented and analyzed. The generating voltage is integrated into the NPC converter with the help of the space vector PWM algorithm. Finally, a control strategy was proposed for converting power to the grid.

Outline of Chapter 4

Chapter 4's organization is based on the performance and simulation result analysis. Therefore, it includes the different case studies of various environmental conditions of an integrated battery-based grid-connected PV system MPPT performance and comparative study. Design parameters and figures are included in the chapter. Data and output key findings figure and the table is given as seem appropriate.

Outline of Chapter 5

Finally, the conclusions and outlook are presented in Chapter 5. A summary and critical insights from this research are outlined, followed by the concluding remarks highlighted. Ethical concerns are also discussed. Some implementation issues and limitations are discussed. A few possible future research directions for integrated systems complete this thesis.

2 Literature Review

This chapter furnishes a historical background of the current structure of Bangladesh's power system and its renewable energy prospects in Section 2.1. Section 2.2 highlights the energy harvesting from solar PV systems. Section 2.3 reviews the existing research and gaps in MPPT and hybrid techniques. In addition, with the research gap of the NPC converter, the pros and cons of earlier studies have been reviewed, and a basic description of a neural network power electronics & solar PV system. Then, epitomize the significance and research contributions in section 2.4. Finally, summarize section 2.5. These dissertations gave an idea of a battery-based grid-connected PV system with affordable distribution utilities.

2.1 CURRENT STRUCTURE OF POWER SYSTEM AND RENEWABLE ENERGY

Under Sustainable Development Goal 7 (SDG-7), about 190 countries have engaged in providing reliable, affordable, and sustainable energy to all citizens by 2030. As a result, SDG-7, which was widely adopted at the Paris Agreement-2015 [21], contains specific regulations for generating power from clean energy. The primary focus is on the percentage of people with access to electricity; numerous nations, most notably Bangladesh, Kenya, and India, have made strides in increasing this access [22]. By 2030, nearly all countries will significantly reduce their electricity output from fossil fuels and focus on renewable energy, which will help lower climate change to 1.5°C [23]. This emphasizes the critical need for climate action investment. COP29 plans for finance to mitigate the effects of climate change and help developing nations transition to more sustainable energy sources. It also intends to increase renewable energy capacity

to 30% by 2030 and diversify its existing energy system to become a principal in clean energy [23]. The upcoming Brazil Agreement-2025 (COP30) promises effective carbon emission policies and eco-friendly green energy systems that align with long-term weather goals.

The energy consumed worldwide has surged in recent years and will continue rising until 2045, after only hydropower and renewables are projected to grow, reaching 30% of total energy use by 2050 [24]. Global energy consumption by source from 2000 to 2022, with projections to 2050, is shown in Figure 2.1.

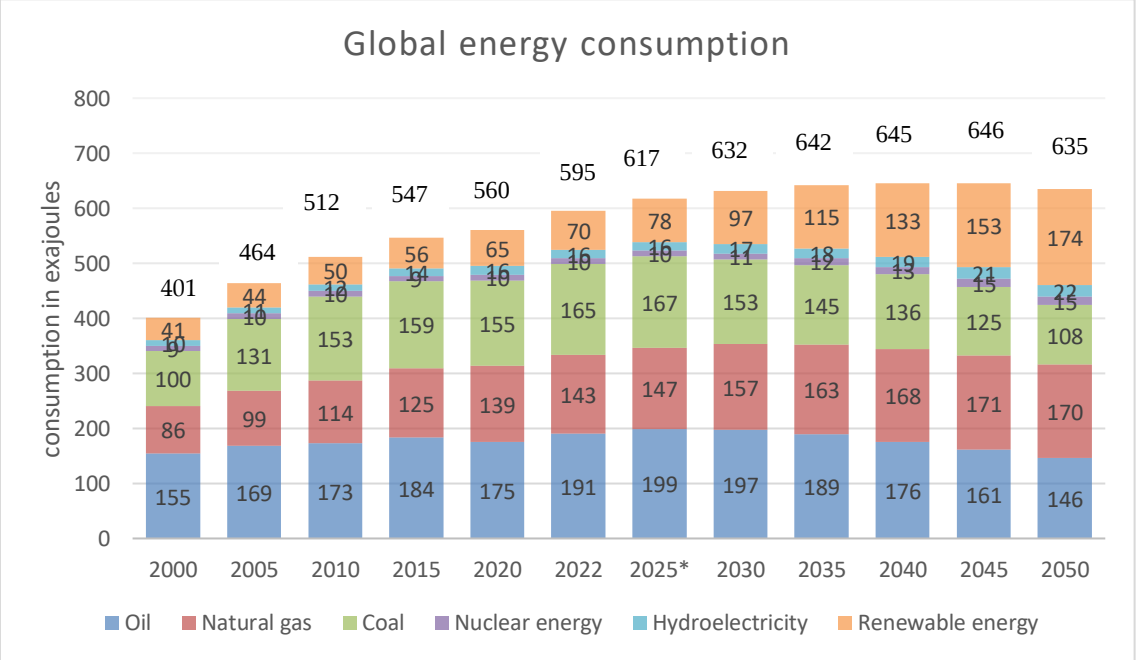


Figure 2.1 Global energy consumption forecast until 2050, by energy source (July 2024).

Currently, Bangladesh has 28,098 MW of installed capacity, and during peak hours, its entire power consumption is around 20,000 MW. The maximum peak generation is 16,477 MW, and its growth rate is just 1.26 percent. It predicts that each person will generate 510 kilowatt-hours of energy [25]. To achieve this development goal, net electricity demand is estimated to reach 61 GW by 2041. Bangladesh must import energy supplies including gas, oil, and occasionally direct power to meet its electrical requirements. Compared to other energy

sources, Bangladesh relies heavily on fossil fuels to generate power. Natural gas provides around 48.52 % of the world's electrical generation, as shown in Figure 2.2. The other sources include coal, imported liquid fuel, hydropower, energy imports, and solar photovoltaics [25].

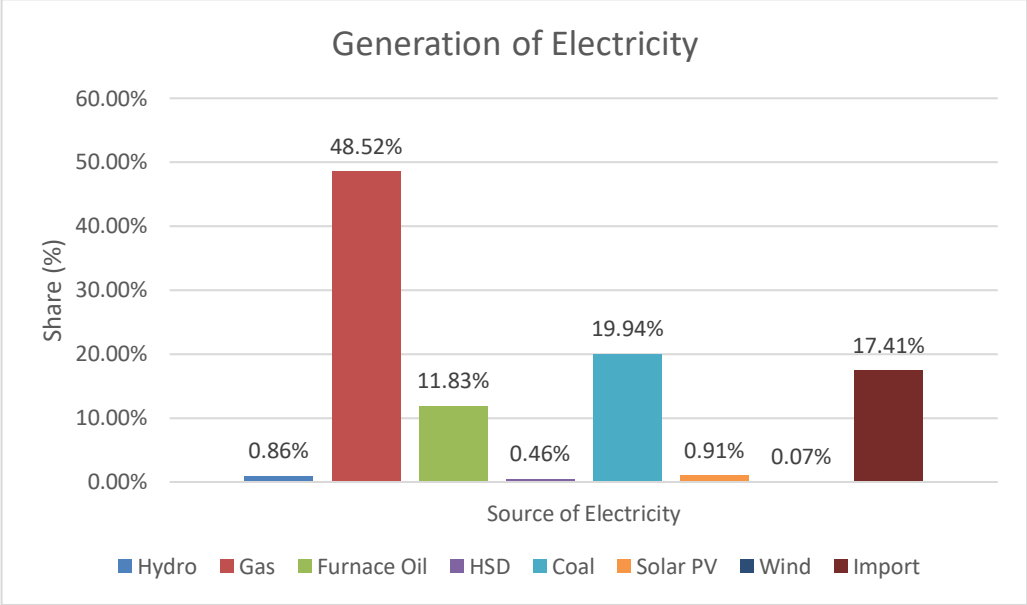


Figure 2.2 Electricity generation in Bangladesh by fuel type (August 2024).

A low-carbon economy requires rapid expansion of RE sources such as hydro, solar PV, wind, biomass, gas CCS, and hydrogen. By 2050, total RE supply is projected to reach 45.5 million toe in the PP2041 GDP scenario and 37.8 million toe in the In-Between scenario. In the PP2041 scenario, the share of clean energy is estimated to rise from near zero in 2019 to 27% by 2050 [26]. Transitioning to 100% RE is crucial to our better future because the environmental costs of combusting carbon-based fuels, along with rising economic concerns, hasten the impacts of climate change, which are detrimental to humans. Nowadays, almost 69% of GHG emissions come from carbon-based fuels like coal, oil, and gas to generate electricity [27].

Bangladesh has had remarkable economic growth and development during the past few decades. To support the nation's growing export-oriented industry, enormous amounts of electricity are needed. By 2023, the Government of

Bangladesh aims to ensure electricity to all. According to World Bank data, Bangladesh had 99.4% electricity coverage in 2022 (see Table 2.1).

Table 2.1. Current electricity structure of Bangladesh (June 2024) [28], [29], [30].

Name	2009	2021	2024
Number of Power Plants	27	152	174
Power Generation Capacity (*Including Captive Power & Off-Grid RE*) (MW)	5,000	25,500	28,098
System Loss (%)	16.85	11.00	10.06
Electricity Access (%)	47.0	99.5	100
Transmission Line (circuit km)	8,000.0	12,283.31	15,948.0
Transmission Loss (%)	8.00	2.93	3.13
Distribution Line (< 33 kV) (circuit km)	2,60,000.0	5,90,000.0	643,000.0
Per Capita Generation (kWh)	220	518	640
Consumers (million)	10.08	25.52	40.9

However, by 2023, Bangladesh will have covered 100% of its population with electricity. Now, GoB wants to use RE reliable source in its energy mix expected to cover 15% by 2030, 40% by 2041, and 100% by 2050 with a population [31]. The government has a detailed goal to boost power capacity to 40 GW by 2030 and 60 GW by 2041 [32]. As of 2024, RE makes up only 4.5% of Bangladesh's total installed capacity of 22,215 MW, with solar power accounting for 80% of the 1,183 MW renewable capacity [33]. However, it is essential to have well-trained professionals and comprehensive infrastructure systems to provide for the country's energy scheme. Natural gas is the primary source of energy generation in Bangladesh. The percentage of energy and electricity produced in Bangladesh by different fuels is shown in Table 2.2. As of June 2024, Bangladesh's total installed capacity reached 28.098 GW (See Fig. 2.3). Fig. 2.4 shows the breakdown of energy usage by multiple sectors. Approximately 57.02% of grid electricity is consumed by the domestic sector [32]. Most power plants in operation are gas-

fired; however, some are oil-fired. The present gas reserves are being exhausted by profuse gas use in the utility, transportation, and domestic. Kaptai, Bangladesh, has only a 230 MW hydroelectric plant [32]. In close collaboration with Russia, a 2,400 MW nuclear power plant is now being built in Rooppur, with power expected to be injected into the national grid by 2025-2026 [32].

Table 2.2 Overview of Power Generation

Various Plants		**Various Fuels**		**Energy Generated (MkWh)**
Hydro	230 MW (0.82%)	Hydro Power	230 MW (0.82%)	825
Steam Turbine	6158 MW (21.92%)	Natural Gas	12441 MW (44.28%)	46579
Gas Turbine	1218 MW (4.33%)	Furnace Oil	6442 MW (22.93%)	11357
Combined Cycle	9283 MW (33.04%)	Diesel	626 MW (2.23%)	440
Reciprocating Engine	7958 MW (28.32%)	Coal	5108 MW (18.18%)	19138
Solar PV (*On & Off-Grid*), Others *RE*	595 MW (2.12%)	Solar PV (*On & Off-Grid*)	595 MW (2.12%)	942
Imported Power	2656 MW (9.45%)	Imported Power	2656 MW (9.45%)	16715
TOTAL	**28098 MW (100%)**	**TOTAL**	**28098 MW (100%)**	**95996 MkWh**

In FY 2023–24, GoB's net energy generation reached 95.996 GWh, an 8.53% increase from 88.450 GWh in the previous year (see Figure 2.5). This included 2,478 MW from joint ventures (BCPCL), 10,478 MW from IPP/SIPP, 989 MW from rental and NENP (No Electricity No Payment) electricity Plants, 251 MW under REB (for PBS), 6,350 MW from the BPDB, and 2,656 MW of electricity imports from India [25],[34]. Bangladesh's energy generation scenario from 2001 to 2024 is depicted in Fig. 2.5. The distribution-based power system loss in Bangladesh decreased from 26.11% in 2001 to 7.23% in 2024 [32]. Bangladesh's public and private sector-based power stations had a total net generation change over the preceding year of 8.53% in 2023-24. It was 3.32% of the previous year in 2022–23 [32]. Under the PP2041 GDP scenario, Bangladesh's final energy consumption is

projected to increase by 3.75 times between 2019 and 2050 (4.4% annual growth), and by 3.14 times (3.8% annual growth) under the in-between GDP scenario. In recent years, energy consumption has increased across all aspects of life worldwide.

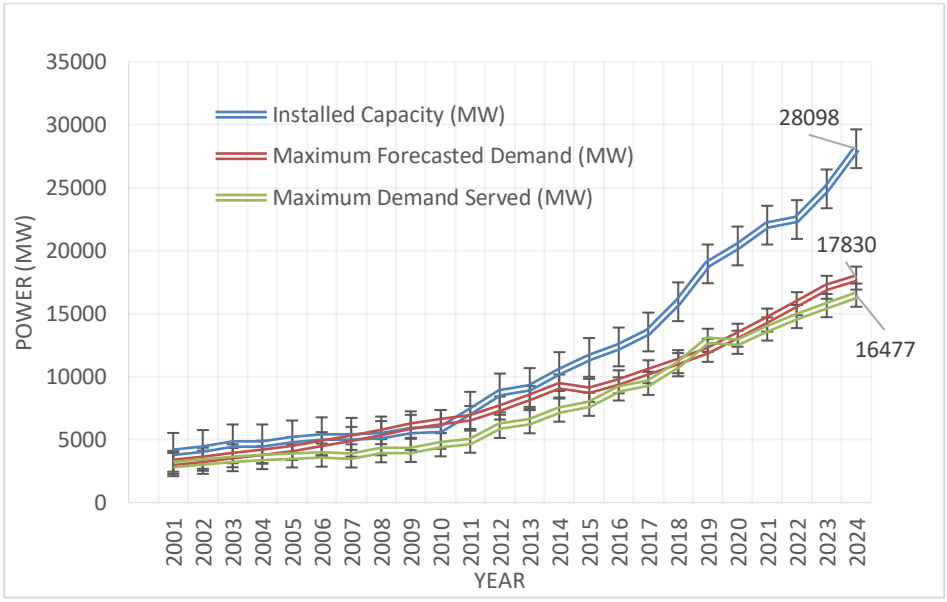


Figure 2.3 Power generation capacity of Bangladesh (June 2024) [25].

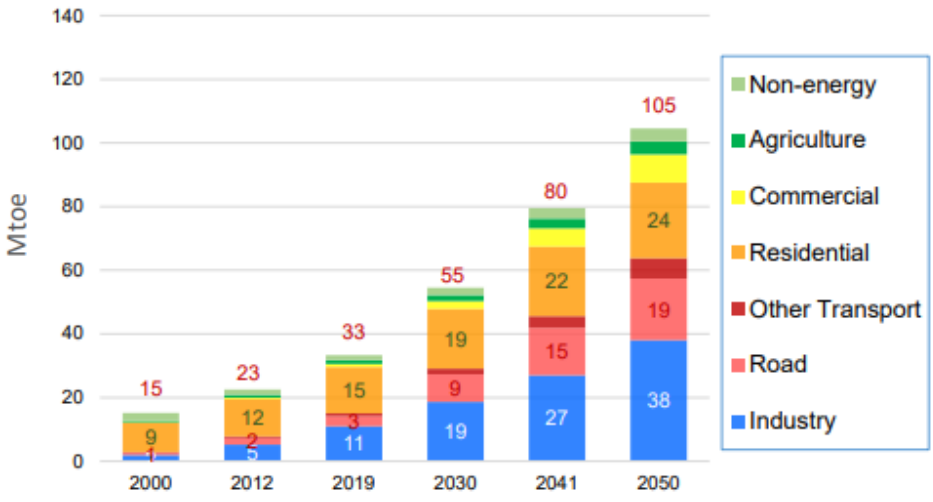


Figure 2.4 Energy consumption by various sectors of Bangladesh [26].

From 2010 to 2030, it is projected to expand by 33%, with an annual growth rate of 2.3% between 2015 and 2040 [35]. BPDB achieves this target by using RE, adopting new technologies, optimizing fuel use, and serving as a single buyer of

electricity. Its main focus is to ensure a consistent electricity supply to encourage economic development.

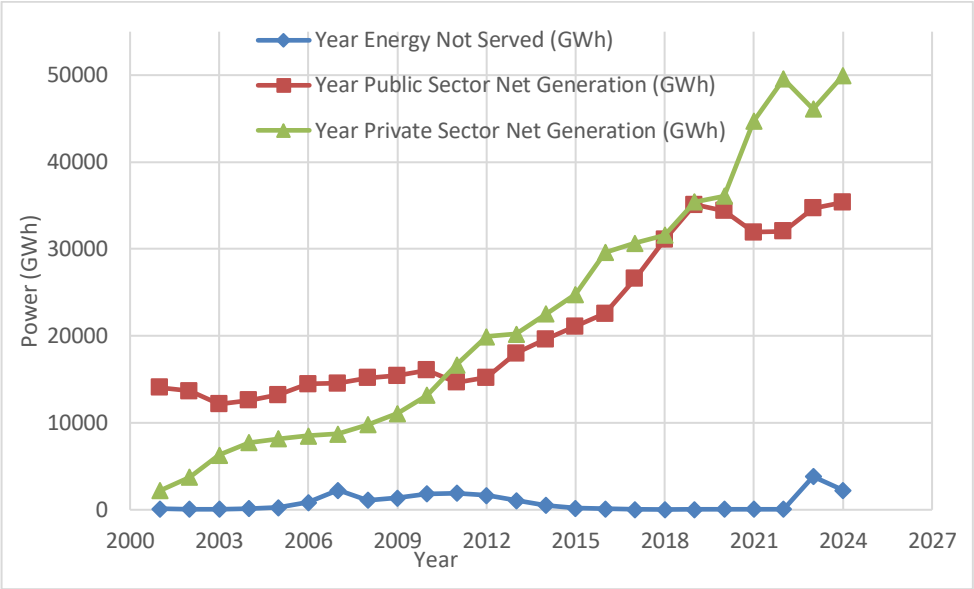


Figure 2.5 Bangladesh Public and Private sector-based energy generation scenario (June 2024) [25].

Bangladesh's goal is to generate mainly from green energy such as sun, biogas, waste materials, wind, and hydro energy. Gas power output has significantly exceeded that of coal and oil. Consequently, the GoB has taken intelligent action to diversify the main fuel supplies to generate electricity.

Table 2.3 RE generation sector of Bangladesh (December 2024) [36].

Technologies (Power Plants)	**Off-grid (MWp)**	**On-grid (MWp)**	**Total (MWp)**
Various SHS (>7 million)	263.793	0	
Rooftop Solar PV System (Public & Private offices)	33.161	166.631	
Various Solar PV Systems (Commercial and Shopping Centers)	25.534	0.016	1155.38 (79.7%)
Various Solar PV Systems (Consumer-based Electricity Connections)	5.806	0	
Solar PV Irrigation Systems	54.616	2.925	
Solar PP	0	778.29	
Biogas PP	0.69	0	0.69 (0.46%)
Biomass PP	0.4	0	0.4 (0.09%)
Wind PP	2.00	60.9	62.9 (4.03%)
Hydro-Electric PP	0	230.00	230.00 (15.7%)
Total			**1449.4 (100%)**

2.2 ENERGY HARVESTING FROM SOLAR PV SYSTEMS

Energy harvesting from solar PV systems involves absorbing sunlight and transforming it into usable electricity via the photovoltaic effect. This method generates renewable energy that can be used to power homes, businesses, and other consumers, while reducing dependence on traditional fossil fuels. According to energy prospects of the place, solar power is the primary source of Bangladesh. Figure 2.6 shows its solar potential based on global horizontal irradiation and terrestrial radiation on a horizontal surface. Located in South Asia at 23.6850° N and 90.3563° E [37]. The location is therefore ideal for optimizing the advantages of solar energy. In Bangladesh, the average daily sun irradiation varies from 4.4 to 6.5 kWh per square meter, as shown in Figures 2.6 and 2.7. According to the graph, maximal solar irradiation is available from March to May, while minimal solar radiation is available in December and January. Sun's irradiation map shows the Chattogram division as the most suitable region for solar energy in Bangladesh. Solar power is reliable, safe, and cost-effective, with potential in rooftop, floating, agro-solar PV, and SHS systems. However, improper panel placement can significantly reduce output. The standard and function panel alignment of 23.69° N and 91.78° E slope angle was observed better [38]. However, this region's performance latitude ranges from roughly 20.34° to 26.38° [38]. The latitudes of key places in Bangladesh are shown in the Figure. 2.6. The latitudes of Chattogram and Rangpur districts are 22.52° and 25.52°, respectively.

Therefore, Bangladesh should be divided into at least five areas, and the inclination angle should be changed as necessary (see Figure 2.6). The PV system energy in Bangladesh is frequently reserved for three days of autonomy. The three-day autonomy ensures that electricity is supplied even in rainy and foggy conditions. However, this type of weather only occurs around three or four times

every year. Most time, the sky is clear and there is enough sunlight for the SHS battery to charge completely.

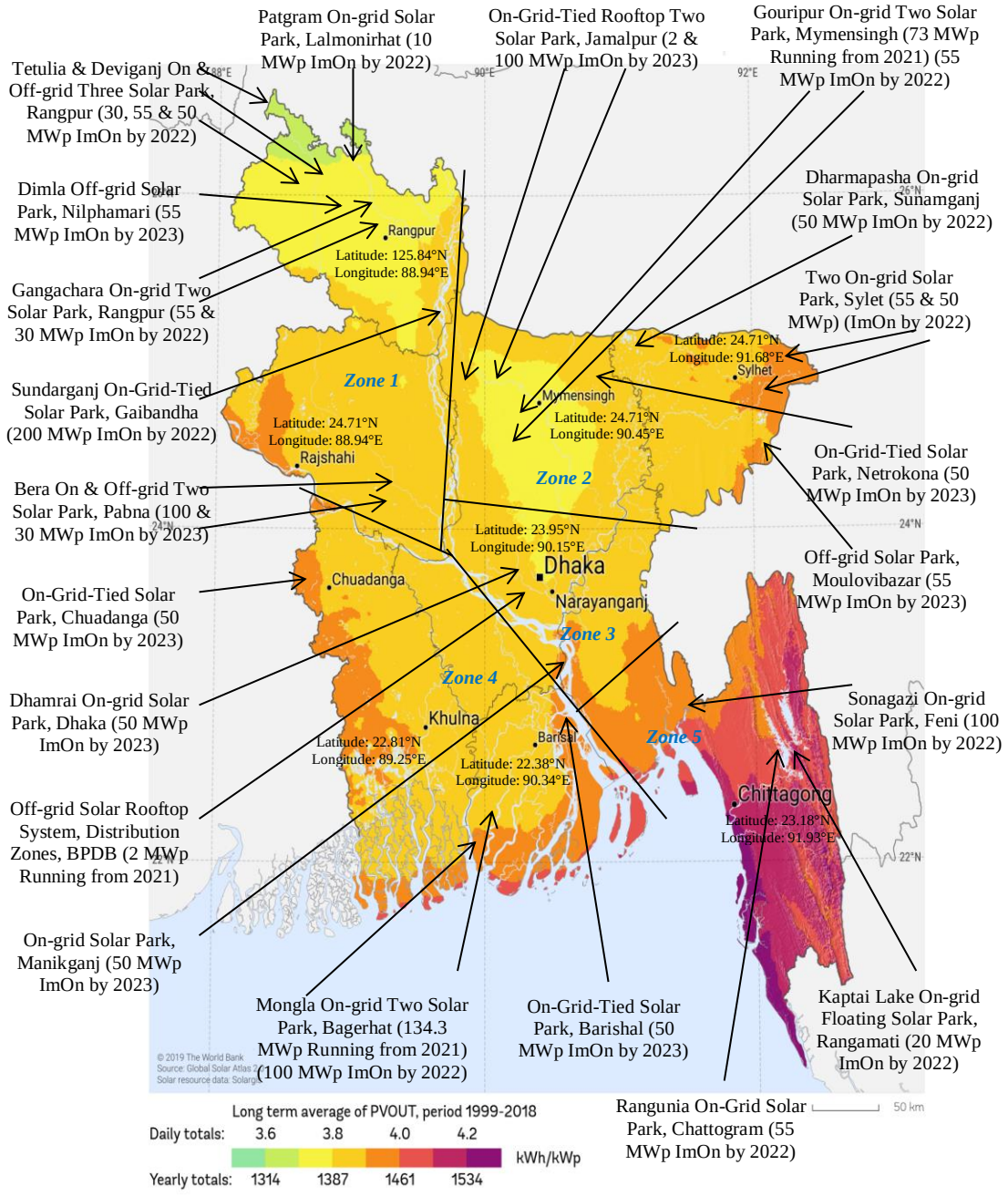


Figure 2.6 Potential of solar PV power generation for Bangladesh and major initiatives of different solar projects [39], [40].

In early 2011, researchers evaluated the possibility and practicability of grid-tied solar PV systems in Bangladesh [41]. After 2012, they conducted a comprehensive review of development in solar PV research and applications in Bangladesh [42]. Solar energy is so reasonably priced and might be a vital

solution to Bangladesh's energy crisis. In 2021, Bangladesh produced 1,156.48 MW of solar energy, apportion of 79.7% for RE capacity [43]. The most practical and reliable choice for Bangladesh to produce power from renewable resources is a variety of solar systems. Levels of Radiation are good from March to May, but lacking in December and January.

Due to the lack of local solar cell manufacturing, Bangladesh is dependent on imported solar PV panels. Although panel prices have generally collapsed, a 16% rise in the dollar over the past 5 years has reduced affordability [44]. Bi-facial solar panels are a cutting-edge technology that increases energy efficiency by capturing sunlight from both sides. When properly placed, they may provide between 8% and 50% more energy generated than conventional mono-facial panels [45]. Bi-facial panels are efficient, economical, and have the ability to save space, according to research conducted in Bangladesh's Hatiya area [46]. Bi-facial panels can therefore be incorporated into Bangladesh's SHS. The government and NGO plan to further research for Bi-facial technology to save more than 8% of space and more than 9% of expenditures when compared to mono-facial technology [47]. In the future, these solar panels will be used in Bangladesh's Agri-PV sector, offering both productivity and cost-effectiveness [48].

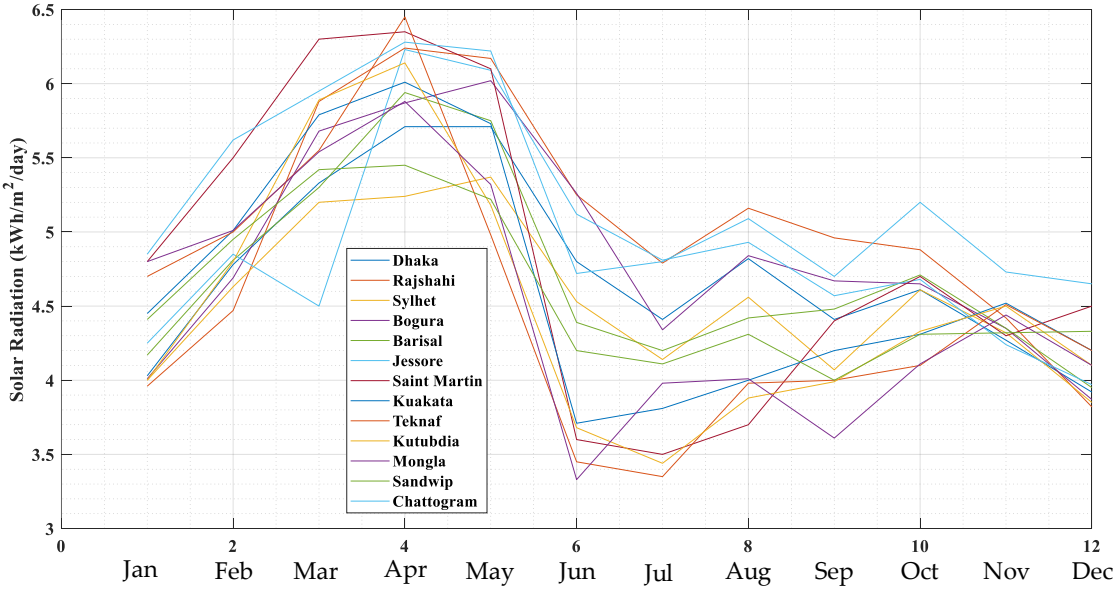


Figure 2.7 Solar radiation level at different locations of Bangladesh [43].

2.3 REVIEW OF EXISTING RESEARCH AND IDENTIFIED GAPS

Renewable energy (RE) is generated naturally by sources such as the sun, hydro, wind, geothermal, and tides, providing year-round electricity. Energy demands such as transportation, heating, irrigation, and power can be met through local generation or imports. Energy storage technologies are essential for balancing these sources efficiently. The leading RE source, solar PV technology, needs the highest harvesting from solar cells. The Researcher can develop and modify the approach for extracting power from PV systems. MPPT is a vital algorithm for maximizing energy extraction from solar PV. MPPT is a method used in solar inverters and charge controllers that optimizes the interface between solar panels and the battery bank or utility grid. It maximizes solar energy extraction under a variety of situations by maintaining the array's operating voltage within the appropriate range [49]. MPPT solar battery charge controllers are the best option for solar systems with batteries because they manage the voltage between the solar panels and the batteries. MPPT battery charge controllers can increase battery longevity and efficiency while also protecting the batteries. Grid-tied inverters also have MPPT tracking; however, some have advanced functions than others.

The main obstacle in developing a flexible and reliable renewable energy-based grid-connected battery is converting current renewable power from off-grid infrastructure. The approaches and technologies suggested as affordable grid-connected PV energy-storing systems for reliable and sustainable power systems are examined in this study, with multiple uses of power extraction techniques and an emphasis on how they can help ease the shift to a post-fossil fuel world. The suggested grid-integrated battery-based model intends to provide the most cost-effective and carbon-free energy-generating option for future energy systems, with advanced energy management technologies playing a critical role in guaranteeing stability and efficiency.

2.3.1 MPPT Technique

A typical solar panel adapts only 30-40% of incoming sun irradiation into electrical energy but the typical efficiency of PV modules that are sold commercially is about 20%. The MPPT approach enhances the efficiency of the solar panel circuit's output power which reaches its maximum source impedance or Thevenin impedance equals the load impedance, defined by the maximum power transfer theorem. As a result, our issue of monitoring the MPP becomes an impedance-matching issue. We utilize a boost converter with a solar panel to increase output voltage for various purposes, such as consumer demand loads. We match the source and load impedance by adjusting the boost converter's duty cycle suitably. By maintaining PV modules at their ideal voltage and current levels, MPPT allows them to provide all of the available power.

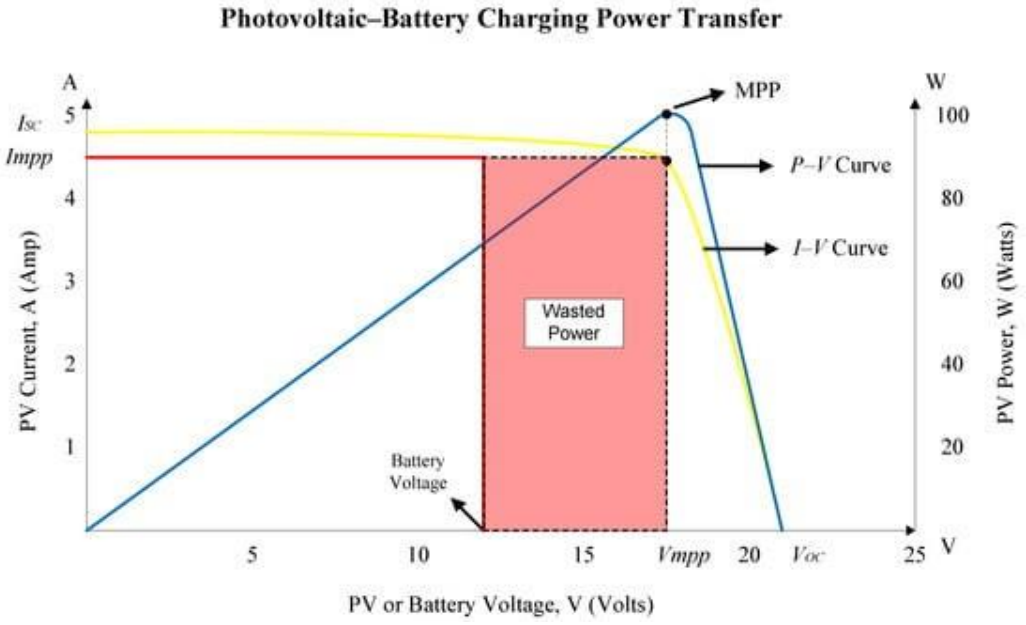


Figure 2.8 PV array battery charging power transfer Graph [16].

Without MPPT, a PV array connected directly to a battery operates at the battery's voltage (for example, 12V), which is frequently less than ideal and wastes electricity. MPPT ensures that the PV module runs at its MPP and optimizes energy harvesting efficiency.

Since a PV module's output depends on meteorological factors temperature, T & irradiance, G. Its generated power can vary significantly, even though PV integration into the power grid has advanced considerably. The MPP is a unique point on a PV module's I-V and P–V curves where the module delivers its maximum power under Uniform Environmental Conditions (UECs). However, under varying environmental conditions such as irregular G, fluctuating T, or Partial Shading Conditions (PSC), the I–V and P–V curves exhibit several peaks, including numerous local maxima and a single global maximum [50]. Consequently, various MPPT approaches are developed to accurately identify the MPP and enhance the lifespan and efficiency of PV systems. It constantly adjusts the electrical operating point of the solar array to ensure that it works at its most efficient power point, regardless of changes in environmental factors such as sunshine and temperature. These MPPT approaches are divided into sextuplets based on their characteristics, as shown in Figure 2.9.

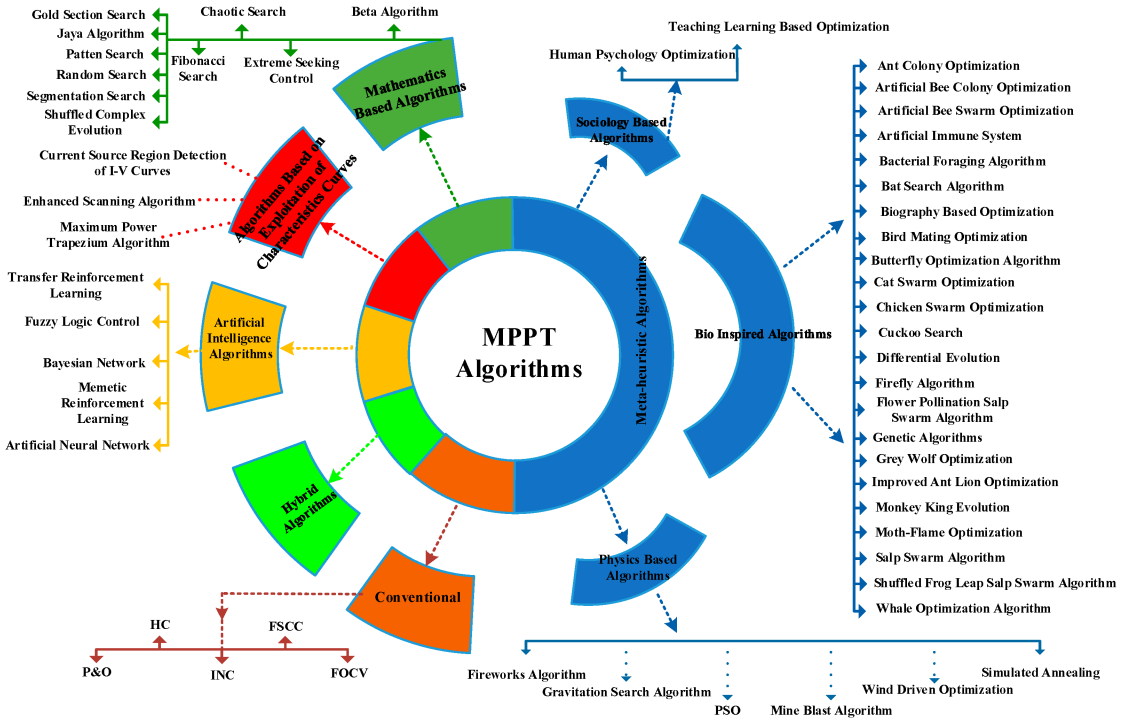


Figure 2.9 Classification of MPPT techniques [51].

The first group consists of traditional MPPT methods such as P&O [52]Hill Climb (HC) [53]Fractional Open Circuit Voltage (FOCV) [54] and other conventional approaches. These methods work well and precisely follow the MPP under uniform environmental conditions. However, using these traditional methods results in steady-state oscillations. As a result, several adjustments have been made to increase their performance, including the following: The reference voltage is specified based on G and T in [55], which presents an enhanced P&O method. Although these improvements have boosted the system's tracking accuracy and efficiency, performance degrades under PSC. A collection of meta-heuristic algorithms, such as Particle Swarm Optimization (PSO) [56], Gravitational Search Algorithm (GSA) [57]Differential Evolution (DE) [58]Artificial Bee Colony (ABC) [59]Human Psychology Optimization [60] and others are developed to track the GMPP under VEC or PSC precisely. Likewise, methods based on mathematics, including the Beta (β) algorithm [61], segmentation search [62], Jaya algorithm [63], etc., provide quick convergence and great tracking accuracy.

Although these advanced MPPT algorithms outperform standard PSC algorithms, they have significant drawbacks. The ANN approach outperforms an FLC because of its autonomy, but it must be trained particularly for PV applications through a rigorous training program [64].

2.3.1.1 Hybrid MPPT Algorithms

MPPT approaches aim to maximize the electricity generated by photovoltaic systems while functioning efficiently under stable environmental conditions. However, under VEC, multiple local maximum power points (LMPP) exist alongside a single global maximum power point (GMPP), making tracking difficult. Many algorithms fail, leading to reliability issues, hotspots, and lower efficiency. Hybrid MPPT methods were developed to precisely track the GMPP and address these problems effectively. Therefore, hybrid algorithms combine

two or more MPPT methods to enhance their strengths while reducing their weaknesses. Combining traditional methods with neural networks can improve accuracy. Hybrid MPPT strategies are categorized into three types: combining conventional algorithms, integrating soft computing techniques (e.g., meta-heuristics, AI), and mixing conventional approaches with soft computing algorithms. Table 2.4 compares the major MPPT methods widely used in some literature.

Table 2.4 Comparative assessment of different hybrid MPPT techniques.

Algorithm	C.	S.U.	T.A.	T.S.	O. L.	PV. M.D.	E.V.	C.T.	Cost	η	Ref. (year)
Combination of Conventional Algorithms											
P&O-FSCC	L	V,I,T	M	L	H	×	×	Buck Boost	H	M	H. Ser et al., 2017 [65]
FOCV-P&O	L	I,V	M	L	M	√	√	Buck	L	M	Al-Soeidat et al., 2016 [66]
P&O-IC	M	V,I	M	M	M	x	√	Boost	H	M	Gökhan et al., 2017 [67]
Combination of Soft Computing Algorithms											
CGSVM trained ANN	VH	V,I	VH	VH	L	x	√	Cuk	H	Vh	Farayola et al., 2018 [68]
GS-PS trained ANN	VH	V,I, G,T	VH	VH	VL	x	x	Buck	VH	VH	Alkhalaf et al., 2022 [69]
ANFIS	H	V,I,P	H	H	L	x	√	Buck	H	VH	Nikolovski et al., 2018 [70]
ANN-GA	VH	V,I	VH	H	VL	x	x	NG	VH	H	Prasad et al., 2016 [71]
ANN-SP	H	I,V,G	H	M	L	√	x	Boost	H	H	Bouselham et al., 2017 [72]
ANN-ACO	VH	V,I	VH	VH	L	x	√	Boost	H	VH	Babes et al., 2022 [73]
ANN-MC	VH	I,V	H	H	L	x	x	NG	VH	H	Chen et al., 2019 [74]
ANN vision-BS	VH	V,I	VH	VH	VL	x	√	Buck Boost	VH	VH	Martin et al., 2018 [75]
Combination of Conventional with Soft Computing Algorithms											
P&O-PInc	M	V,I	M	L	M	x	√	Buck	M	M	Al-Soeidat et al., 2016 [66]
P&O-PSO	H	I,V	VH	VH	L	x	√	Boost	H	H	manickam et al., 2016 [76]
P&O-IPSO	H	V,I	H	VH	L	x	√	Buck Boost	H	VH	yang et al., 2017 [77]
P&O-FLC	M	I,V	H	M	L	x	x	Boost	M	H	bataineh et al., 2018 [78]
P&O-SSA	H	V,I	H	H	L	x	√	Boost	H	VH	premkumar et al., 2021 [79]
P&O-GWO	H	I,V	VH	VH	L	x	√	Boost	M	VH	mohanty et al., 2016 [80]

P&O-AIDSM	VH	I,V	H	VH	L	x	√	Boost	VH	VH	kihal et al., 2019 [81]
P&O-FWA	H	I,V	H	H	M	√	√	Boost	H	H	manickam et al., 2016 [82]
P&O-ACO	H	I,V	VH	VH	L	x	√	Boost	H	VH	sundareswaran et al., 2015 [83]
P&O-GA	H	I,V	H	H	L	x	√	Boost	VH	H	sundareswaran et al., 2015 [84]
ANN-IC	H	I	M	H	L	x	x	Boost	H	H	phan et al., 2010 [85]
ANN-P&O	H	V,I	VH	H	L	x	√	Buck Boost	VH	H	jiang et al., 2014 [86]
P&O-ANN	**H**	**V,I, G,T**	**VH**	**VH**	**L**	**√**	**√**	**Boost**	**H**	**VH**	**M.E. Haque & N. Mohammad, 2024** [87]
Legend: C: complexity; S.U.: sensors used; T.A.: tracking accuracy; T.S.: tracking speed; O.L.: oscillation level; PV.M.D.: PV module dependency; E.V.: experimental validation; C.T.: converter topology; S.A.: stand-alone; G.C.: grid-connected; L: low; M: medium; H: high; V.H.: very high; N.P.: not provided.											

2.3.2 Neutral Point Clamped (NPC) Converters

The Neutral Point Clamped (NPC) converter is a multilevel inverter widely used in solar energy systems to convert electricity from solar panels for grid usage. Compared to conventional converter topologies, these converters provide benefits including lower switching losses and better output waveform quality. Because of their reputation for delivering greater efficiency and reducing total harmonic distortion, NPC converters are a popular option for grid-tied solar projects. Solar energy systems may optimize power output while preserving grid stability and reliability by employing NPC converters. Figure 2.10 shows the classification of several types of converter drives available for electric-powered applications.

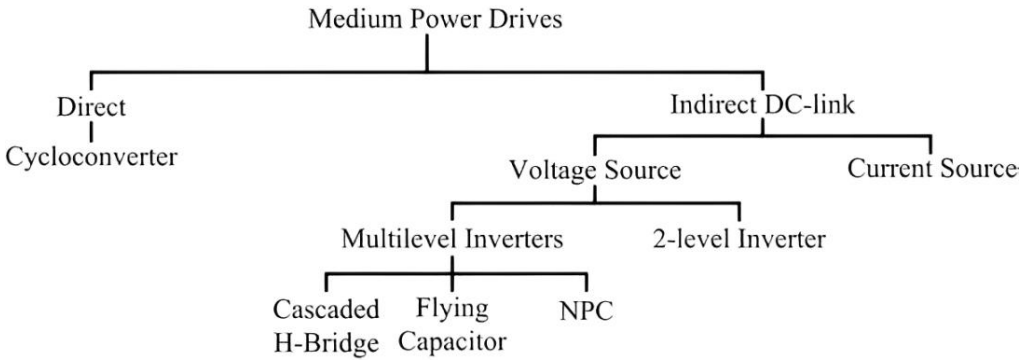


Figure 2.10 Different DC/AC power converters used for applications.

Essentially, Voltage-regulated PWM schemes can be categorized into two approaches: continuous and discontinuous conduction (CPWM, DPWM). There are two subclasses of the continuous and discontinuous conduction modes: Sine PWM (SPWM) and Space-vector PWM (SV-PWM). SV-PWM may generate a maximum phase voltage peak of 57.77% of the total DC-link voltage. It is around 15% more expensive than the sine-PWM method [88]. SPWM is the simplest constant switching frequency PWM scheme used in an adjustable Duty cycle. Hence, SV-PWM techniques are the most widely used for generating switching pulses for DC or AC traction inverters [89],[90].

Designing an ANN-based MPPT system with an NPC converter for grid-connected PV systems is an important field of renewable energy research. Several studies have looked at how AI approaches, notably neural networks, might improve MPPT productivity and accuracy in PV systems [91]. The authors [92] employ an advanced three-phase, 3L NPC inverter design to criticize the integration of solar systems with MPPT and battery storage. To solve imbalanced DC capacitor voltages, an enhanced three-level vector modulation approach is presented to provide precise AC voltages. However, this system can be improved by using a better management algorithm to regulate power supply between the PV array, battery storage, and grid circumstances in battery operations. Some research also evaluates the action of the integrated energy storage systems with the NPC converter to improve the efficiency of the entire PV system. Research on NPC in solar energy systems is still in its early stages but provides vital guidance to enable the efficient recovery of the highest power from a solar PV. A hexagonal space vector hysteresis current control (SVHCC) approach to improve voltage balancing and current control in NPC multilevel inverters is reported in this research [93]. The technique effectively reduces error and maintains the capacitors' voltage balance. However, the modulation index to balance the capacitor DC-link voltages improves NPC-MLI efficiency and reliability. The

author [94] claim the widespread usage of Common DC-Link Multilevel Converters in industrial applications, focusing on their potential to replace bulky transformers and allow shared DC connections for back-to-back setups. The improvements in wide-bandgap devices that improve the power density in these converters are also highlighted. Still, some issues need to be looked at further, such as flying capacitor voltage management and capacitor pre-charging. An NPC multilevel converter voltage balancing for solar PV systems contends [95]. It increases input voltage and lowers system weight by doing away with magnetic components. It boosts and balances voltage in grid-connected applications efficiently. However, the converter has switching and conduction losses, necessitating more study to enhance efficiency under changing environmental circumstances. A three-level NPC inverter duty cycle-based SVPWM technique solution incorporates overmodulation and neutral point balancing [96]. While it has promising dynamic and steady-state performance, issues like nonlinear phase distortion and difficult neutral-point voltage balancing remain. Generalized SVM-based NPC multilevel inverters [97] combining Nearest Level Modulation (NLM) and a switch matrix to ease gate pulse derivation. Dual-input NPC inverter-based control approach [98] for PV systems that maximizes power extraction through linearization of asymmetric PV array control. However, scalability in bigger systems is not yet clear. Nevertheless, we propose to mitigate it using a raw single integration source and the suggested approach in the chapter methodology section. Nowadays, intelligent techniques [99] provide faster responses and greater accuracy than traditional methods, allowing maximum power extraction from PV cells.

Table 2.5 Analysis of grid-connected multilevel inverters.

MLT Topology	NOP	NOL	MT	C	SF (kHz)	CP (kW)	Ref.
CHB	$3-\Phi$	5	SV-PWM	PI	10	-	[100]
NPC back to back	$3-\Phi$	-	PWM	MPC	10	0.28	[101]
Quasi Z-Source based NPC	$1-\Phi$	5	LS-PWM	PI	10	0.5	[102]
NPC	$3-\Phi$	3	SV-PWM	-	2	1.1	[103]

NPC	**$3-\Phi$**	**3**	**SV-PWM**	**PI**	**5**		**Present study**
Legend: MLI Topology: Multilevel Topology; NOP: Number of Phases; NOL.: Number of Levels; MT: Modulation Technique; C: Controller; SF: Switching Frequency; CP: Capacity; SV: Space Vector: LS: Level Shift.							

The overview covers several inverter features and different MLI topologies used for system integration are tabulated in Table 2.5.

Table 2.6 Main characteristics of different controllers proposed in scientific articles.

MT	NOP, CRF	CC	DLC	FL	CP	F	A	Ref.
SVM	$3-\Phi$, (dq)	MPC	-	S-L	C	L	PV	[104]
SV PWM	$3-\Phi$, $(\alpha\beta)$	SMC-DPC	SMC-DPC	M-L	V, P	L	PV	[105]
PWM	$3-\Phi$, (abc)	Fuzzy NN	Fuzzy NN	M-L	V, P	L	PV	[106]
SV PWM	$3-\Phi$, (dq)	Adaptive	PI	M-L	V, C	LC	DG	[107]
SV PWM	$3-\Phi$, (dq)	PI	PI	M-L	V, C	L	PV	[108]
SVM	$3-\Phi$, $(\alpha\beta)$	H-infinity	-	S-L	C	LCL	G	[109]
SV PWM	**3-Φ, (αβ)**	**PI**	**-**	**M-L**	**V, C**	**LC**	**PV**	**Present study**
Legend: CRF: Control Reference Frames; NOP: Number of Phases; CC: Current Controller; DLC: DC-Link Controller; FL: Feedback Loop; CP: Control Parameters: A: Application; M-L: Multiple loop; S-L: Single loop; V: Voltage; C: Current; P: Power; DG: Distributed Generation; and G: General.								

Table 2.6 highlights the various current and DC-link controllers utilized in different reference frames to manage power, current, and voltage in single-phase and three-phase inverters. Control feedback loops, modulation methods, and filters are key features in grid-tied applications. The research identifies shortcomings of these controllers, including the inability of PI and PID techniques to completely eradicate steady-state errors.

2.3.3 Neural Networks in Power Electronics & PV Systems

Through the neural networks' enhanced performance and advanced control strategies, power electronics and photovoltaic systems are undergoing a revolution [110]. Neural networks can adjust to shifting conditions, including quickly changing temperature and irradiance, to trace the MPP in MPPT more effectively than traditional techniques [111]. They can also manage challenging scenarios such as partial shading local maxima in the power-voltage curve. Neural networks may also be utilized for problem detection and predictive

maintenance in power electronic converters, improving reliability and minimizing downtime. More intelligent, reliable, and efficient renewable energy systems are being made possible by neural networks, which are utilizing artificial intelligence [112].

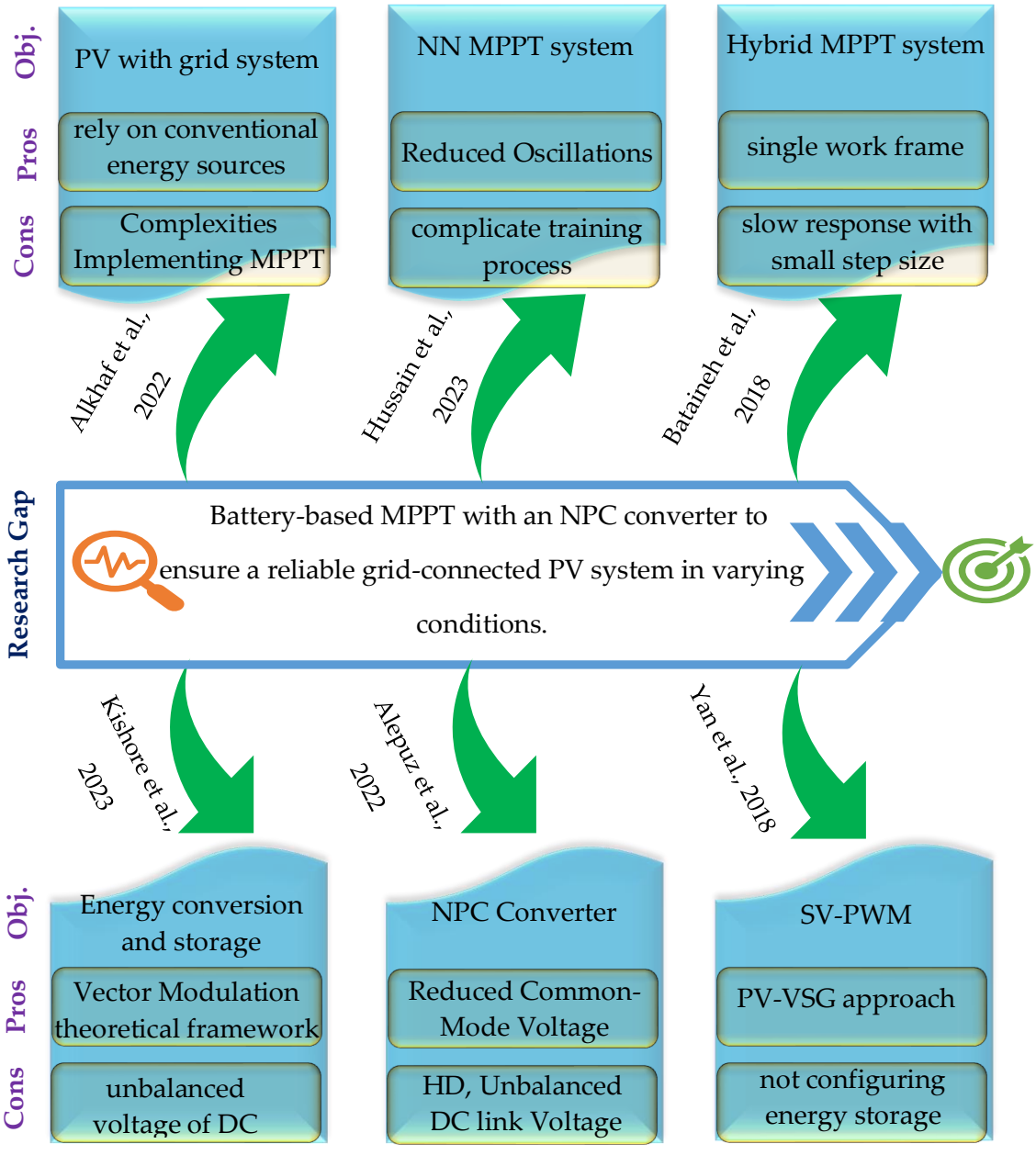


Figure 2.11 Research gap by reviewing a few key papers by comparing and contrasting the objectives, the pros and cons of a neural network-based grid connected MPPT PV system and NPC converter.

A research gap is assessed in Figure 2.11 by studying a few important studies and comparing and contrasting the goals, advantages, and disadvantages

of a grid-connected MPPT PV system and NPC converter. In most research studies on the MPPT technique.

- The MPPT technique of energy harvesting supplies energy to the storage by using a converter (DC Boost).
- Power quality and active or reactive power balance must be maintained in the grid with the NPC converter via a modulation technique.

If the MPPT control and NPC converter analysis are successful, they could greatly enhance power quality and grid stability, yielding several benefits from the proposed model system.

2.4 SIGNIFICANCE AND CONTRIBUTION

This study presents a battery-based photovoltaic model highlighting grid-connected systems with energy storage. This PV system converts the generated power using an NPC converter.

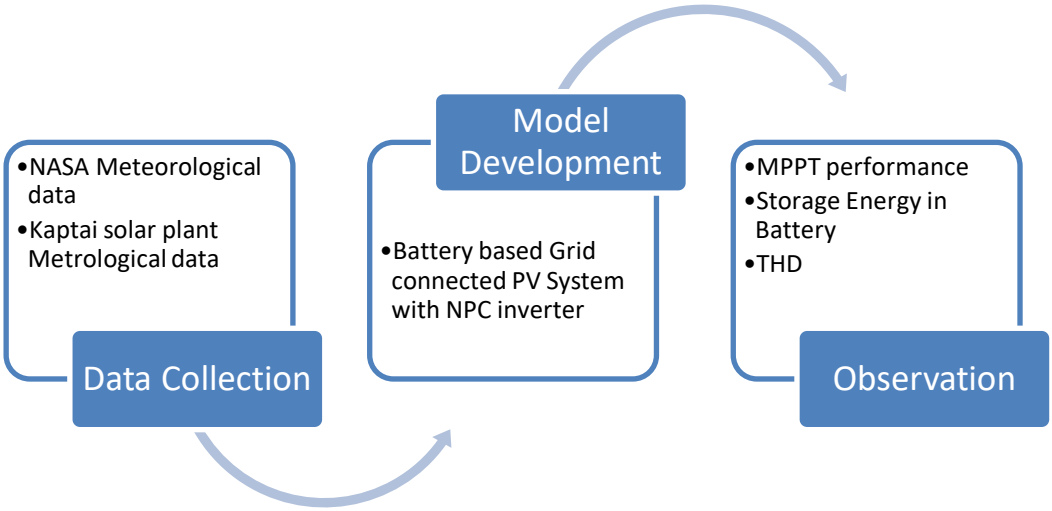


Figure 2.12 The working flow of the Research framework.

Weather variations and PV system erratic behaviour are monitored via an automated meteorological station and compared with real field data. The weather variations and the erratic behaviour of solar PV systems are monitored

and studied using data from an automated meteorological measurement center and compared with real field data. When solar output is insufficient, stored energy meets the load demand, and the grid feed-in mode draws power from the central grid into the integrated system.

2.5 SUMMARY

This chapter discusses neural network-based MPPT for PV systems and clean RE production, the current structure of Bangladesh's power system and renewable energy sector, existing research on solar MPPT, NPC converters, and the significance and contributions of this thesis. The study examines both conventional and renewable energy scenarios. Neural networks in power systems, combined with electronics and NPC converters, are used to analyze the PV system. The problem faced by grid-connected PV systems and the work of researchers in Bangladesh are likely to benefit from these key findings, which inform the actual study of solar PV energy harvesting systems and the implementation of suitable battery-based energy conservation and management policies. The operational performance of various MPPT PV systems is discussed, with a focus on the NPC converter of the grid-connected battery as a crucial enabler for DSM. The literature on the operation mechanisms of MPPT is reviewed, and relevant studies on the effectiveness of PV-based grid-connected systems in power electronics with NPC converters are presented. The machine learning-based MPPT techniques of the proposed models are discussed for battery-based grid applications. Several relevant studies are critically reviewed, with a detailed comparison of their objectives, strengths, and limitations. Research gaps and problems are identified. The significance and contributions of this study are outlined at the end of the literature review.

3 Research Methodology

This chapter describes the design adopted by this research to achieve the aims and objectives stated in Section 1.7 of Chapter 1. It also explains an elaborate battery energy management PV system framework with an NPC converter. After evaluating the machine learning-based hybrid MPPT performance state and converting DC power integration to the grid. The parameters of the solar PV energy storage management system simulation setup are explained. Sections 3.5 and 3.6 detail and analyse the design of MPPT and NPC converter ideas, as well as their functions. The study system's integration, including grid synchronization, voltage stability management, and proposed control strategies, is discussed in Section 3.37. Then, it discusses the harmonic distortion in the operating model. Finally, Section 3.8 includes the summary and concluding remarks of Chapter 3.

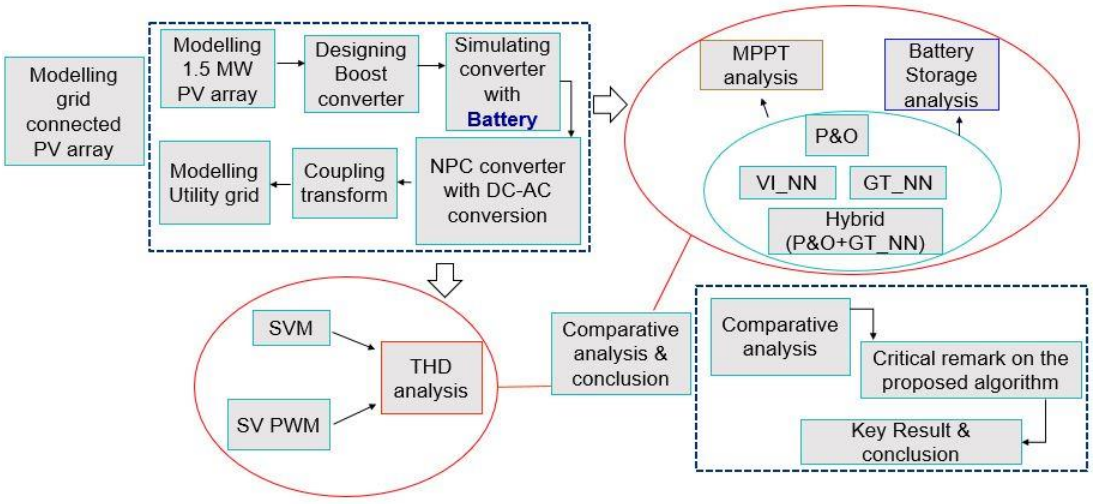


Figure 3.1 The Overall Research Methodological Framework.

3.1 SYSTEM OVERVIEW

The proposed system overview frameworks entail modeling various scenarios and combining neural network-based MPPT systems to enhance performance through on-grid PV installations, where a neutral point clamped

converter maintains the DC link voltage up to 1000 V, irrespective of the active power delivered. The controller of reactive power generates or absorbs up to 1 Mvar. This method intends to enhance the proficiency and reliability of converting solar power in grid-connected applications and deploying advanced control systems. We consider battery management for a hybrid energy supply for the grid-tied PV system. The model shown in Figure 3.2 represents a significant advancement in extracting more power and improving system performance overall. It reduces the unpredictability of solar output and optimizes the use of RE through a stand-alone or grid system. The combined concept of power plants has a real effect on the example.

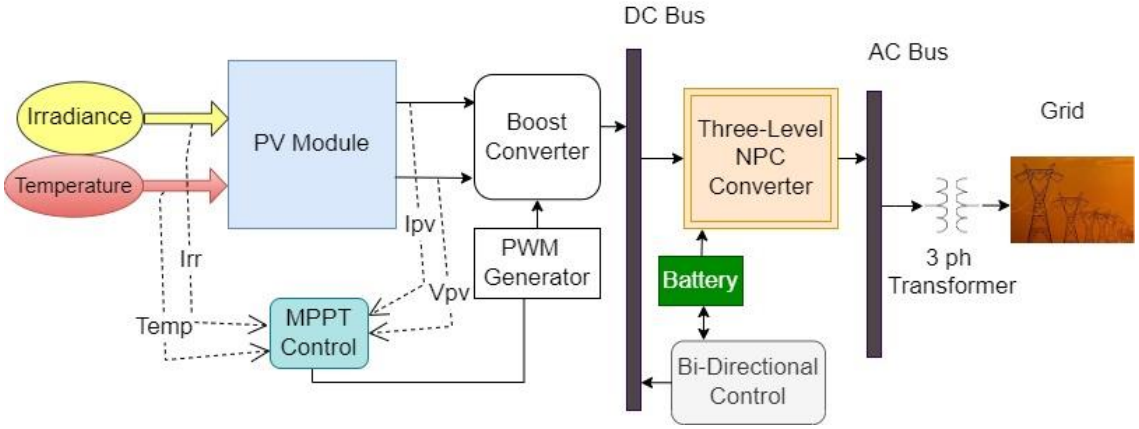


Figure 3.2 Simplified diagram of the proposed battery-based grid-connected PV system model.

3.2 DATA COLLECTION AND ANALYSIS

The electricity generation and hours of operation data were collected from the Daily logbook of the Kaptai Solar Power Plant, Chittagong. Comparatively, under varying irradiance and temperature conditions, we also collected metrological data on PV panel output voltage, current, and power at [113]. That data was obtained using the specifications of the PV panel and analyzed with MATLAB/Simulink software. Meanwhile, the data on wind patterns, weather, and solar irradiation are monitored at a common automated meteorological measuring center next to the integrated grid power plant. A central server uses

the SCADA technique to examine observed statistics. On after 5 minute or hourly basis, the server monitors different solar PV panel data (e.g., current, voltage, efficiency), sensor data, power quality, other device performance, and inverter via busbar data. The data files are automatic sent to the server for retrieval. The server and SCADA system are housed in a control booth. Experimental solar radiation data is gathered from those centers for the planned integrated microgrid at Raozan, Chattogram, Bangladesh (22.5349° N and 91.9104° E). At the Institute of Energy Technology, Chittagong University of Engineering and Technology, Environmental Lab, Raozan-4349, Chattogram, Bangladesh, STC is testing this sun radiation data.

3.3 SIMULATION SETUP AND PARAMETERS

The simulation setup for evaluating MPPT algorithms in solar energy systems considers temperature, shading effects, irradiance levels, and solar panel efficiency. These parameters are critical in correctly analyzing the performance and usefulness of various MPPT algorithms for optimum energy harvesting from solar panels. Figure 3.3 shows solar PV technology using semiconductor cells like silicon. Sunlight generates electron-hole pairs in the cell, and when a load is connected, electrons cross the p-n junction, producing current. The electrical equivalent model is shown in Figure 3.4.

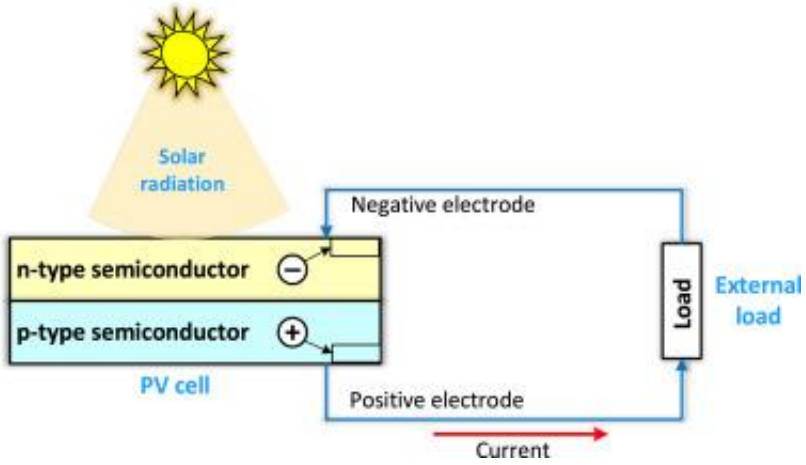


Figure 3.3 Operating principle of a PV cell [8].

3.3.1 Modeling of PV cell

The photovoltaic cell is considered a current source that includes a parallel diode. The STC is calculated using 25°C ambient temperature and 1 W/m^2 solar irradiation. The solar radiation data include global irradiance data (W/m^2) for horizontal, optimally inclined, and dual-axis tracking surfaces over daily, monthly, and annual averages. For analysis, daily irradiance on an optimally inclined surface is used, as measuring stations are aligned accordingly. Solar panel efficiency is denoted by,

$$\eta_{PV} = \frac{Output\ electrical\ energy\ per\ second}{Incidned\ light\ energy\ per\ second} = \frac{P_{max}}{G\ or\ P_{in(irra)}} = \frac{I_{SC} \times V_{OC} \times FF}{G\ or\ P_{in(irra)}} \quad (3.1)$$

The short-circuit current I_{sc} occurs with zero voltage drop and depends on cell technology, area, and solar radiation. The open-circuit voltage V_{oc} occurs with zero current and depends on cell technology and temperature. This study uses monocrystalline cells. We used monocrystalline solar cells in this research study.

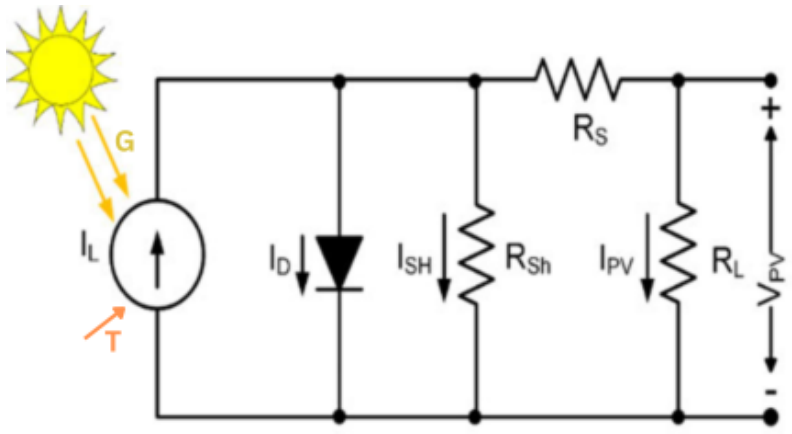


Figure 3.4 The equivalent electrical circuit model of a solar cell.

The solar-induced temperature (T) and irradiance (G) as input parameters, the system is comprised of regulated current sources, diodes, series resistors and parallel resistors for output parameters of current and voltage. The given operating equation (3.2-3.4) calculates the output current of the characteristics of the PV cell.

$$I_{pv} = I_L - I_{sat}\left(e^{q\frac{(Vpv+IpvRs)}{NKTpv}} - 1\right) - \frac{(V_{pv}+I_{pv}R_S)}{R_{sh}} \quad (3.2)$$

$$I_L = (I_{L0} + K_0(T - T_n))\ \frac{G}{G_n} \quad (3.3)$$

$$I_{sat} = I_{sat,n}\left(\frac{T_n}{T}\right) e\ [\ \frac{qE_g}{ak}\ (\frac{1}{T_n} - \frac{1}{T})] \quad (3.4)$$

The solar-induced currents I_{L0} and I_L are measured at standard test conditions. $I_{sat,n}$ represents the nominal saturation current, whereas I_{sat} represents the saturation diode current. Boltzmann's constant K, the elemental charge q, the thermal coefficient K_0, and the parameters R_s, R_{sh}, G_n,G,T_n, T, E_g and n given in Figure 3.3 are all significant constants.

The quality or state of the solar cell is indicated by the fill factor (FF). A higher FF score indicates higher-quality solar cells. The FF value lies between 0.8 to 0.9. The avg. measured irradiance value at STC is, $G\ or\ P_{in(irra)} = 1000\frac{W}{m^2} = 1\frac{kW}{m^2}$. The solar PV panel having, $I_{SC} = 355\frac{A}{m^2}, V_{OC} = 0.74V,\ and\ FF = 0.81$. So, $\eta_{PV} = \frac{355\times0.74\times0.81}{1000} \times 100 = 21.28\%$. The proposed solar PV panel area in this experimental microgrid area (A_{PV}) is around 2650 m^2, with an array efficiency is = 21.28%. The P_{PV} forecast PV power is revealed in Chapter 4 (See Fig. 4.1), which is calculated from equation (3.5). The calculation of power provides grid loads (residential, commercial, industrial, and others) with the 11-kV substation system, as measured for the integrated microgrid system.

$$P_{PV} = Irra_{day} \times A_{PV} \times \eta_{PV} \quad (3.5)$$

The PV panel takes the time necessary to supply an array's DC energy output (E_A) per day, also known as the array yield (Y_A). The reference yield (Y_R) is the ratio of the PV panel's reference irradiance to its total in-plane irradiation (H_T). It indicates the ideal conditions for generating solar energy. Monthly and annual weather changes, as well as the location and orientation of the PV array, all have an impact [114]. The ratio of the system's daily, monthly, or yearly net AC power production and the installed PV array's peak power at STC is referred

to as the overall yield (Y_{All}). Additionally, it permits the evaluation of various solar systems within a certain area [115].

PR_Y represents the ratio of overall yield to reference yield, indicating the correlation between actual and theoretical system performance [116]. It compares actual results to expected output and considers module function, size, radiation, panel temperature, modifications, mounting, space, grid access, and nominal power [117].

$$Y_A = \frac{E_A}{P_{nominal}} = \frac{V_{DC} \times I_{DC} \times t}{P_{nominal}} \tag{3.6}$$

$$Y_R = \frac{H_T}{G_{STC}} = \frac{\frac{kWh}{m^2}}{\frac{kW}{m^2}} \tag{3.7}$$

$$Y_{All} = \frac{E_{PV(AC)}}{P_{G,\max(STC)}} = \frac{kWh}{kW_p day} \tag{3.8}$$

$$PR_Y = \frac{Y_{All}}{Y_R} \tag{3.9}$$

3.3.2 Boost Converter Design

DC/DC boost converters step up the input voltage. In our application, it acts as an interface between the solar panel and the supplied resistive load. The two alternative states of the switch, whose schematics are shown separately in Figure 3.4, may be used to analyze the converter. When the switch is turned ON, the inductor current (iL) may be determined using Equation (3.10). The circuit model for the switch's OFF state is shown in Figure 3.5(b).

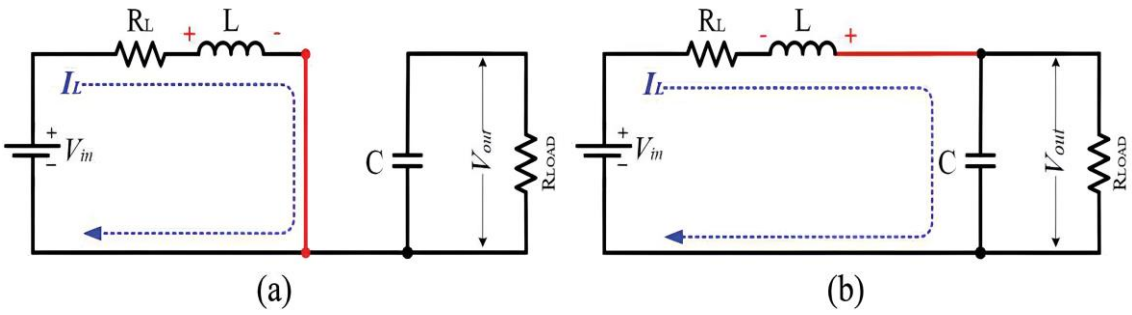


Figure 3.5 Converter Circuit Design. (a) Switch is ON (S=1). (b) Switch is OFF (S=0).

In this instance, both the input source and the inductor provide power to the load. Equation (3.11) may thus be used to represent the input current as OFF.

$$V_L = L = \frac{d_{iL}}{d_t} = (V_{in} - R_L i_L)S \tag{3.10}$$

$$V_L = L\frac{d_{iL}}{d_t} = (V_{in} - R_L i_L - V_{out})(1 - S) \tag{3.11}$$

Where;

L, inductance and resistance values of the inductor, respectively

Input and output voltage is V_{in}, V_{out},

i_L: Inductor current

From equations 3.10 and 3.11 combine into equation 3.12, we can get the input current during a switching period.

$$V_L = L\frac{d_{iL}}{d_t} = [V_{in} - R_L i_L - V_{out}(1 - d)] \tag{3.12}$$

$$d = \begin{cases} 0 \ \ for\ OFF\ position\ of\ the\ S \\ 1 \ \ for\ ON\ position\ of\ the\ S \end{cases}$$

Table 3.1 Different parameters of the proposed model.

Parameter	Specifications
Solar PV	- Microgrid area (A_{PV}) = 2650 m^2
	- Solar PV system capacity = 1.5 MW
	- Solar PV system efficiency = 86 %
Inverter	- Capacity = 1,000 kW
Battery	- Battery power = 450 kW
	- Min discharge rate = −400 kW
	- Max charge rate = +400 kW
	- Battery efficiency = 95 %
	- Battery SoC minimum = 20 %
	- Battery SoC maximum = 80 %
	- Autonomy = 18 hrs
Boost Converter	- Input voltage = 25 V
	- Switching Freq. = 20000 Hz
	- Initial output voltage = 48 V
	- Converter power = 2.40 kW
	- Efficiency = 0.9
	- Percentage of output voltage = 1

3.4 ENERGY STORAGE MANAGEMENT SYSTEM (ESMS)

Solar energy must be reserve in robust battery banks due to its intermittent nature. In this investigation, we used lithium-ion batteries. The storage system plays a critical role in effective load DSM. The recommended integrated grid-based battery backup storage capacity (autonomy days) is about one day. About 250 Ah ranged single battery ($Batt_{size(single)}$) bank is used for superior performance. In generally, total battery bank size ($Batt_{size(general)}$), Lithium-ion battery size $Batt_{size(li-ion)}$ and single storage (battery bank) capacity, $Batt_{cap(single)}$ is regulate by equation (3.15) and equation (3.16) [118],

$$Batt_{size(general)} = \frac{P_{load} \times t}{V_{DC}} \tag{3.13}$$

$$Batt_{size(li-ion)} = \frac{100 \times I_{DC} \times t}{100 - Q} \tag{3.14}$$

$$Batt_{cap(single)} = Batt_{size(single)} \times V_{DC} \tag{3.15}$$

$$Batt_{cap(total)} = Batt_{cap(single)} \times N_{Batt(single)} \tag{3.16}$$

In a single li-ion battery, the V_{DC} is selected as 48 V, then $Batt_{cap(single)}$ is calculated as 12 kWh. The number of single battery banks, $N_{Batt(single)}$, is measured as 210 times the capacity of $Batt_{cap(single)}$ to create the total battery bank capacity, $Batt_{cap(total)}$. Therefore, $Batt_{cap(total)}$ is calculated as around 2,520 kWh.

The autonomy (backup time) method, based on the battery bank's daily load profile, uses manufacturer-provided data such as temperature, capacity, float voltage, total charge, electrolyte density, and end-of-discharge voltage. The number of battery banks required may be established more precisely to fit the load tolerance better [119]. The planned series or parallel battery bank ratio should be within these limits:

$$N_{Batt(max)} = \frac{V_{DC}(1 - V_{load(\max)})}{V_{DC}} \tag{3.17}$$

$$N_{Batt(min)} = \frac{V_{DC}(1 - V_{load(\min)})}{V_{eodv}} \tag{3.18}$$

To support the load beyond the stated autonomy, a minimum battery ban capacity in ampere-hours (Ah) is required [120]. The battery charging current is the DC needed to charge the 2,520-kWh bank, while the solar panel's total current ($I_{PV(total)}$) supplies the load and charges the battery.

$$C_{Batt(min)} = \frac{E_{DC}(k_{af} \times k_{tcf} \times k_{crt})}{(V_{DC} \times k_{mdod} \times k_{sc})} \tag{3.19}$$

$$I_{Batt,char(DC)} = \frac{1}{10}^{th} \, of \; Batt_{cap(total)} \tag{3.20}$$

$$I_{PV(total)} = I_{DC} \times I_{Batt,char(DC)} \tag{3.21}$$

Maintaining the battery's SoC energy limitations between 20% and 80% will enhance its life cycle and overall health. The initial battery energy, E_{max} is calculated by equation (3.22), where 50% SoC is assumed for the ideal condition. In this proposed system, a lithium-ion battery is utilized starting at the lowest 10% state of charge (SoC) to ensure that more stored energy can be injected into the grid-connected photovoltaic (PV) system when needed. Battery Energy, $Batt_{Energy} = Batt_{cap} \times 3.6 \times 10^6 = 2500\, kWh \times 3.6 \times 10^6 = 9 \times 10^9\, W,$ where the energy generated by a kW power source in 1 hour is $1kWh = 3.6 \times 10^6\, Joule$. When, maximum power, P_{max} is around +400.0 kW then SoC_{max}= 80% and minimum power, P_{min} is around -400.0 kW then SoC_{min}= 20%.

$$E_{batt(max,min)} = SoC_{min,max} \times Batt_{Energy} \tag{3.22}$$

$$E_{max} = SoC_{max} \times Batt_{Energy} \tag{3.23}$$

$$E_{min} = SoC_{min} \times Batt_{Energy} \tag{3.24}$$

Total solar PV system power ($P_{PV(total)}$) or installed capacity of the PV plant identified by equation (3.25),

$$P_{PV(total)} = V_{DC} \times I_{PV(total)} \tag{3.25}$$

An electric battery's charge amount SoC is related to its capability. Percentage points are used to quantify it; 0% represents empty and 100% represents filled. In addition, the depth of discharge (DoD) is an alternative

means of quantifying the same subject (SoC). The DoD and SoC are opposed; 100% represents empty, and 0% represents full.

3.5 DESIGN OF MAXIMUM POWER POINT TRACKING

The suggested integrated model is represented in Figure 3.2, where the combination of MPPT design with various environmental PV systems conditions. The design of MPPT systems includes selecting appropriate algorithms and control techniques to guarantee that solar panels perform at peak efficiency. These devices are critical for maximizing power output and enhancing the overall performance of grid-tied solar arrays. Neural network-based MPPT design provides a more dynamic and efficient approach for tracking solar panels' maximum power points. Real-time modifications may be made using this technology to maximize energy output and improve system performance as a whole. Similarly, neural network-based MPPT design may increase the overall reliability and stability of solar energy systems by constantly fine-tuning the power output. Optimizing the potential of renewable energy sources under diverse environmental situations requires this cutting-edge technology.

3.5.1 MPPT algorithm used in this study

Energy efficiency varies depending on integrating solar power performance, which MPPT controls to optimize energy levels for the supplied load. In this research, we utilize Perturb & Observe (P&O), Neural Networks, and its combination of hybrid MPPT.

3.5.1.1 Perturb and Observe (P&O) MPPT

The P&O approach is commonly used in PV systems. It works by keeping an eye on the power-voltage (P-V) relationship. The operational points of this algorithm are classified into five modes which described in regions Figure 3.6 [121]. The perturbation is adjusted to attain the MPP. When the voltage perturbation raises power ($dp/dv > 0$), the point changes toward the MPP. When

power reduces (dp/dv < 0), the perturbation reverses. The following duty ratio is calculated using power and voltage variations, and this cycle is repeated until attained MPP.

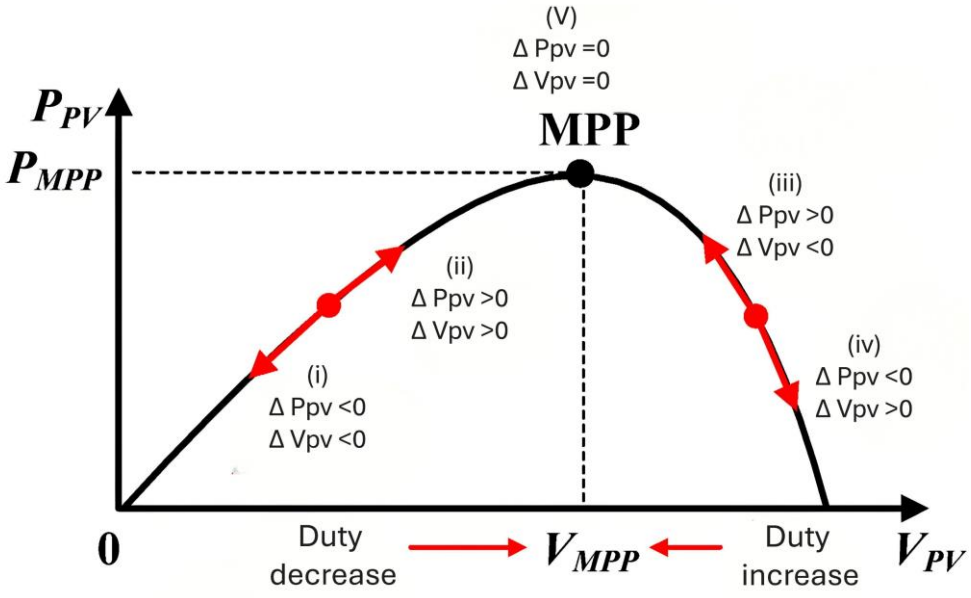


Figure 3.6 dp/dv sign at various points of the curve [121].

The flowchart method is presented in Figure 3.7. It causes a perturbation when the voltage and PV power both rise, increasing the duty cycle D by a step size ΔD, which modifies the pulse-width modulation. The operating point approaches the MPP as a result of this repeated process. In contrast, if PV power falls but voltage rises, the algorithm reverses and steers towards the MPP. However, the approach has drawbacks in settings with significant solar irradiation changes. It usually causes voltage fluctuations near the maximum power point without exactly reaching the ideal value. The function methodology of the P&O algorithm follows the theoretical equation 3.26.

$$d(k) = d\,(k-1) \pm \frac{\frac{\Delta P}{\Delta d}}{\frac{P}{d}} \tag{3.26}$$

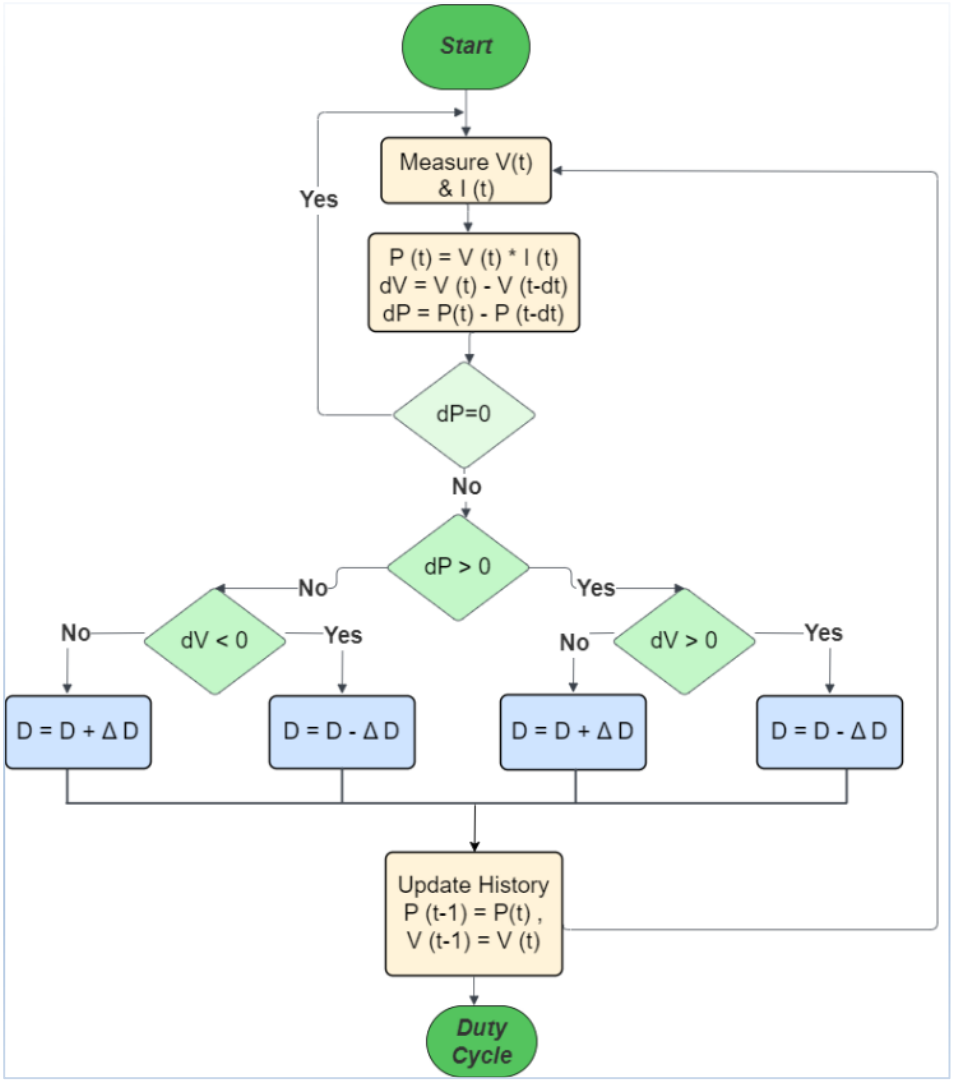


Figure 3.7 P&O algorithm flowchart.

For **performance benchmarking**, the P&O algorithm's effectiveness is determined by its MPPT efficiency. To calculate the instantaneous MPPT efficiency, use the following equations 3.27 & 3.28.

$$\eta_{MPPT} = \frac{P_{MPP}(t)}{P_{MPP*}(t)} \times 100 \tag{3.27}$$

$$\eta_{MPPT(avg)} = \frac{\int P_{MPP}(t)\,dt}{\int P_{MPP*}(t)\,dt} \times 100 \tag{3.28}$$

This algorithm focuses on obtaining maximum theoretical power P_{MPP*}. The PV model is used to calculate it. The real power that is extracted using the MPPT method, however, is known as P_{MPP}. It depends on how closely the algorithm tracks the irradiance at any instant of time and compute with the measured

values of V_{PV} and I_{PV}. For the adaptive P&O, the logarithmic scheme [122] is used. The pseudocode for the P&O MPPT algorithm is provided in the Appendix (Algorithm A1).

3.5.1.2 Neural Network-based MPPT

Neural Network-based MPPT algorithm model calculates output and input variables. The system takes data inputs such as temperature and irradiance and outputs as a power value. The duty cycle processes through input VI in the NN model as shown in Figure 3.8. The multilayer network is made up of 3 layers: an input layer (two neurons), a hidden layer (ten neurons), and an output layer (one neuron), with the activation function used for processing.

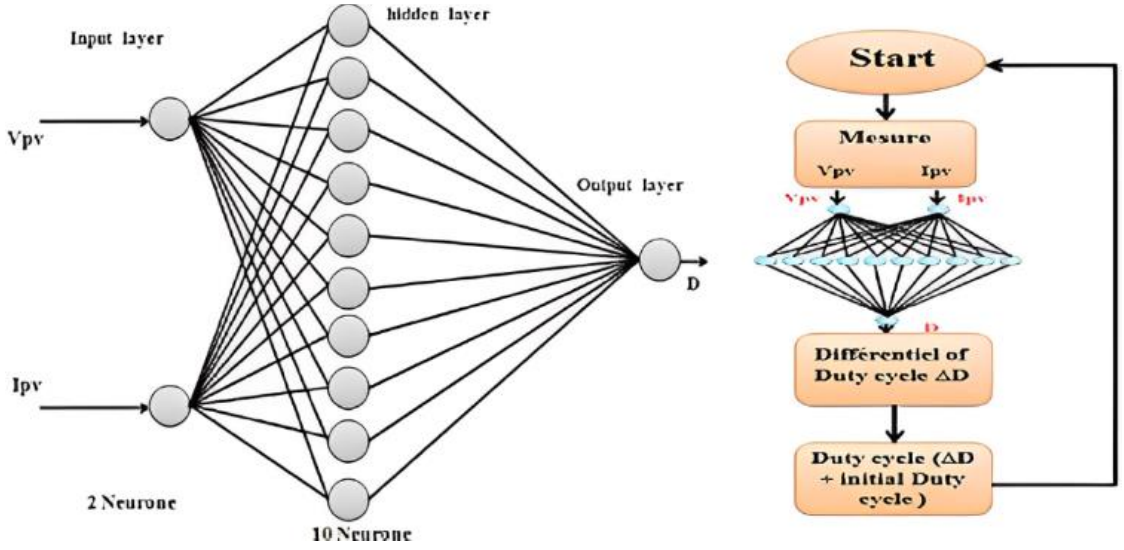


Figure 3.8 Neural Network Model & flowchart of MPP.

In the power extraction optimization, the PV array is connected to the DC bus via a boost converter controlled by the neural network MPPT algorithm. The controller of the MPPT algorithm predicts the prime duty cycle for the boost converter. The boost converter extracts the maximum power from PV. The correlation of the target and trained value of the neural network algorithm ensures a steady duty cycle for PWM. The subsystem delivers solar data to PV with a sequential simulation transfer time. Solar panels require solar radiation to

generate energy. Therefore, it depends on input data (irradiance and temperature), which is computed through equations (3.29) and (3.30). The function of neural network MPPT is created using solar power plant data, where irradiance and temperature generate maximum power (voltage) from the PV. Equations (3.31-3.33) are used to calculate which maximum generated voltage V_{MP}, maximum current I_{MP}, and maximum power P_{MP} for a given temperature and irradiance various data. These data that are considered to be the output of the neural network are the voltage that is produced by the solar panel.

Irradiance, G (W/m2):

$$G = [(G_{max} - G_{min}) \times \text{rand}\,] + G_{min} \tag{3.29}$$

Temperature, T (°C):

$$T = [(T_{max} - T_{min}) \times \text{rand}\,] + T_{min} \tag{3.30}$$

Maximum Voltage, V_{MP}(V), at given G and T

$$V_{MP} = [(T - T_S) \times \text{beta}\,] + V_{OC} \tag{3.31}$$

Where Voc is refer at open circuit of the panel and Ts is in the standard.

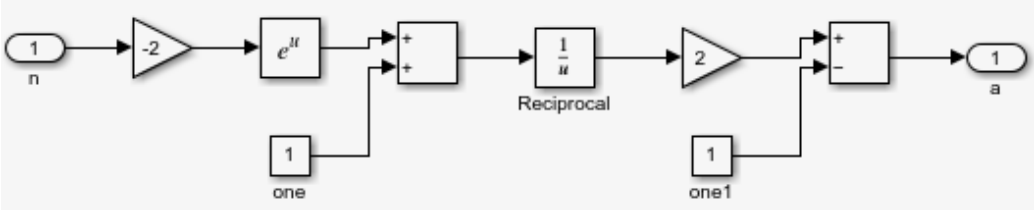
Maximum Current, I_{MP} (A), at given G and T

$$I_{MP} = \left[1 + \left((T - T_S) \times \text{alpha}\right)\right] \times I_M \times \left(\frac{G}{G_S}\right) \tag{3.32}$$

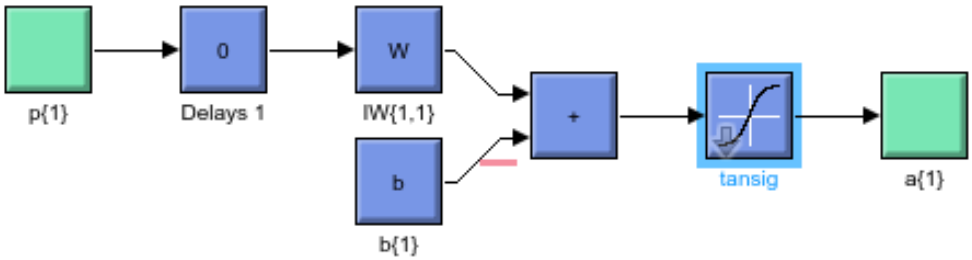
Maximum Power, (P_{MP}) at given G and T

$$P_{MP} = V_{MP} \times I_{MP} \tag{3.33}$$

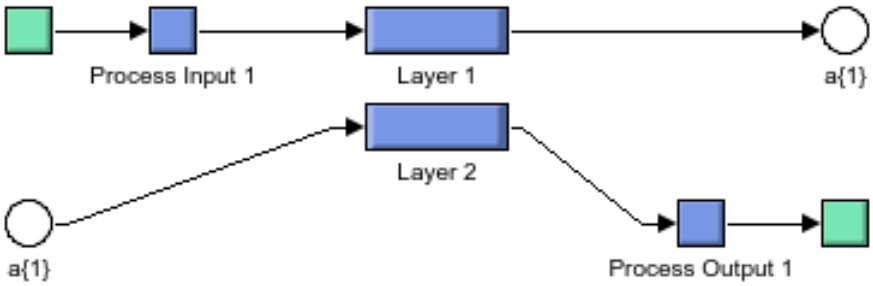
The produced voltage is considered the neural network's output data. The Technology MPPT is designed with a rated solar panel coefficient input-output dataset.



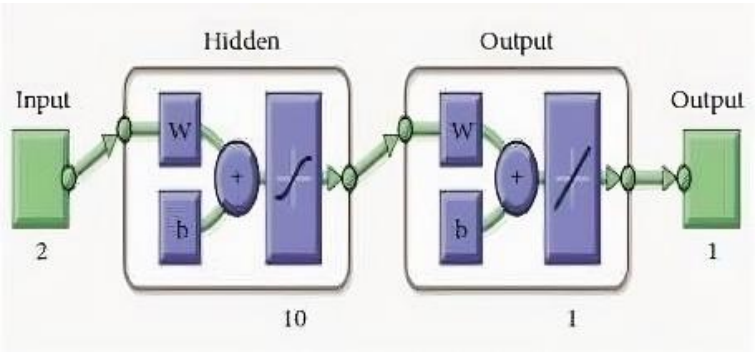
(a)



(b)



(c)



(d)

Figure 3.9 Neural Network's (a) Function block (b) Layer configuration (c) Process layer (d) Final trained neural network.

The approach employed in this research is according to the three-layer feedforward network configuration. Figure 3.9 shows the sigmoid activity function in hidden neurons and multi-dimensional mapping fit for linear output.

3.5.1.2.1 Neural Network Architecture

Neural network design often comprises multiple layers of linked nodes that process and evaluate data to make accurate predictions and modifications. The MPPT system's intricate structure allows it to adjust to shifting environmental conditions and ensure maximum energy harvesting efficiency.

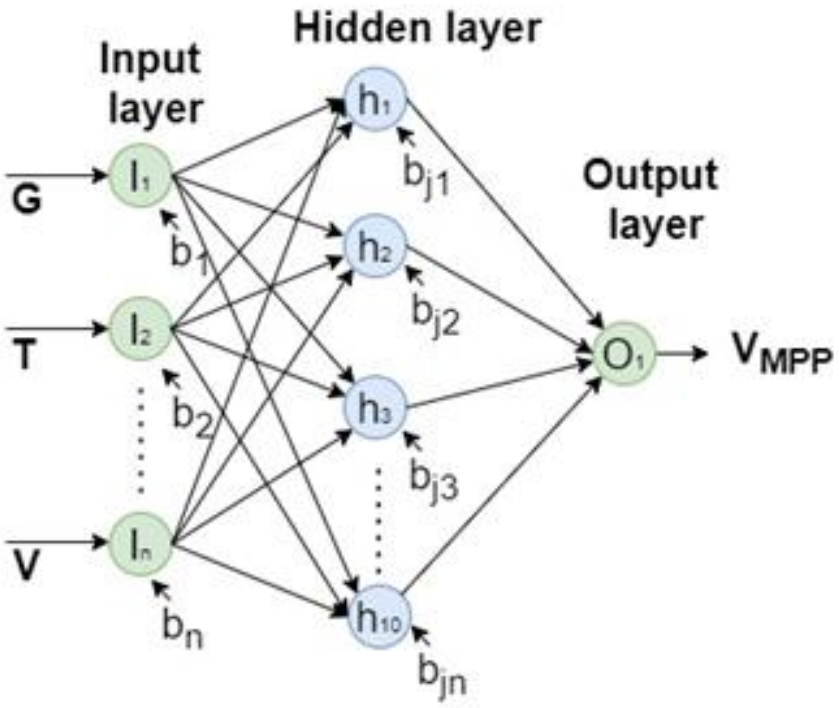


Figure 3.10 Structure of basic neural network model.

3.5.1.2.2 Developing Neural Network System

The dynamic application data investigated the performance of the connectionist model and produced predicted results. The basic structure of the Neural Network-based MPPT system calculates output and input variables, as illustrated in Figure 3.10. The system takes data inputs such as temperature and irradiance and outputs the maximum voltage. The duty cycle (PWM) is processed using the input voltage and current in the developed ANN structure model, as shown in Figure 3.11. The development of the ANN structure model flowchart integrates algorithm input parameters to improve the accuracy and reliability of the MPPT system. This model process has passed tough steps with testing and validation to guarantee its efficacy in practical applications.

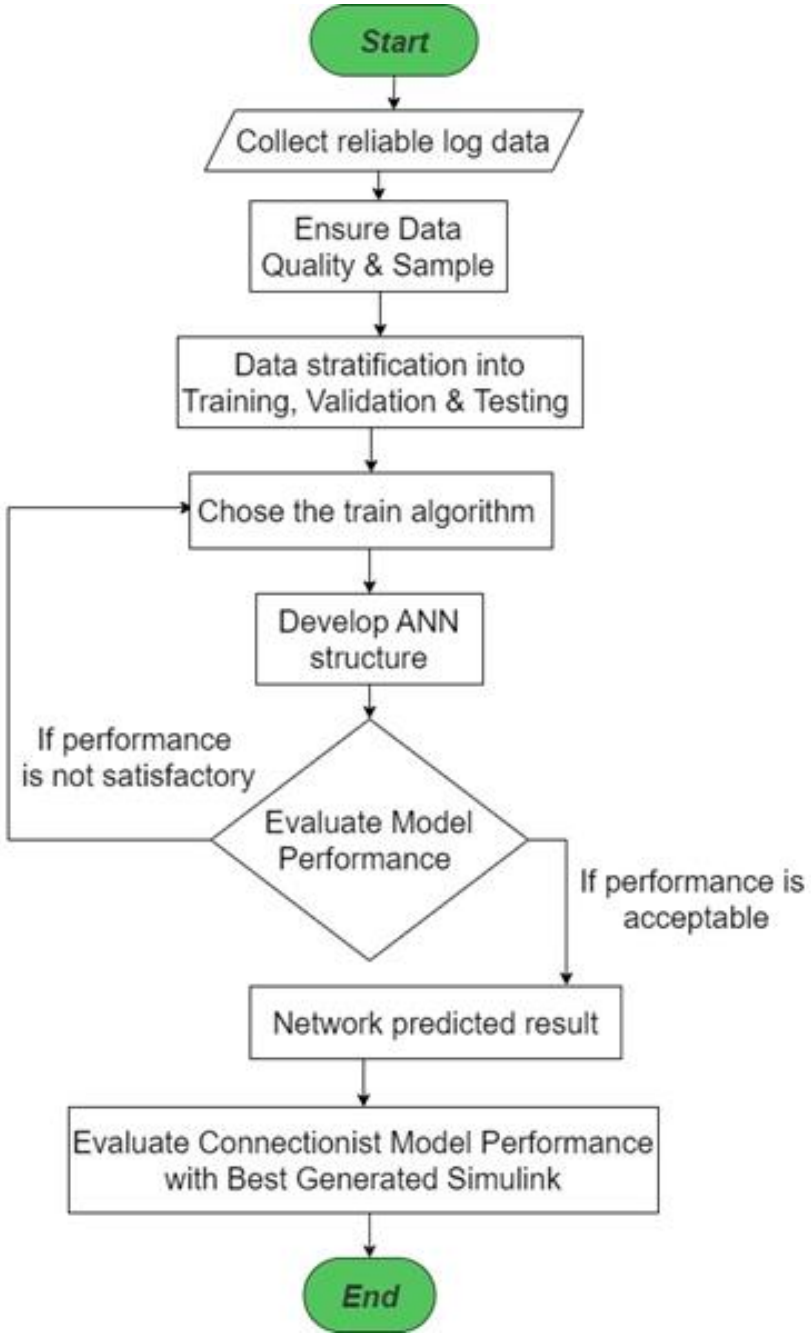


Figure 3.11 Development of the ANN flowchart.

In the neural network function fitting system, the ANN's output layer and hidden layers perform calculations using the tansig and purelin activation functions respectively, as shown in Figure 3.12. This set of linear and nonlinear processes is used to provide practical ANN training. Equation (3.34) provides the function of tansig, whereas Equation (3.35) illustrates the idea of updating the weights (Wi,j). Equation (3.36) provides the function of purelin, whereas Equation (3.37) provides the idea for updating the weights ($W_{j,o}$).

$$\emptyset\,(V_j) \;=\; \frac{2}{1+e^{-2vj}} - 1 \qquad (3.34)$$

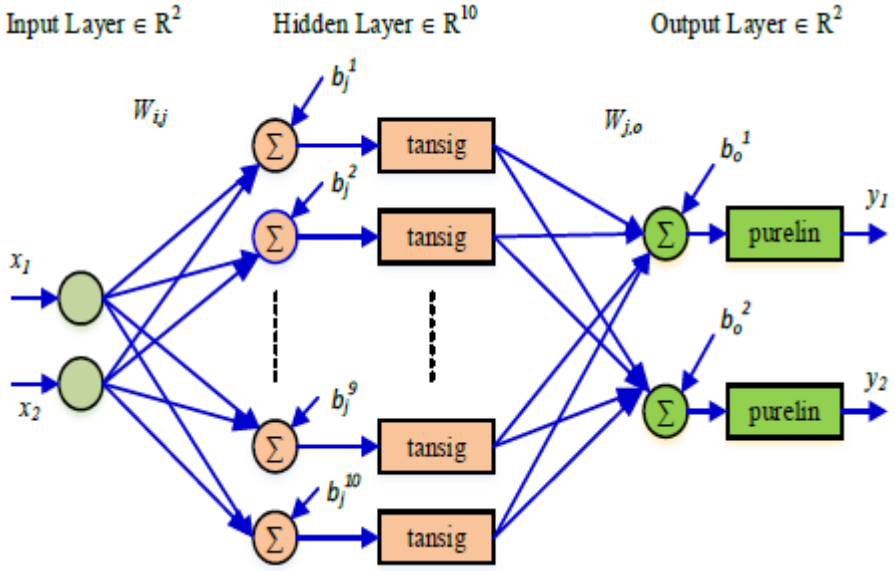


Figure 3.12 Ten hidden layer nodes (ANN model architecture).

For modifying the weights between nodes in the first two layers, use the delta rule,

$$W_{ij} \;=\; W_{i,j} + \mathrm{l}_r\, \acute{\emptyset}\,(V_j) e_j x_i \qquad (3.35)$$

$$\varphi\,(V_o) \;=\; V_o \qquad (3.36)$$

The learning rate is l_r, which ranges from 0 to 1; the error value of the j^{th} hidden node is e_j, the weighted sum of inputs and the bias b_j is v_j, the first derivative of the tansig function is $\phi'(v_j)$, and x_i is the i^{th} (i = 1 & 2) input node present value, $W_{i,j}$ is the weight among i^{th} input node and j^{th} hidden node. To adjust the weights between the output layer and hidden layer nodes, the delta rule is given as follows:

$$W_{i,o} \;\leftarrow\; W_{j,o} + \mathrm{l}_r\, \acute{\emptyset}\,(V_o) e_o y_i \qquad (3.37)$$

Considering y_j to be the present value of the j^{th} (j = 1, 2,…, 10) hidden node, $W_{j,o}$ is the weight between the o^{th} output node and the j^{th} hidden node, e_o is the error value of the o^{th} output node, v_o is the weighted total of the hidden layer nodes with their bias b_o, and $\varphi'(v_j)$ is the first derivative of the purelin function. The study adopted the Levenberg-Marquardt (LM) optimization algorithm to train,

validate and test the ANN model. Equation (3.38) provides a procedure for updating weights ($W^*_{i,j}$ and $W^*_{j,o}$). The value of regression, R is 1, as shown by the training, testing, and validation results and discussion chapter in Figure 4.4. The pseudocode for the proposed ANN-based MPPT algorithm is provided in the Appendix (Algorithm A2).

$$\left.\begin{aligned} W_{i,j} &= W_{i,j} - [\, J^T J - \mathrm{I}_p I]\hat{}-1\ (J^T e) \\ W_{i,o} &= W_{i,o} - [\, J^T J - \mathrm{I}_p I\,]\hat{}-1\ (J^T e) \end{aligned}\right\} \quad (3.38)$$

Where J, is the Jacobian matrix, I, is the identity matrix, e, is the cumulative error vector, and lp, is the learning parameter.

3.5.1.2.3 Training & Performance Metrics

We train the neural network using real-time data, which is detailed in the results section. After providing solar input and necessary data throughout a specific observation period. The requirements for fitting a neural network model for the necessary parameters are given in Table 3.2.

Table 3.2 Neural Network function

Specification	***Data***	***Data information***	
Toolbox	nnstart	Types of Sample, (%)	Samples
Input-Output and Curve Fitting	Fitting app	Training 70%	420001
Input data to the Network	1000 points Irradiation, Temperature input data	Validation 15%	90000
Target data	1000 points Voltage data	Testing 15%	90000
Samples	Matrix-rows		
Hidden Layer	10		
Training Algorithm	**Levenberg-Marquardt**		
Performance	Mean squared error		

3.5.1.3 Proposed Hybrid (P&O, Neural Network) MPPT

The suggested hybrid MPPT system combines the benefits of Perturb and Observe (P&O) and neural network algorithms to increase overall performance and efficiency. This novel methodology tries to maximize energy harvesting from solar panels by using each method's capabilities under various environmental conditions. The combined intelligent MPPT method was utilized to enhance the performance of both standalone and grid-connected PV systems. Using this novel supervised approach, this research improves the efficacy and reliability of solar energy production, thereby augmenting the efficiency and sustainability of the energy infrastructure.

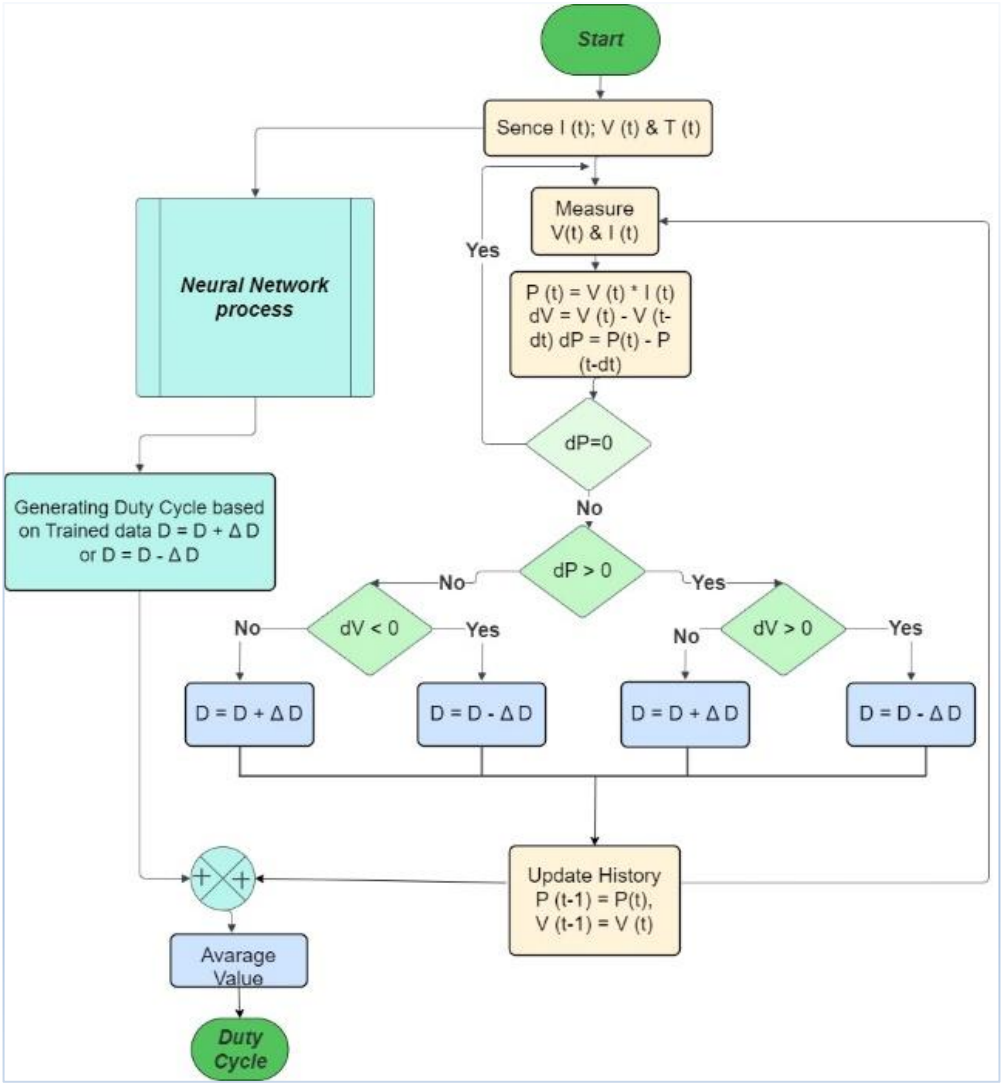


Figure 3.13 Proposed Hybrid (P&O, NN) model algorithm flowchart.

The hybrid MPPT technology combines neural network (NN) and P&O controllers presented in Figure 3.13 to optimize solar panel efficiency under various environmental conditions. In this hybrid system, the solar irradiance (G) and temperature (T) feed the neural network, while the P&O algorithm based on solar voltage and current. Both techniques complement the hybrid method of merging their outputs and averaging the duty ratio. The system reduces oscillations around the MPP and this hybrid approach exhibits variations in operating speed, measurement precision, hardware implementation, sensor count and predictability. Figures 3.9 & 3.12 show a graphical diagram and the architecture of the intelligent algorithm. It's conjunction with nonlinear systems like PV panels. The central nervous system of multilayer information flow is unidirectional. It is fabricated of input, hidden and output layers where thousands of neurons have weight links passing messages. Equations 3.39 & 3.40 compute the calculation of bias terms (b) of preceding level weights (w) and feedforward backpropagation Mean Squared Errors (MSE) function. P&O algorithm results are combined with weight adjustments in neural network processing.

$$Output, y \; = \; \sum_{i=1}^{n} W_{ij} \, Xj \; + \; b_j \tag{3.39}$$

$$MSE \; = \; \frac{1}{n} \sum_{i=1}^{n} \sum_{j=1}^{m} [Y_j(i) \; - \; T_j(i)]^2 \tag{3.40}$$

The combined duty cycle (D) is precisely calculated as the average of the separate D1 and D2, generated by the P&O algorithm and NN controller respectively, as given by equation (3.41).

$$D = \frac{(D1+D2)}{2} \tag{3.41}$$

This predicted final average duty cycle (D) is supplied to the PWM generator for switching pulses to control the boost converter adjusting the input voltage to match the MPP prediction reference.

3.6 NPC CONVERTER TOPOLOGY & CONTROL DESIGN

The Neutral Point Clamped (NPC) converter topology and control design play a vital role in efficiently converting the harvested solar energy into usable power for the utility grid. The NPC converter can ensure harmonic performance, optimal energy conversion, and grid integration by employing modulation techniques like space vector. These design considerations are critical for increasing the efficiency and reliability of solar energy systems, particularly in grid-connected applications. The NPC converter is a multilevel architecture inverter extensively used in medium to high-power applications. Its three-level structure reduces harmonic distortion and voltage stress on switching devices by using clamped diodes to maintain DC bus voltage levels. The proposed methodology outlines how this converter operates and explores its benefits to the on-grid PV systems. The total possible states on each lag of the NPC inverter is 4 transistors. The converter topology Figure 3.14, shows a three-phase NPC inverter is $2^4 = 16$.

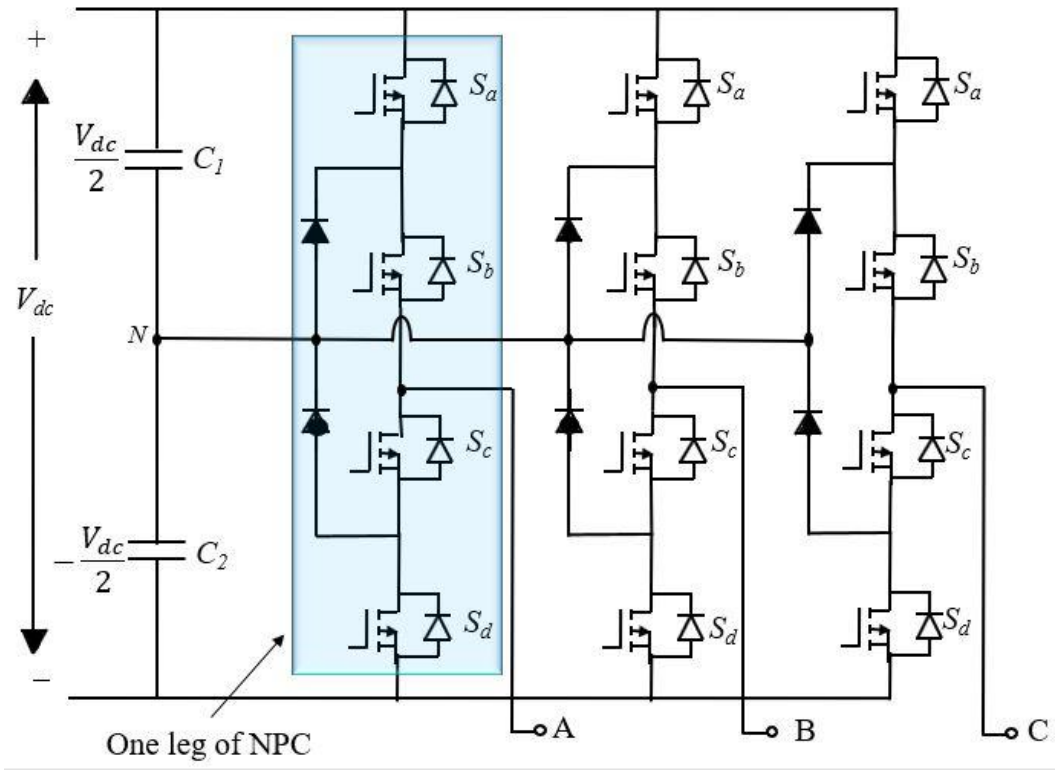


Figure 3.14 Neutral-point diode clamped Three level inverter.

While three are feasible and one creates a short circuit on the DC link. The output voltage profile is distinct in Table 3.3.

Table 3.3. NPC Switching States (ONE LEG)

Switching State	*Sa*	*Sb*	*Sc*	*Sd*	*Output Voltage*	*Leg State*
1	ON	ON	OFF	OFF	Vdc/2	P
2	OFF	ON	ON	OFF	0	0
3	OFF	OFF	ON	ON	-Vdc/2	N
4	ON	OFF	OFF	ON	Invalid	-

For one leg, we can observe the n-level output, an (n-1) level capacitor, 2(n-1) split input DC sources, and 2(n-2) clamping diodes to switch. The balance-imbalance potential midpoint issue has an impact on the inverter's performance. It is assuming the three-phase load. Equations (3.42) through (3.45) can resolve the midway potential imbalance issue. The capacitor voltage should ideally be equal to Vdc/2, with the output voltage ranging from +Vdc/2 to -Vdc/2. The three states are P, O and N. The symmetric inverter output voltage synthesis is represented by the instantaneous values of the three-phase voltage output (Va, Vb, and Vc), where the vector is Vref.

$$V_a = V_m \sin(wt) \tag{3.42}$$

$$V_b = V_m \sin\ (wt - \tfrac{2}{3}\pi) \tag{3.43}$$

$$V_b = V_m \sin\ (wt + \tfrac{2}{3}\pi) \tag{3.44}$$

$$V_{ref} = \tfrac{2}{3}\ (V_{an} + V_{bn}e^{j\ 2/3\pi} + V_{cn}e^{j-\ 2/3\pi}) \tag{3.45}$$

The three-phase coordinate system a-b-c is converted to a 2-dimensional α-β frame using the Clark transformation, which is helpful in sector identification as shown in Figure 3.15. The equation that results is as follows:

$$\begin{bmatrix} V_{r\alpha} \\ V_{r\beta} \end{bmatrix} = \frac{2}{3} \begin{bmatrix} 1 & -\frac{1}{2} & -\frac{1}{2} \\ 0 & \frac{\sqrt{3}}{2} & -\frac{\sqrt{3}}{2} \end{bmatrix} \begin{bmatrix} V_a \\ V_b \\ V_c \end{bmatrix} \tag{3.46}$$

Where $V_{r\alpha}$ and $V_{r\beta}$ are the Components of the reference vector in α-β coordinate system. The reference voltage vector can be positional in any area (1-4) or sector (I-VI) of the space vector diagram.

3.6.1 Space Vector Modulation (SVM)

The SVM method is a digital modulation approach and was first introduced in 1964, where the vector control signals are compared to the reference waveform to get the output waveforms[123]. It uses the vector representation to produce PWM. Digital signals are supplied directly to switches, which are controlled using vector representation. The vectors are arranged in a hexagonal pattern to show their respective phases and magnitudes. Space vector modulation is applied to the NPC converter. The NPC converter comprises two different states of three switching states for each leg, with common points connected to the common neutral point of the two DC-link capacitors. Any three-phase n-level Space Vector Diagram (SVD) can be separated into six sectors (Si), where i = 1 to 6. The sectors are then divided into $(n-1)^2$ sub-triangles ($\Delta i,j$), with j = 1 to 4 and i = 1 to 6. Thus, the n-level SVD contains of n^3 switching states. As a reference the three phases are combined, there are 27 switching states ($x^n = 3^3 = 27$) and 24-sub-triangles (No. of sub-triangles in each sector is $(3-1)^2 = 4$; therefore, $4 \times 6 = 24$). Considering the three-level MLI SVD, the sector is classified into six categories depending on each switching state category, as shown in Figure 3.15. The various pairing states are classified into four vectors depending on the combination of output phase voltages; *large vector* (vertices of outer hexagon), *medium vector* (mid-points of sides of outer hexagon), and *small vector* (vertices of inner hexagon) and *null vector*. As a result, this combination determines the converter's output voltage and NP current flow. Large vectors do not affect the NP current and the medium vectors do not affect the NP current when all loads have broken poles. Begin with the expansive voltage vector PNN/200; the whole area is delineated as sectors I, II,... and VI spaced every 60 degrees.

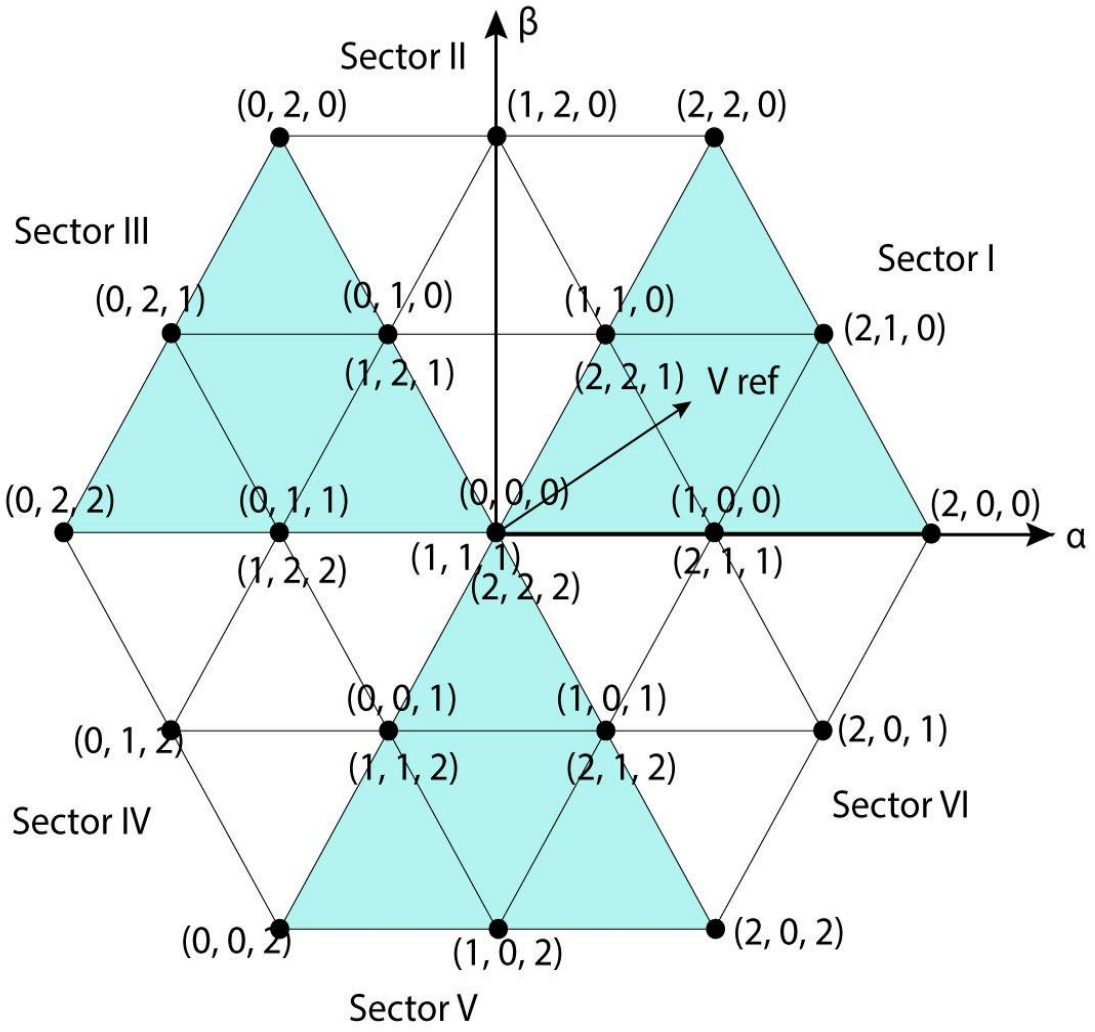


Figure 3.15 Three-level inverter Space Vector Diagram (α, β) frame.

In three-level SVD, the small and null vectors have 12 and 3 redundancy switching states, respectively. As the MLI level increases, the number of redundancies switching states for null and small vectors also increases. The most challenging part of the SVD realizations is fixing the Vref in the sub-triangle. Figure 3.16 depicts how each sector is split into four sub-triangles. Firstly, Sector I, is typically examined as the initial step. Subsequently, applying its symmetry feature facilitates the derivation of results for the entire 360-degree region. The main purpose of the SVM approach is to find the sector and sub-triangle that contains a specific reference vector Vref. From there, this reference vector is formed by its Nearest Three Vectors (NTV) following the voltage-second

balancing principle[124]. The point of the reference voltage vector in these sectors controls the switching sequence as **0 = N (-), 1= O & 2 = P (+)** shown in Table 3.4.

Table 3.4 Different Switching States and Vectors in NPC Converter.

Active			
Small Voltage ($V_{dc}/3$) **(Redundant vectors)**	***Medium Voltage Vectors*** ($V_{dc}/\sqrt{3}$)	***Large Voltage Vectors*** ($2\,V_{dc}/3$)	***Null Vectors (0)*** **(Redundant vectors)**
(+ 0 0), (0 - -)	**(+ 0 -)**	**(+ - -)**	**(- - -), (0 0 0), (+ + +)**
(+ + 0), (0 0 -)	**(0 + -)**	**(+ + -)**	
(0 + 0), (- 0 -)	**(- + 0)**	**(- + -)**	
(0 + +), (- 0 0)	**(- 0 +)**	**(- + +)**	
(0 0 +), (- - 0)	**(0 - +)**	**(- - +)**	
(+ 0 +), (0 - 0)	**(+ - 0)**	**(+ - +)**	

The switching states and associated **on-time calculations** are determined using the rotating reference vector, Vref, within any of the four sub-triangles. For instance, if Vref lies in the fourth sub-triangle of the first sector (Δ1,2), the nearest three vectors VS2, VM1, and VS1 are used to synthesize Vref.

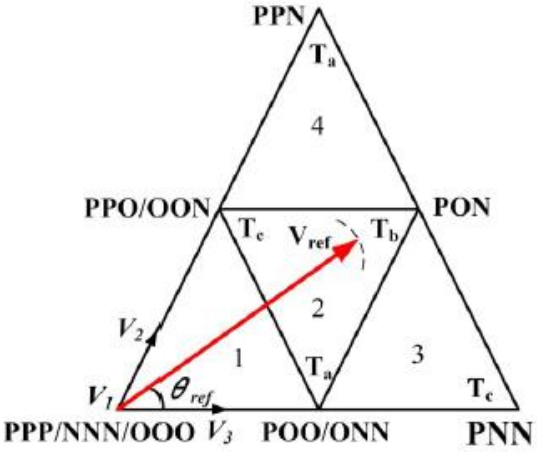


Figure 3.16 Vector map of (Sector I).

The duty cycle of the nearest switching vectors POO/ONN (V1), PON (V2), and PPO/OON (V3) may be calculated and applied to pulse generation. Hence, V_{ref} can be represented as:

$$\left.\begin{array}{c} V_{ref}.T_s = T_a.V_1 + T_b.V_2 + T_c.V_3 \\ T_s = T_a + T_b + T_C \end{array}\right\} \quad (3.47)$$

Here, T_s is the sampling time, T_a , T_b and T_c are the on times for the voltage vector respectively. The movement of V* angle (θ) within the sector is computed by

$$\theta = \tan^{-1}\left(\frac{V_\alpha}{V_\beta}\right) \quad (3.48)$$

The θ values sample the V* in different sectors; for instance, the V* approaches sector-2 when θ is 115° because sector-2 falls on an angle between 61° and 120°.

The obtaining times of switching each state for dwell time in the inverter leg can be evaluated from the Table 3.5 equation that follows:

Table 3.5 Switching Vector Times of a Three-Level Inverter in Sector I.

Triangle Number	**Switching Vectors**	**Switching Times**
1	$V_1 = 0$ $V_2 = \frac{1}{3}V_{dc}$ $V_3 = \frac{1}{3}V_{dc}\, e^{j60°}$	$T_a = T_s\,[1 - 2\,m_a\, sin(\frac{\pi}{3} + \theta)]$ $T_b = T_s\,[2\,m_a\, sin(\frac{\pi}{3} - \theta)]$ $T_c = T_s\,[2\,m_a\, sin\,\theta]$
2	$V_1 = \frac{1}{\sqrt{3}}V_{dc}\, e^{j30°}$ $V_2 = \frac{1}{3}V_{dc}$ $V_3 = \frac{2}{3}V_{dc}$	$T_a = T_s\,[2\,m_a\, sin\,\theta]$ $T_b = T_s\,[2 - 2\,m_a\, sin(\frac{\pi}{3} + \theta)]$ $T_c = T_s\,[2\,m_a\, sin\left(\frac{\pi}{3} - \theta\right) - 1]$
3	$V_1 = \frac{1}{\sqrt{3}}V_{dc}\, e^{j30°}$ $V_2 = \frac{1}{3}V_{dc}$ $V_3 = \frac{1}{3}V_{dc}\, e^{j60°}$	$T_a = T_s\,[2\,m_a\, sin\left(\frac{\pi}{3} + \theta\right) - 1]$ $T_b = T_s\,[1 - 2\,m_a\, sin\,\theta]$ $T_c = T_s\,[1 - 2\,m_a\, sin\left(\frac{\pi}{3} - \theta\right)]$
4	$V_1 = \frac{1}{\sqrt{3}}V_{dc}\, e^{j30°}$ $V_2 = \frac{2}{3}V_{dc}e^{j60°}$ $V_3 = \frac{1}{3}V_{dc}e^{j60°}$	$T_a = T_s\,[2\,m_a\, sin\left(\frac{\pi}{3} - \theta\right)]$ $T_b = T_s\,[2\,m_a\, sin\,\theta - 1]$ $T_c = T_s\,[2 - 2\,m_a\, sin\left(\frac{\pi}{3} + \theta\right)]$

Where $m_a = \sqrt{3}\frac{V_{ref}}{V_{dc}}$.

3.6.2 Switching Strategy

The switching strategy used in SVM plays a crucial role in enhancing the overall performance of NPC converters. The switching sequence of the NPC converter operates at a lower switching frequency and has reduced switching losses, exposing it to less voltage stress than two-level converters. In the conventional SVM approach, the reference vector is determined based on the three vectors that are set up closest to it. Hence, it is also known as the Nearest Three Vector method. Table 3.6 presents the conventional SVM switching sequence for the six sectors of the 3L NPC MLI. SVM generates PWM signals that control the switches of an inverter. These signals produce the required modulated voltage to ensure the output voltage vector is synthesized correctly. Redundant states in the NPC converter balance the neutral-point voltage and reduce switching losses by selecting the optimal equivalent switching configurations. This switching signal controls the power of electronic switches to provide the required output voltage. Due to such advantages, the NPC converters with SVM are a recognized method for high-power applications.

Table 3.6 Conventional switching sequence of the three-level inverter SVM.

Sector	*Sub-Sector*	*Switching Sequence*
1	1	nnn-onn-oon-ooo-poo-ppo-ppp-ppo-poo-ooo-oon-onn-nnn
	2	onn-oon-pon-poo-ppo-poo-pon-oon-onn
	3	onn-pnn-pon-poo-pon-pnn-onn
	4	ppo-ppn-pon-oon-pon-ppn-ppo
2	1	ppp-ppo-opo-ooo-oon-non-nnn-non-oon-ooo-opo-ppo-ppp
	2	non-oon-opn-opo-ppo-opo-opn-oon-non
	3	oon-opn-ppn-ppo-ppn-opn-oon
	4	non-npn-opn-opo-opn-npn-non
3	1	ppp-opp-opo-ooo-noo-non-nnn-non-noo-ooo-opo-opp-ppp
	2	opp-opo-npo-noo-non-noo-npo-opo-opp
	3	non-npn-npo-opo-npo-npn-non
	4	oop-nop-nnp-nno-nnp-nop-oop

Sector	*Sub-Sector*	*Switching Sequence*
4	1	ppp-opp-oop-ooo-noo-nno-nnn-nno-noo-ooo-oop-opp-ppp
	2	nno-noo-nop-oop-opp-oop-nop-noo-nno-
	3	opp-npp-nop-noo-nop-npp-opp
	4	oop-nop-nnp-nno-nnp-nop-oop
5	1	ppp-ppop-oop-ooo-ono-nno-nnn-nno-ono-ooo-oop-pop-ppp
	2	pop-oop-onp-ono-nno-ono-onp-oop-pop
	3	oop-onp-nnp-nno-nnp-onp-oop
	4	pop-pnp-onpono-onp-pnp-pop
6	1	ppp-pop-poo-ooo-ono-onn-nnn-onn-ono-ooo-poo-pop-ppp
	2	pop-poo-pno-ono-onn-ono-pno-poo-pop
	3	pop-pnp-pno-ono-pno-pnp-pop
	4	poo-pno-pnn-onn-pnn-pno-poo

3.6.3 Space Vector PWM (SV-PWM) Algorithm

SV-PWM is a sophisticated approach for generating the required output voltage by selecting the proper switching states. The vector space is divided into sectors and switching times for each sector are calculated. This technique uses the switching states of all three legs to balance the DC-link capacitor voltages and generate the desired output voltage. For the current requirement, one needs to reorder the sequence, the switching state vector's on-time, or both. Thus, the output voltage is controlled by the combination of the switching states and the duration of a switching state's activity during a switching period. These specified modulation schemes (SVPWM) increase the maximum output voltage by 15%. It enables more precise control and performance in specific applications.

The duty cycles for the switches are determined using the location of the reference vector inside a sector. It’s necessary to determine the periods for applying each vector during a switching cycle. The balancing of the SV-PWM bus voltage is achieved by utilizing redundancy among small vectors. These produce

identical line-to-line voltages corresponding to different switching states, which charge or discharge the DC link capacitors C_1 and C_2, respectively.

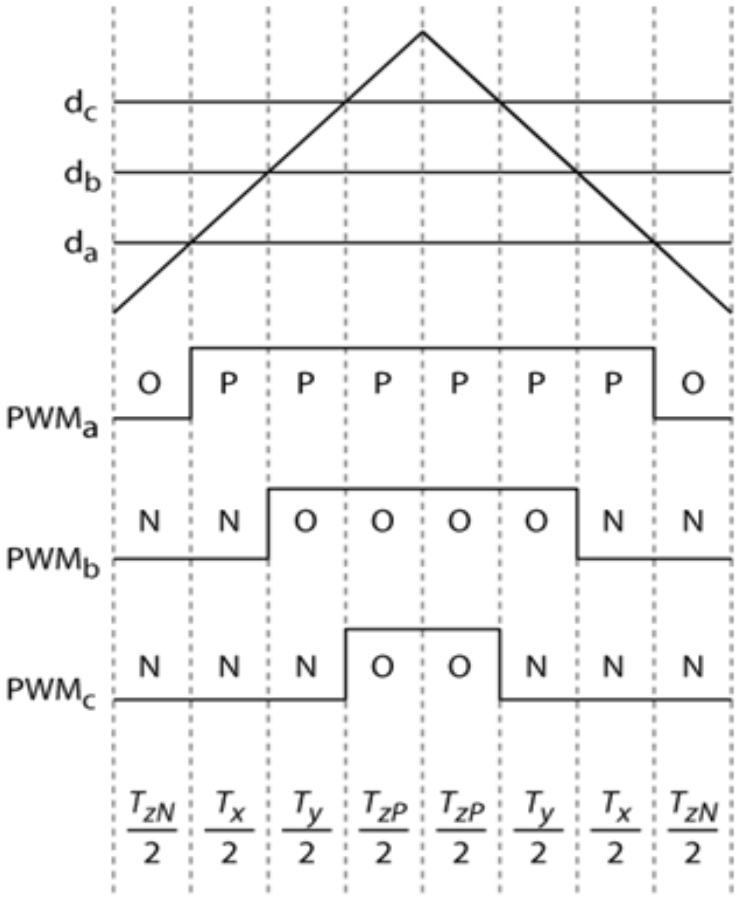


Figure 3.17 Pattern of SV-PWM duty cycles switching application.

The appropriate duty cycles (dx, dy & dz) illustrated in Figure 3.17 are computed to match the average output voltage with Vref. After determining the three vectors in the $\alpha\beta$-plane closest to the required reference value Vref. The duty cycle dz is divided into two components, dzP and dzN, which represent various vector applications and are applied in a certain order to reduce switching occurrences. The duty cycles da, db and dc are efficiently shifted by adjusting dzP and dzN, which optimizes the switching process. It can also be calculated by following equation (3.49-3.51).

$$d_a = d_x + d_y + d_{zP} \tag{3.49}$$

$$d_b = d_y + d_{zP} \quad (3.50)$$

$$d_c = d_{zP} \quad (3.51)$$

Where $d_{zP} = \frac{d_z}{2} + x$ and x is multiplied $I_d$with voltage ratio difference.

- The terms SVM (Space Vector Modulation) and SVPWM (Space Vector Pulse Width Modulation) are often used interchangeably in literature, but there's a subtle distinction that helps in understanding their roles in multilevel inverter control:

Aspect	**SVM (Space Vector Modulation)**	**SVPWM (Space Vector PWM)**
Definition	**SVM is the** modulation technique **that models the inverter output as a** space vector in a rotating reference frame**.**	SVPWM is the **practical implementation** of the SVM method using **pulse width modulation** techniques.
Role	Modulation theory and vector analysis	PWM signal generation method
Focus	How to represent and approximate vectors	How to switch the inverter accordingly
Output	Vector durations and selection	Actual gate pulses to switches
Abstraction Level	Higher-level, **mathematical modeling**	Lower-level, **practical implementation**

3.7 INTEGRATION OF THE STUDY SYSTEM

This integration allows for seamless connection to the grid, enhancing effective power transmission and reducing energy losses. Solar energy systems can achieve higher efficiency and better grid compatibility by combining MPPT technology and NPC converters. It also boosts overall system performance by delivering optimal power output under various environmental conditions. Additionally, it enables more effective monitoring and operation, which increases the system's longevity and reliability. For an imbalanced DC capacitor

voltage, the approach involves integrating solar PV and battery storage with an advanced three-phase, 3L NPC inverter shown in Figure 3.18. In this study, we proposed a grid-connected solar PV system with battery storage.

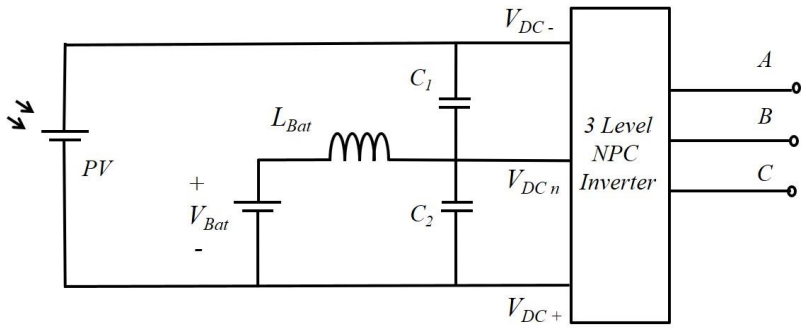


Figure 3.18 Solar PV and battery control integration with NPC inverter configuration.

This system transfers electricity from renewable energy sources to the grid while managing battery charge and discharge via the control system. The setup regulates battery charging and discharging while performing MPPT via precise control of capacitor voltages C1 and C2. The effectiveness of the NPC inverter structure and control algorithm has been verified through simulations in various scenarios. It has presented robust AC side current regulation and efficient battery operations under different solar irradiation levels. When renewable energy sources are unavailable, the relays transmit or absorb power between the DC bus and the grid. The devices are considered either ON or OFF based on specific criteria. While in operation, it manages electricity from renewable sources or the grid to charge the batteries. To prevent relay damage and interruptions in current, it is important to make sure that the inductor current (L_{batt}) is zero before opening the relay. Besides, this system efficiently manages PV and battery storage, ensuring a steady and reliable power supply to the grid.

3.7.1 Grid Synchronization:

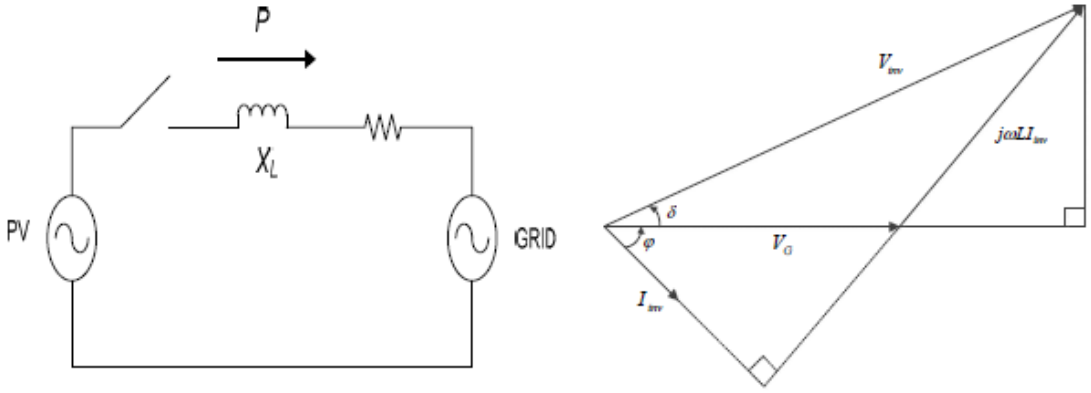
As earlier discussed, the grid-connected PV generating system has drawn considerable interest as more academics concentrate on the integrated and smart-grid distribution power system. Implementing these systems involves thorough

knowledge, critical review, and detailed analysis of aberrant operations. Four requirements must be satisfied to connect a single or 3-phase inverter system to the grid distribution network, as shown in Table 3.7.

Table 3.7 Grid-synchronization Parameters.

Parameters	Description
Phase Sequence	The phase sequence or phase rotation of the three-phase inverter must match the phase sequence of the three phases of the grid.
Voltage Magnitude	The magnitude of the sinusoidal voltage produced by the inverter must be equal to the grid.
Frequency	The frequency of the sinusoidal voltage produced by the inverter must be equal to the grid.
Phase Angle	The phase angle between the sinusoidal voltage produced by the inverter and the sinusoidal voltage generated by the grid must be zero.

A grid-connected PV system consists of two sources and an intermediate reactance as shown in Figure 3.19 (a).



(a) (b)

Figure 3.19 PV grid configuration; (a) Equivalent circuit diagram, (b) Phasor diagram.

Important components are depicted in the phasor diagram Figure 3.19 (b), such as the grid voltage (V_G), current (I_{inv}), and inverter output voltage (V_{inv}). Grid and inverter current relationships are controlled by the power angle (δ), whereas the load angle regulates the voltage phase difference. The relations are governed by equations 3.52 and 3.53, respectively.

$$P = |V_G||I_{inv}|\cos\varphi = \frac{|V_{inv}|\,|V_G|}{X_L}\sin\delta \tag{3.52}$$

$$Q = \frac{V_G}{X_L}(|V_{inv}|\cos\delta - |V_G|) \tag{3.53}$$

The inverter voltage magnitude and phase difference are adjusted to control the direction of power flow, while the phase sequence and frequency are closely monitored.

Electricity converters are essential for connecting renewable sources to the grid and integrating high-quality power. The grid voltage phase angle must be properly measured for the grid-tied inverter system to regulate the inverter voltage and current. Additionally, the amplitude and inverter frequency voltage must be synchronized with those of the grid voltage. By appropriately matching the grid's and the inverter's voltage amplitude and frequency, the inverter and the grid are synchronized at the point of common coupling (PCC). For 3-phase grid-tied inverters, a d-q reference-based phase-locked loop (PLL) is commonly used for its easy construction and precise amplitude and phase determination. In order to synchronize the grid, it uses the frequency, phase angle, and voltage amplitude measurements of the inverter and the grid. The grid synchronization approach is the foundation of the grid-tied inverter's control strategy. Clark's transformation converts three-phase grid quantities (ABC) into balanced two-phase stationary quantities ($\alpha - \beta$), which are then converted to a two-phase using Park's transformation then maps to a rotating reference frame as direct (d) and quadrature (q) components. When the predicted angle is q, the transformation from a-b-c to d-q may be expressed as

$$\begin{bmatrix} V_d \\ V_q \\ V_0 \end{bmatrix} = \sqrt{\frac{2}{3}} \begin{bmatrix} \cos\theta & \sin\theta & 0 \\ -\sin\theta & \cos\theta & 0 \\ 0 & 0 & 1 \end{bmatrix} \tag{3.54}$$

$$= \sqrt{\frac{2}{3}} \begin{bmatrix} \cos(\omega t)\cos(\theta) + \sin(\omega t)\sin(\theta) \\ -\sin(\theta)\cos(\omega t) + \cos(\theta)\sin(\omega t) \\ 0 \end{bmatrix} \tag{3.55}$$

After reducing the equation:

$$\begin{bmatrix} V_d \\ V_q \\ V_0 \end{bmatrix} = \sqrt{\frac{2}{3}} \begin{bmatrix} \cos\theta & \sin\theta & 0 \\ -\sin\theta & \cos\theta & 0 \\ 0 & 0 & 1 \end{bmatrix} \tag{3.56}$$

According to the mathematical model of three phase grid connected PV system, the output voltage of the synchronous (rotating) reference frame are given by equation 3.57 and 3.58 respectively.

$$V^*_d = K_p(I^*_d - I_d) + K_i \int (I^*_d - I_d)dt - \omega L I_q + V_d \tag{3.57}$$

$$V^*_q = K_p(I^*_q - I_q) + K_i \int (I^*_q - I_q)dt - \omega L I_d + V_q \tag{3.58}$$

here the grid voltage and current are represented by the DC components V^*_d, V^*_q, I^*_d, and I^*_q, respectively, and the inverter output is represented by V_d, V_q, I_d, and I_q. These DC quantities are converted back to the ABC frame to serve as reference signals for sinusoidal PWM (SPWM), which creates a three-phase inverter switching sequence with a proportional duty cycle. Under ideal grid conditions, q matches the grid phase angle ωt, and vq is zero. When $\omega t - q$ is small, it can be linearized for PI control.

$$V_q = \sin(\omega t - \theta) \approx (\omega t - \theta) \tag{3.59}$$

In a balanced three-phase system, when the PLL locks, vq is near zero. A low-pass filter or PI controller is used by the phase detector (PD) to reduce steady-state error. After that, the VCO produces the sine and angle waves using the PLL transfer function, which is provided by:

$$H(s) = \frac{k_p S + \frac{k_p}{T_s}}{S^2 + k_p S + \frac{k_p}{T_s}} \tag{3.60}$$

3.7.2 Proposed Control Strategies

The proposed control strategies aim to further details implementation of power generation and grid interaction. The system control strategies and the combination of converter with grid provide a comprehensive solution for effectiveness of the solar energy system. Figure 3.20 presents the proposed

control schematic diagram approach for grid-tied, three-phase, 3L NPC converter systems.

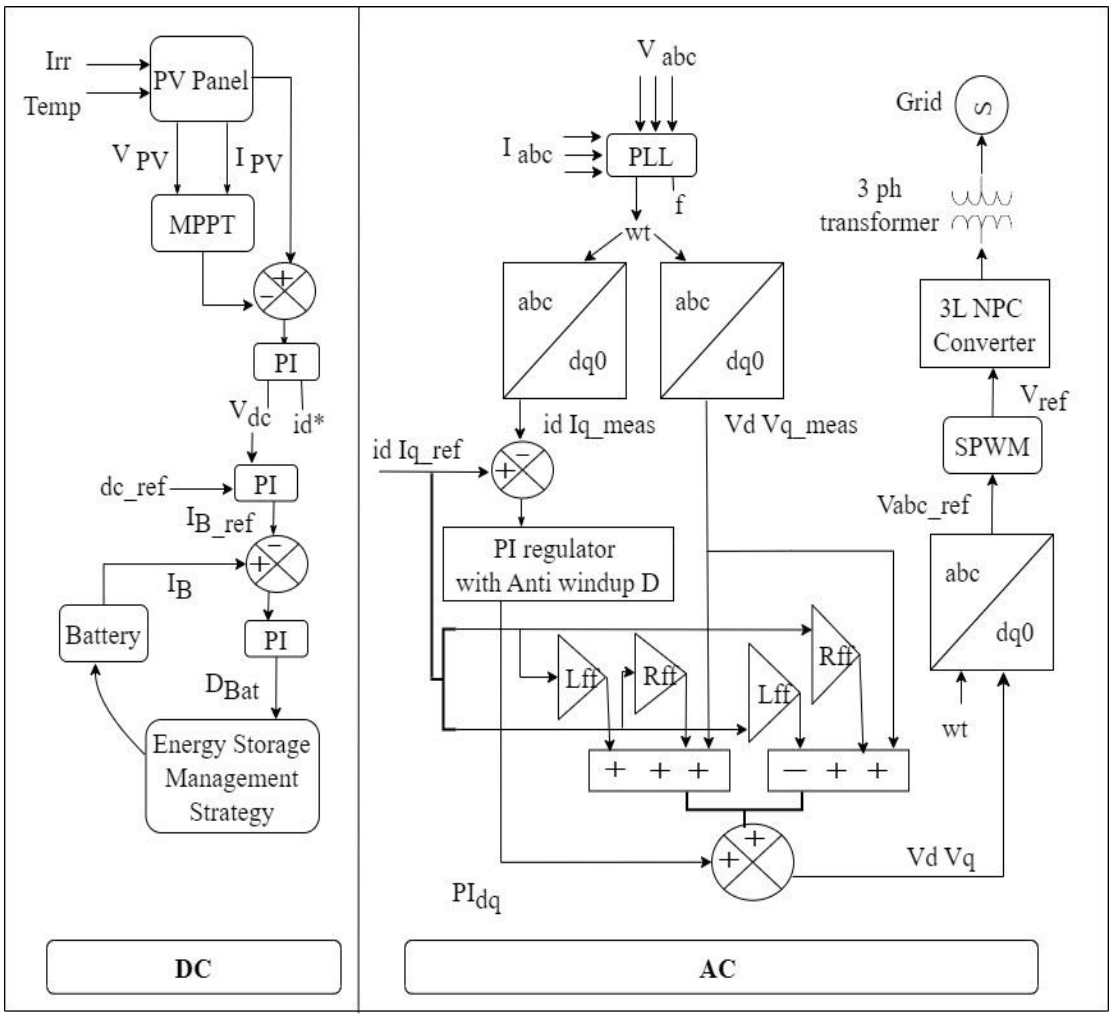


Figure 3.20 Control Block diagram of a 3-Level NPC inverter system.

It consists of two main controls: the AC-side controller for the inverter and the DC-side controller for the bidirectional DC-DC converter. The DC side controller block implements MPPT on the input side of the converter. The voltage and current of PV module are set as the input and duty cycle is the output parameter. The AC side controller produces PWM signals for the three-phase inverter. These controllers are built into the overall system controller in the inverter circuit, which is controlled by DC link voltage, PLL and Measurement current controller. In this grid synchronization, the three technical aspects are very crucial. The primary function is to regulate the DC-link voltage and keep it

constant. The second is to control the active power injected into the grid, and the third is to manage reactive power compensation. The feedforward PI regulator with anti-windup D regulates the inverter and grid current. It also reduces the steady-state error. Using a Park transform transforms the voltage into a gate pulse to produce in the d-q coordinate system. Therefore, the clamped converter is linked to a neural network architecture to enable real-time monitoring and control of power flow. The MPPT algorithm is integrated with the converter and a neural network model, which allows one to track and adjust to actively changing environmental parameters. In this system, three-phase coupling transformers link up to the controller power supply. In that way, the system offers optimal performance and efficiency. Moreover, the system exhibits increased stability and reliability in energy production. Table 3.8. Describe the system parameter of the experimental model.

Table 3.8 System Parameter

Parameter	Value
DC-link Voltage	*1000 V*
DC-link capacitors	*$150e^{-3}$ F*
Capacitor initial voltage	*500 V*
Output resistance	*1e-4/2*
Output inductance	*44.2e^-6*
Carrier frequency	*2340 Hz*
Switching frequency	*5 KHz*
Grid	*60 Hz, 3ph, 380 V(LL)*

3.7.3 Voltage Stability Management for Solar PV System

Solar PV impacts the stability of the microgrid system. It is going to make things worse in both cases of high penetration and low penetration. Consider solar PV on low-voltage networks as part of the distributed generation initiative.

The old unidirectional power flow has now turned bidirectional, converting consumers into prosumers in microgrid systems. As a result, solar PV has caused some new power quality problems in this microgrid system. Voltage stability concerns (voltage increase and voltage imbalance) are given significant consideration in the microgrid system.

According to the IEC 61000-430 class-A standard, a voltage increase of +6% over the nominal voltage is permitted, as is a 2% voltage imbalance factor. To determine how the penetration affects the stability of the system, we must assess the microgrid system's anticipated generation and load demand metrics. In our microgrid system, EMS automatically adjusts and balances voltage stability to maximize microgrid area power capacity concerning load demand by altering power factors and apparent power within the defined limits. This will occur when the overvoltage and voltage imbalance requirements are satisfied. MATLAB Simulink power system simulation is used to do mathematical optimization to achieve maximum power availability in the microgrid system while balancing generation and load demand.

The solar panel, MPPT charge controller, and battery should be as close together as feasible to minimize voltage drop in the solar PV/battery-based microgrid system. If we set the MPPT charge controller near the panels, then transmit the energy to the battery, and load the electricity grid region from a distance, we will see a large voltage decrease in the microgrid system. There will be less voltage drop in the microgrid system if we replace the battery with a recognized range of voltage and current ratios and keep the solar panel and battery close to one another. We should maintain a higher voltage in the microgrid region to prevent voltage drop. When we increase the current while decreasing the voltage, such as when charging a battery or wiring in parallel, we require a larger diameter wire to reduce energy losses. The energy storage system (battery) should have a voltage drop of less than 2% to function effectively. We

should (1) keep the distance between the solar panel, MPPT charge controller, and battery as little as possible, (2) increase the cable diameter if the voltage drop exceeds 3%, and (3) lower the cable's temperature to balance the voltage stability issue. The voltage drop problem in the solar PV/battery-based microgrid system may be managed in this manner.

3.7.4 Harmonic Distortion

Power electronics-based devices create harmonic voltages and currents, causing significant power quality issues in PV systems. In PV power systems, harmonics are rising daily. Heat losses, electricity costs, and a decrease in system efficiency follow as a result. The most important harmonic sources in PV power systems are inverters, DC/DC boost converters, and battery chargers. Considering the output waveform quality, Total Harmonic Distortion (THD) is measured by the given equation (3.61-3.62).

$$THD_v = \frac{\sqrt{\sum_{n=2}^{\infty}\left(V_{n,RMS}\right)^2}}{V_{1,RMS}} = \frac{\sqrt{\sum_{n=2}^{\infty}(V_{RMS})^2-\left(V_{1,RMS}\right)^2}}{V_{1,RMS}} \tag{3.61}$$

$$THD_i = \frac{\sqrt{\sum_{n=2}^{\infty}\left(I_{n,RMS}\right)^2}}{I_{1,RMS}} \tag{3.62}$$

Where n is the number of harmonics, THD is calculated by substituting harmonic voltage, V with harmonic current, I.

3.8 SUMMARY

All the parts of the proposed study's theoretical and mathematical model have been addressed in the methodology chapter. This chapter is organized based on research methodology and modeling of the integrated battery-based solar PV system. The system overview, simulation setup and modeling for the PV cell and boost converter are all described in detail. The energy storage management system was addressed in the calculation. A collection of data methods (historical and simulated) was described and examined. The most suitable procedure and measurements for a grid-connected solar PV system were

created using predictions of generation and demand under environmental conditions. Three different MPPTs are designed and used in this study. The details analysis of developing a neural network-based MPPT was explained. The NPC converter topology and control design function operation are applied and investigated in the integrated grid system. The switching strategy and function of space vector modulation are discussed for the SV-PWM algorithm. The optimization framework and approach with different objectives have been identified. P&O, NN, and hybrid MPPT algorithm techniques were employed; hybrid approaches maximized the power extracted from solar PV. This chapter covered the methodology and solution approach in detail. Consequently, the MPPT PV model based on grid-connected batteries was proposed. The grid's integration with the study system is synchronized. This model's grid control system is designed and described to convert DC to an AC power supply. Furthermore, the system analyzes THD using a grid current and voltage formula.

4 Results Analysis and Discussion

This chapter provides the overall evaluation of results and their performance analysis of MPPT and battery-based Neutral Point Clamped Converter in a grid operation. Section 4.1 describes the performance evaluation, where solar energy generation is production. Section 4.2 analysis the performance of the MPPT simulation result, where machine learning based MPPT training and dynamic performance are evaluated under varying irradiance and temperature. Section 4.3 describes the storage capacity. Therefore, Section 4.4 analysis the battery operation in 3 different MPPT algorithm and comparative analysis is discussed in section 4.5 details with considering several scenarios. In Section 4.6, the NPC converter performance on an integrated grid for NPC operation, the Total Harmonic Distortion is evaluated which is a permissible level. Then, discuss the power quality assessment and reliability in Section 4.7. Finally, Section 4.8 includes the summary and concluding remarks of Chapter 4.

4.1 PERFORMANCE EVALUATION

The ground-mounted solar PV system in this thesis research uses monocrystalline solar panels. Consequently, the entire integrated solar system has a 1.5 MW generating capacity. This study assumes solely a ground-mounted PV system for experimentation purposes. Section 4.1.1 provides an analysis of the daily load curve. The predicted grid load or base load is 400 kW, with a pick-up load of around 200 kW. The MPPT techniques are used for optimization under various conditions.

4.1.1 Solar Irradiance

The performance of the simulated MPPT algorithms is tested under various sun irradiance and temperature conditions to demonstrate their

characteristics, as shown in Table 4.1, which illustrates how irradiance and temperature vary over time. The sample was collected from the daily logbook on 28 May 2019 at the Kaptai Solar Power Plant, Chittagong.

Table 4.1 Changing environmental conditions data on a day.

Time (hours)	Global Horizontal Irradiation (W/m^2)	Ambient Temperature (˚C)	Time (hours)	Global Horizontal Irradiation (W/m^2)	Ambient Temperature (˚C)
09:45	697.215	32.825	13:55	843	36.2
09:50	699.6	33.128	14:00	833	36.6
09:55	709.935	33.128	14:05	816	36.6
10:00	715.5	33.229	14:10	803	36.7
10:05	726.63	33.532	14:15	790	36.7
10:10	928	33.1	14:20	777	36.7
10:15	909	33	14:25	760	36.7
10:20	767	33	14:30	750	36.8
10:25	770	33.4	14:35	733	37
10:30	921	33.5	14:40	715	37.1
10:35	981	34.1	14:55	665	37.4
10:40	980	33.7	15:00	629	37.4
10:45	985	33.7	15:15	576	37.8
10:50	894	33.9	15:20	559	37.3
10:55	855	34	15:25	546	37.3
11:00	1016	34.3	15:30	522	37.3
11:05	1008	34.2	15:35	506	37.7
11:10	1004	34.3	15:40	493	37.6
11:15	998	34.4	15:45	475	37.8
11:20	1054.2	34.4	15:50	454	38
11:25	1047.9	34.7	15:55	431	38
11:30	1057.35	34.6	16:00	410	37.7
11:35	1046.85	34.6	16:05	394	37.5
11:40	1040.55	34.3	16:10	373	37.6
11:45	993	34.6	16:15	337	37.7
11:50	987	34.8	16:20	327	37.6
11:55	989	35.3	16:25	322	37.3
12:00	1005	35.4	16:30	284	37
12:05	834	35.4	16:35	269	36.7
12:10	989	35.4	16:40	259	36.9
12:15	998	35.4	16:45	244	36.6
12:20	995	35.5	16:50	222	36.5
12:25	892	35.2	16:55	193	36.4
12:30	989	35.5	17:00	178	35.8
12:35	988	36	17:05	160	35.2
12:40	983	36.2	17:10	128	34.7
12:45	976	36.4	17:15	95	34.5
12:50	971	36.2	17:20	84	34.2
12:55	964	35.9	17:25	81	33.6
13:00	951	35.9	17:30	67	33.2
13:05	928	35.9	17:35	63	33
13:10	917	35.9	17:40	55	32.8
13:15	924	36	17:45	48	32.6
13:20	919	36.5	17:55	38	32.5
13:25	911	36	18:00	31	32.4
13:30	897	36.2	18:05	0	32.4
13:35	892	36.4	18:10	0	32.1
13:40	879	36.4	18:15	0	31.9
13:45	867	36.4	18:20	0	31.6
13:50	857	36.2			

4.1.2 Solar Energy Generation

The forecast maximum PV power, P_{PV} is depicted in Fig. 4.1(a), which is calculated from equation (3.2). Daily temperatures are analyzed, as the measurement stations are optimally aligned (See Fig. 4.1(b)).

4.1.2.1 Power Production

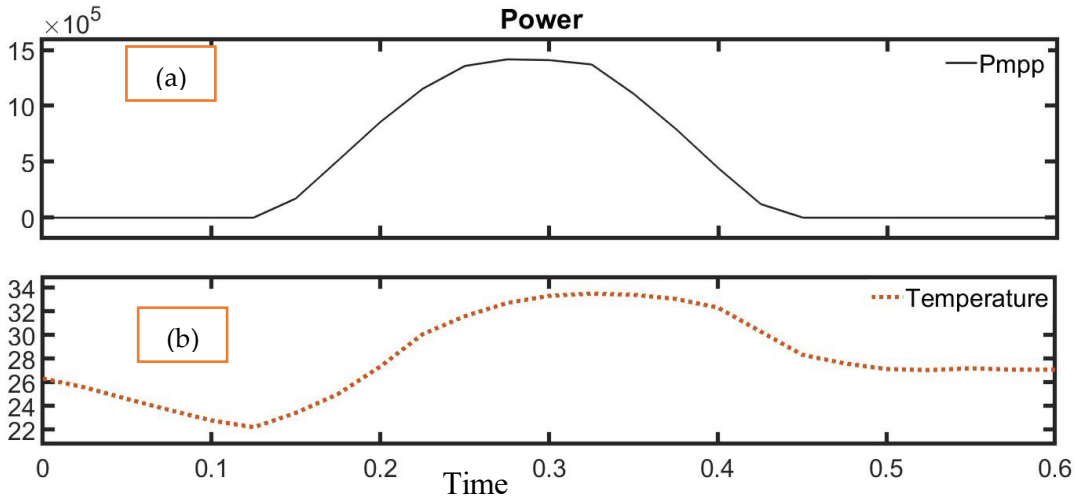


Figure 4.1 The measurement of Solar (a) PV maximum power production (b) Temperature data.

Figure 4.1 discloses the measurement of solar irradiation data[113]. It is observed that solar power production directly depends on solar irradiation. Due to the environmental weather, solar PV power production fluctuates based on irradiation.

4.2 PERFORMANCE ANALYSIS OF MPPT ALGORITHMS

The following section discusses the MATLAB simulation performance results with dynamically varying environmental conditions.

4.2.1 Simulation Result of MPPT$_{(P\&O)}$ Power

The results demonstrate the output power of P&O control MPPT in tracking and extracting the maximum power from the solar panels. Details explanations and comparisons are discussed in section 4.5.

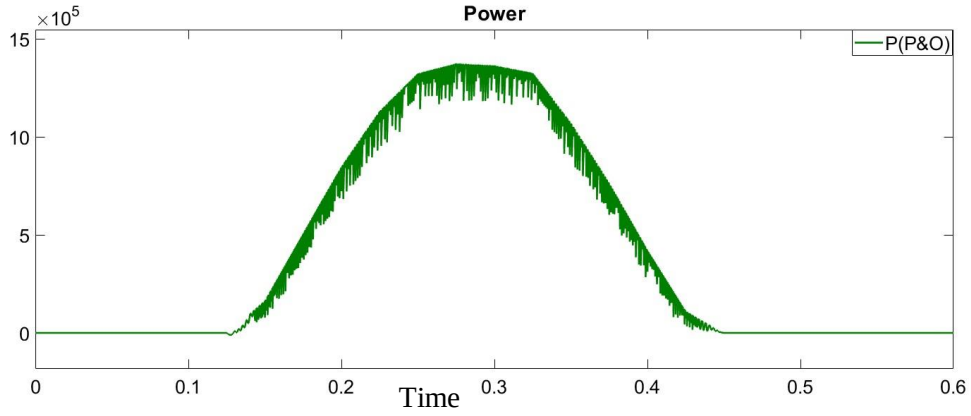


Figure 4.2 Whole-day Observing P&O MPPT PV power.

4.2.2 Simulation Result of MPPT$_{(NN)}$ Power

The results demonstrate the output power of irradiance-temperature (GT) and voltage-current (vi) based NN control MPPT, in tracking and extracting the maximum power from the solar panels. Detailed explanation and comparison will be discussed in section 4.5.

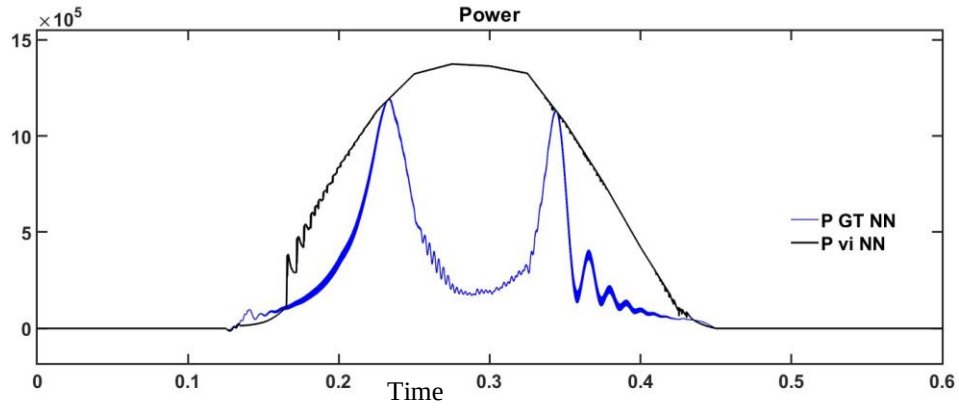


Figure 4.3 Whole-day Observing NN MPPT PV power.

4.2.2.1 Training, Testing & Validation Process

The proposed solar MPPT PV system simulates 1000 seconds of data from a PV array to correlate the sequential transfer function concerning simulation time. The ANN prediction accuracy depends on dataset size, training procedure efficacy and a discrete simulation is employed for optimal analysis. In huge datasets, it neglects the lowest possible error and feeds the solar panel input irradiance and temperature data into clock-synchronized lookup table. In this research, we represent the applicability of solar energy where parameters such

as regression, mean square error, gradient, momentum parameter (Mu), and validation check are often used to evaluate the performance and accuracy of algorithms using training data. The regression model predicts output based on inputs, whereas error is measured by subtracting output from the target. The neural network uses 70% of data for training, 15% for validation, and 15% for testing of samples. The dataset is used for training, and the network is modified based on the resulting error. The network's generalization, which stops training while managing errors, is accomplished by validation. Testing is an independent network performance metric that does not affect the dataset while training.

4.2.2.1.1 Analysis of Levenberg-Marquardt (LM) trained ANN algorithm

The LM-trained ANN algorithm parameters of the research simulation, where the value sample (S), regression (R), mean squared error (MSE), epoch and iteration (E&I), and performance (perform) are described in Table 4.2.

Table 4.2 Levenberg-Marquardt ANN Parameters.

States	**S**	**MSE**	**R**	***E&I***	***Perform***
Training	420001	1.0890e-09	1	1000	1.14e03
Testing	90000	1.0824e-09	1		
Validation	90000	1.0970e-09	1		

The regression curve for the ANN, R =1 shows a precise prediction of output based on input and the correlation between the solar cells' output voltage and target voltage. Often, an error is computed by subtracting the target from the output. The Levenberg-Marquardt method effectively trains data with minimal errors, as illustrated by the regression plot in Figure 4.4, where the output line with the expected values. Figure 4.5 also confirms the ANN method, demonstrating zero errors throughout the training, validation, and testing conditions of data matching. It shows the number of vertical bars in the bin error histogram. The total error of ANN varies from -0.000157 (leftmost bin) to 0.0001106 (rightmost bin). 20 smaller bins with a bin width of 0.000015 are created

from the error range. Every vertical bar indicates how many samples in the dataset fall into a specific bin. From Figure 4.5, for 75 samples of the validation dataset, the bin's error is -0.0000023, which is almost the middle of the error distribution. The neural network-based MPPT demonstrates zero error by the error histogram's convergence at 20 bins.

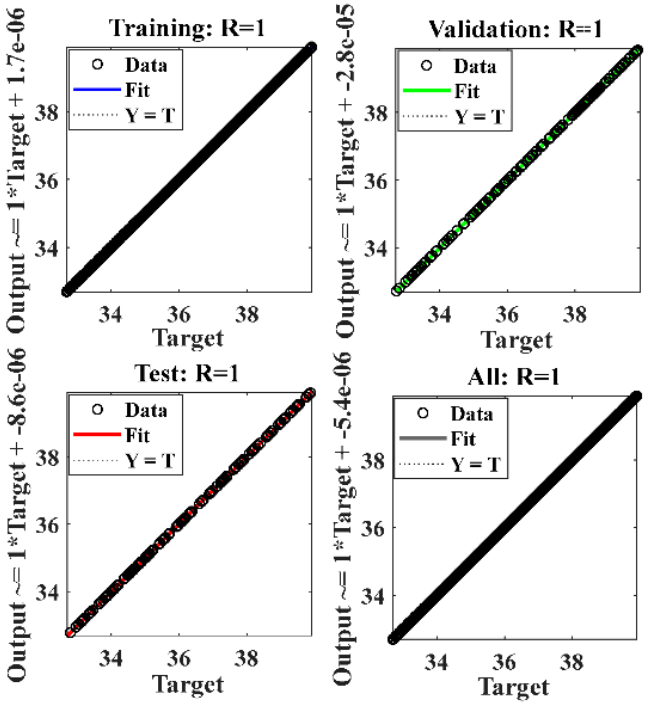


Figure 4.4 Regression plot of the proposed ANN model.

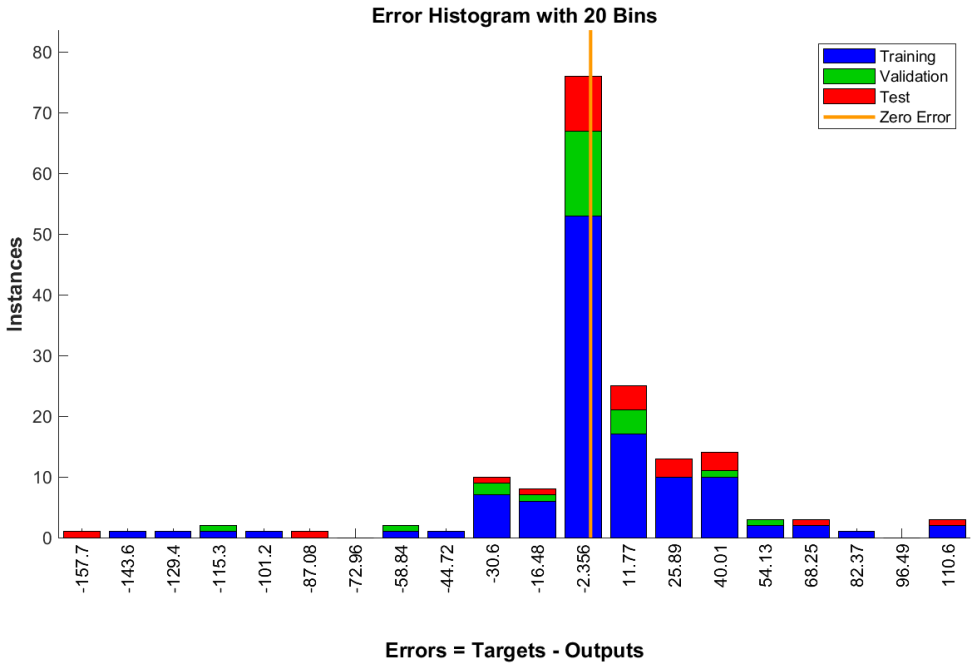


Figure 4.5 Error histogram plot of the proposed ANN PV model.

The ANN's training state and performance phase for managing the chosen dataset are displayed in Figures 4.6 and 4.7. The trained dataset's gradient, momentum parameter (Mu), and validation check are shown at 1000 epochs in Figure 4.6.

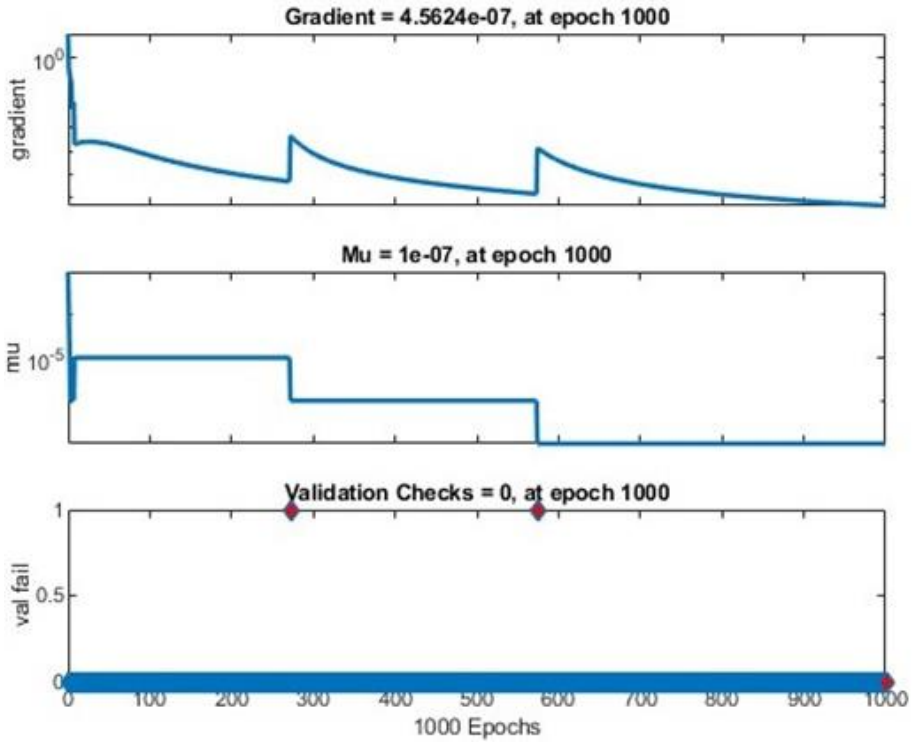


Figure 4.6 Training state plot of the proposed ANN MPPT.

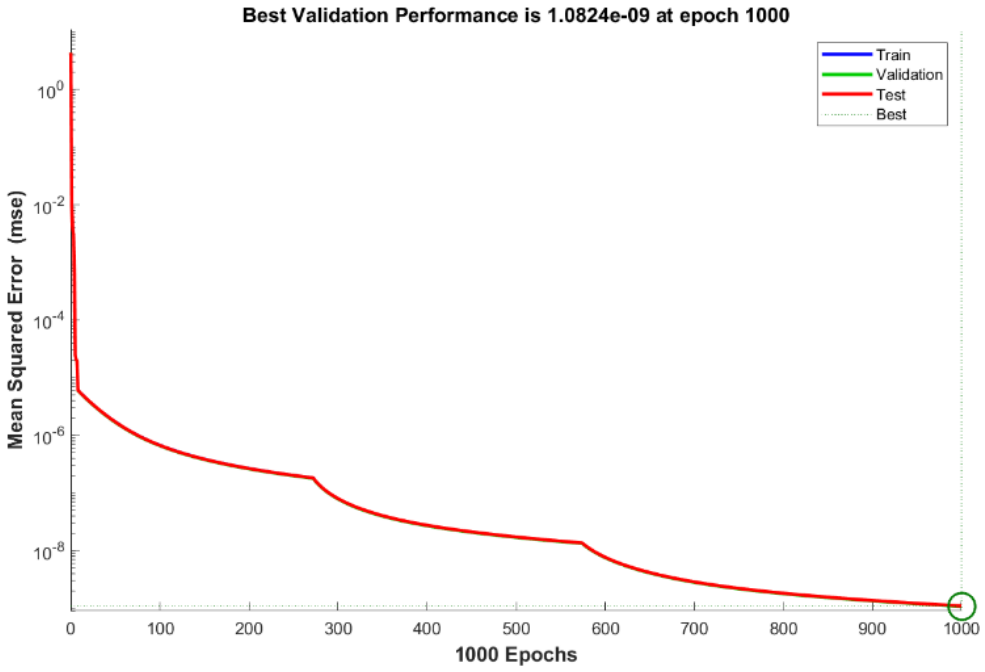


Figure 4.7 Proposed Neural Network Algorithm Performance Test.

The simulation shows a gradient value of 0.0000004562, indicating a small loss function and insignificant departure from training data. The simulation result of a zero-output decision and the mean for each input vector create the combined error. The LM method fit for the MPPT is justified by the training dataset's validation checks, gradient, and a small value of Mu, which is near zero. Figure 4.7 depicts the mean squared error over several epochs, showing that samples from the training dataset converge best at 1000 epochs. At epochs, the result of the training dataset's best validation performance is obtained. The simulation results show that at 1000 epochs, it is 0.0000001. The near-zero validation performance shows negligible error for MPPT prediction using the LM method. For the insights study, this model is an optimization details flowchart illustrated in Figure 3.11. There is a rigorous analysis of ANN algorithms in the study [125]. Table 4.3 summarizes the important performance metrics parameters for the algorithm, considering regression, gradient, middle bin error, performance, momentum parameter, and epochs. The simulation results show that the LM method outperforms the Bayesian Regularization (BR), Gradient Descent Momentum (GDM), Scaled Conjugate Gradient (SCG) and Broyden Fletcher Goldfarb Shanno (BFGS) algorithms for this study regarding precise dataset training and perfect correlation between input and output with low error.

Table 4.3 Comparative Analysis of Levenberg-Marquardt Train ANN Algorithm.

Parameters	***ANN Algorithm Name***				
	LM	***GDM***	***BR***	***SCG***	**BFGS**
Regression	**1**	0.996	0.999999	0.99176	1
Gradient	**4.5624e-07**	11.485	0.00010493	0.26139	1.0211e-7
Middle bin error	**-0.0000023**	-	-0.000037	0.001985	-
Performance	**1.0824e-09**	0.15378	1.583e-7	0.065951	9.98e-17
Momentum parameter	**1e-07**	-	5000	-	-
Epochs	**1000**	2	1000	24	10

The large gradient and error values render the SCG method unsuitable for this study, even though it processes the whole set of data in fewer than 24 epochs [126]. Similarly, the LM algorithm outperforms, with BFGS coming close in gradient and all performance metrics. Besides, BR also performs well across metrics, but SCG and GDM are less effective in resolving this issue. So, the BR method is less suitable than the LM algorithm due to its large momentum parameter and lengthy prediction processing time. The suggested LM approach has several significant benefits for this study. Its simplicity of use stems from the fact that it just needs a few factors, including temperature, solar voltage, and solar irradiance, to produce precise output forecasts. This ease of use improves user-friendliness and expedites the deployment process. However, the LM method may have limitations when dealing with huge volumes of data or in commercial-scale deployment. Despite its challenges, the LM algorithm is a powerful tool for optimizing solar PV integration and improving energy harvesting efficiency in NN-based MPPT PV systems.

4.2.3 Simulation Result of MPPT$_{(Hybrid)}$ Power

The results demonstrate the output power of Hybrid (P&O, NN) control MPPT, in tracking and extracting the maximum power from the solar panels.

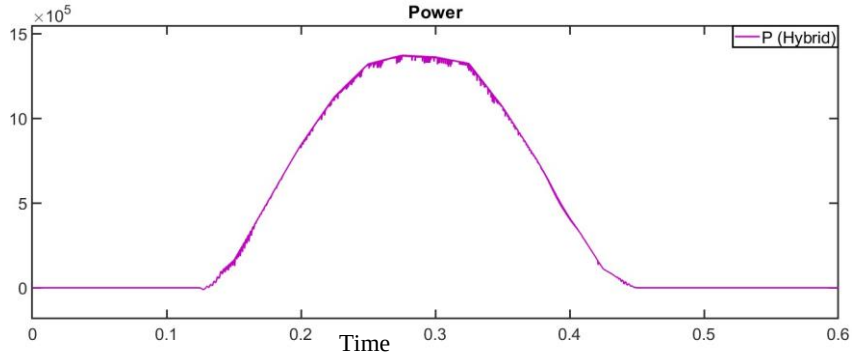


Figure 4.8 Whole-day Observing Hybrid MPPT PV power.

4.3 STORAGE CAPACITY

The battery SoC energy constraints will be kept between 20% and 80% SoC, which will be good for battery health and life cycle. The initial battery energy,

E_{max} is calculated in Chapter 3 using equations (3.22), (3.23) and (3.24), with a 50% SoC assumption, is adjusted for this microgrid using a lithium-ion battery with a minimum 10% SoC, allowing more stored energy to be injected when needed. Battery Energy, $Batt_{Energy} = Batt_{cap} \times 3.6 \times 10^6 = 2500\, kWh \times 3.6 \times 10^6 = 9 \times 10^9\, W$, where the energy generated by a kW power source in one hour is $1kWh = 3.6 \times 10^6\, Joule$. If maximum power, P_{max} is around +400 kW then SoC_{max}= 80% and minimum power, P_{min} is around -400 kW, Thus SoC_{min}= 20%.

Daily basis analysis is performed and evaluated for a battery based integrated grid system. For performance evaluation, the time step for MATLAB simulation operations is set to one day (24 hours, 1440 minutes or 86400 seconds).

4.4 BATTERY OPERATION

The inverter can maintain a relatively low THD on the AC output, even under moderate DC-link capacitor voltage imbalance, depending on the modulation and control strategy used. The battery's simulation results utilizing the case of system operation provide vital details on power, voltage, current, and percentage state of charge (SOC) level. This information has significance for determining the overall performance and efficiency of the solar energy system in reality. The following section describes the result output and Section 4.5 are comparative analysis.

4.4.1 Simulation Result of Battery (P&O)

In the P&O method, the observation and ease of response of battery current, voltage, power and percentage of charge level are illustrated according to irradiance. In this system, the battery current and voltage fluctuate in the high level of irradiance function.

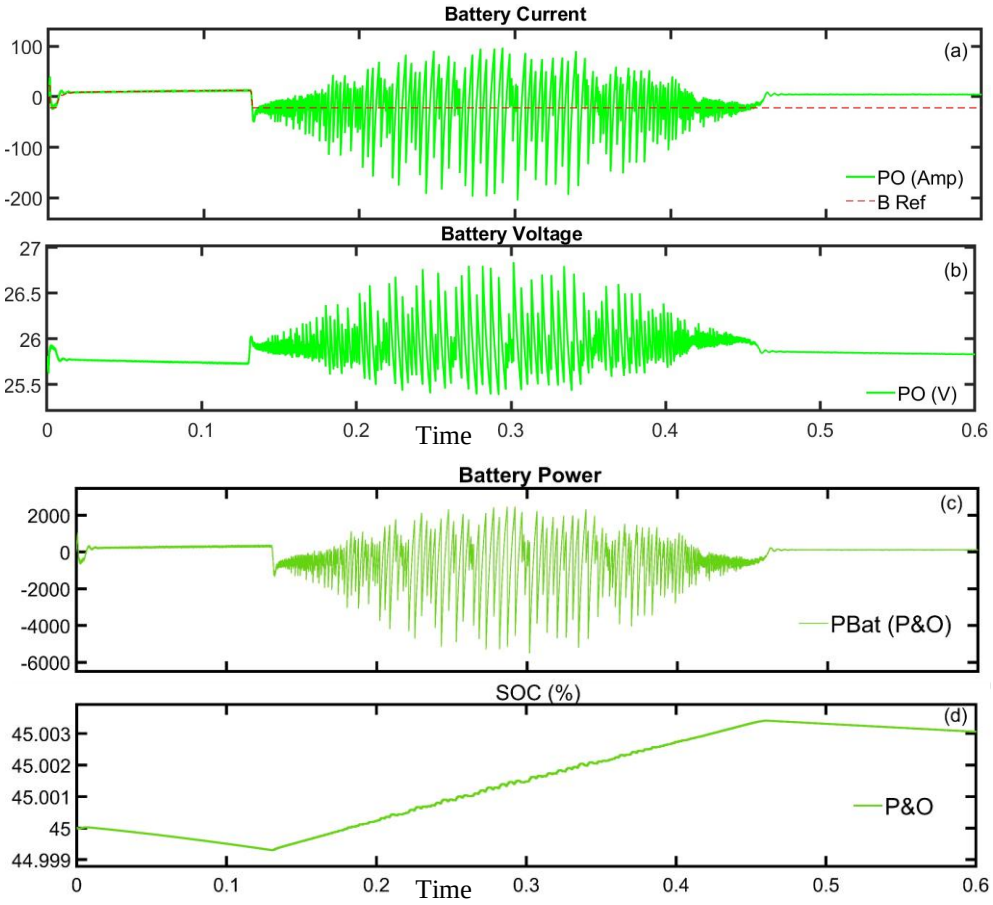
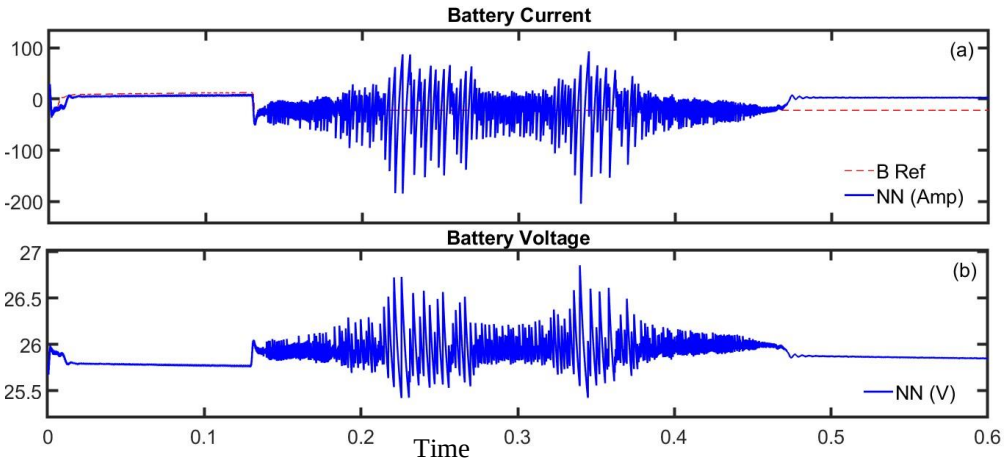


Figure 4.9 Response of Battery (a) Current, (b) Voltage, (c) Power & (c) SOC (%) with varying irradiance and load conditions for P&O System.

4.4.2 **Simulation Result of Battery (NN)**

The NN method presents the observation and ease of reaction of battery current, voltage, power, and % charge level in relation to irradiance. In this system, the battery current and voltage fluctuate at high levels of irradiance but in the case of temperature at the peak point area, it becomes a slow response due to the NN function.



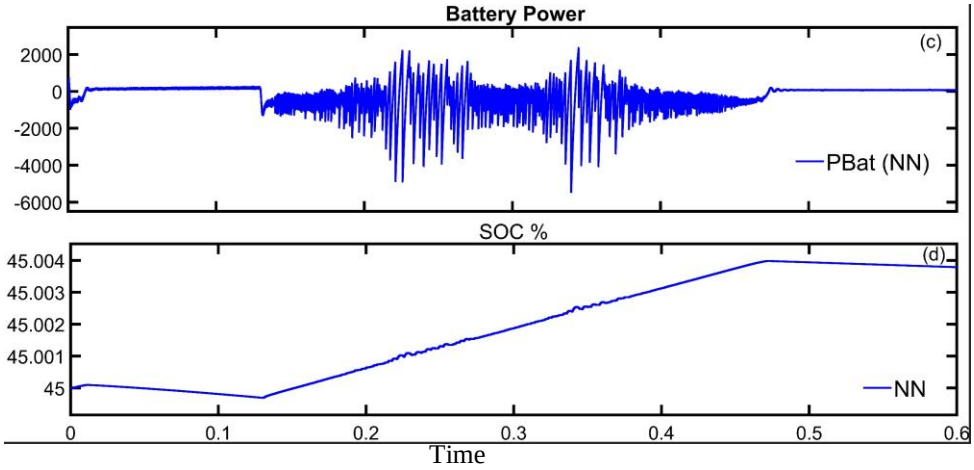


Figure 4.10 Response of Battery (a) Current, (b) Voltage, (c) Power & (c) SOC (%) with varying irradiance and load conditions for Neural Network System.

4.4.3 **Simulation Result of Battery (Hybrid)**

The Hybrid method observation and ease of reaction of battery current, voltage, power, and % charge level in relation to irradiance. In this system, the battery current and voltage are performed superior.

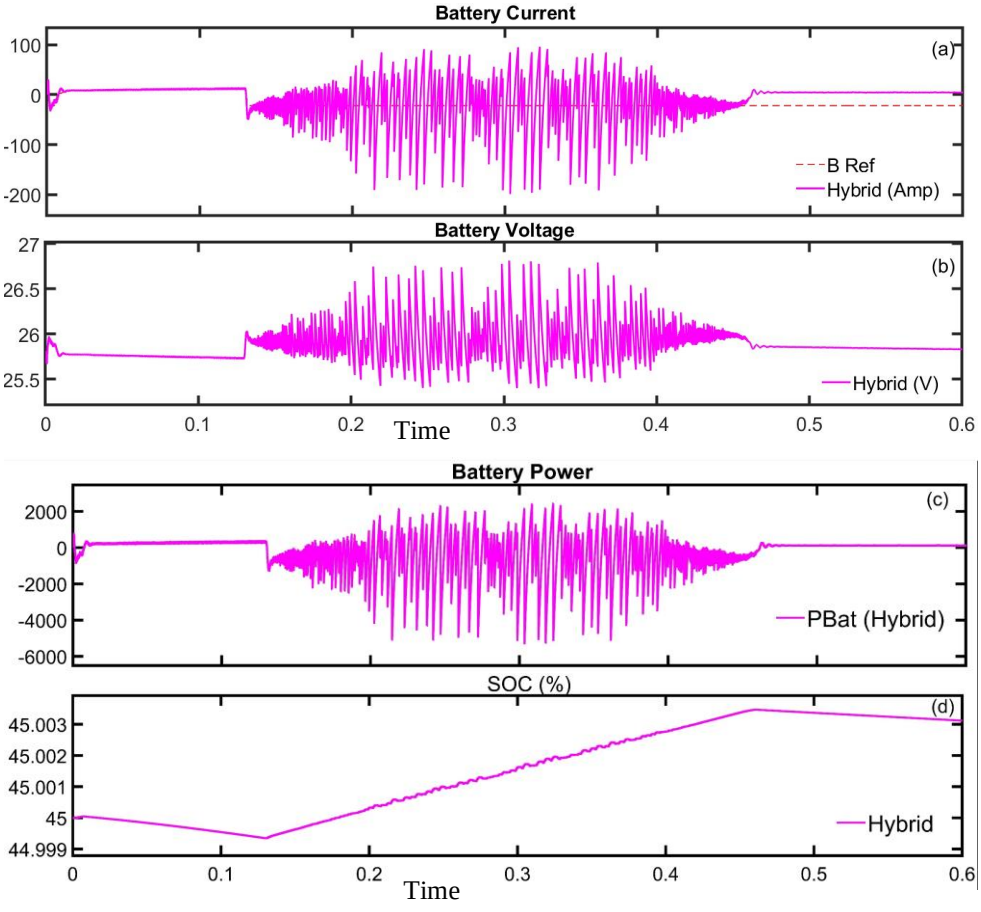


Figure 4.11 Response of Battery (a) Current, (b) Voltage, (c) Power & (c) SOC (%) with varying irradiance and load conditions for Hybrid system.

4.5 COMPARATIVE ANALYSIS

The simulation results depict the system's response to different scenarios, including ambient temperature and sun irradiation inputs for the solar PV module. Based on the findings, the P&O, neural networks, and hybrid (P&O + neural network) methods are denoted by the colors green, blue, and pink. All day long, the time is stepping from 0.1 to 0.6 seconds. Each portion is denoted as 24 hours to 4 hours, respectively, as shown in experiment simulation figure. In the case of a null irradiance level, all performance values start at 0. After a 0.1-second rise and before 0.5 seconds, the curve's level is measured under the irradiation level. The changing level of a power curve at points 0.233 to 0.343 for succinct demand loads of the neural network is observed in Figure 4.12. The change with the P&O power curve starts at 0.131 and is linearly increased till the peak point of 0.277 and then shows a decrease in the lacings of input irradiation on the given Figure 4.12. The response of MPPT at point A is shown in Table 4.4. The simulation results indicate that the neural network-based hybrid MPPT system outperforms traditional methods in both accuracy and efficiency. Point A is increasing power by comparing the cases with maximum PV power.

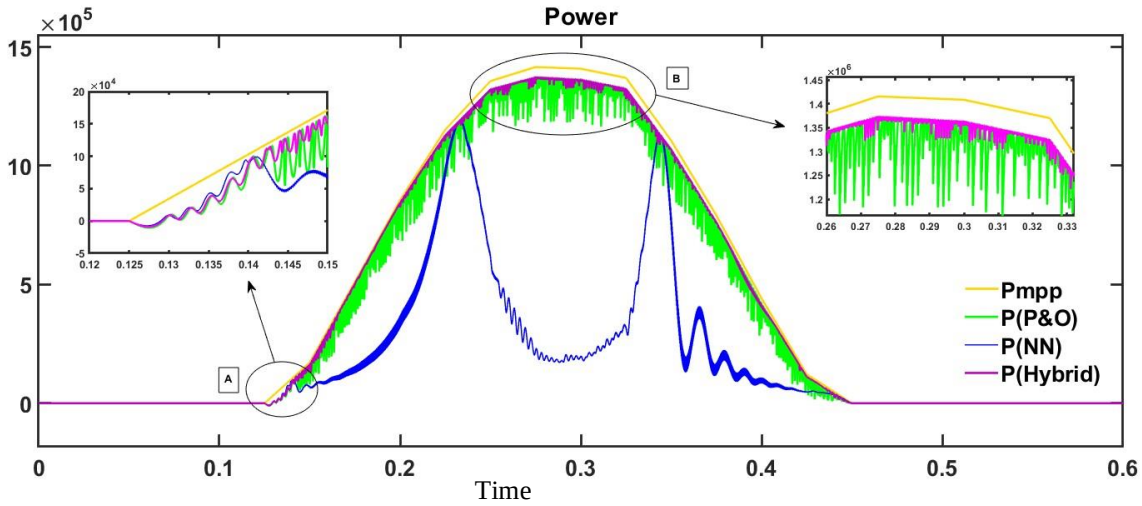


Figure 4.12 Power response comparison of Pmpp, PP&O, PNN, PHybrid.

This system is a dependable choice for optimizing power extraction and grid integration capabilities. It also exhibits resilience and adaptation to shifting environmental circumstances; the power is extracted maximally at Point B.

Table 4.4 Response of Simulation MPPT.

MPPT	*Convergence times*		*Efficiency %*		*Comment*
P&O	0.14	0.145	70	80	Occurs of Oscillation
NN	0.14	0.145	90	72	Dynamic performance
Hybrid	0.14	0.145	96	96	Fast response

The hybrid power curve exhibits the highest level of performance, as shown over the peak condition. The photovoltaic system provides effective power transfer to the load. The photovoltaic system's voltage, current, v bus (DC) and boost current characteristics are shown in Figure 4.13.

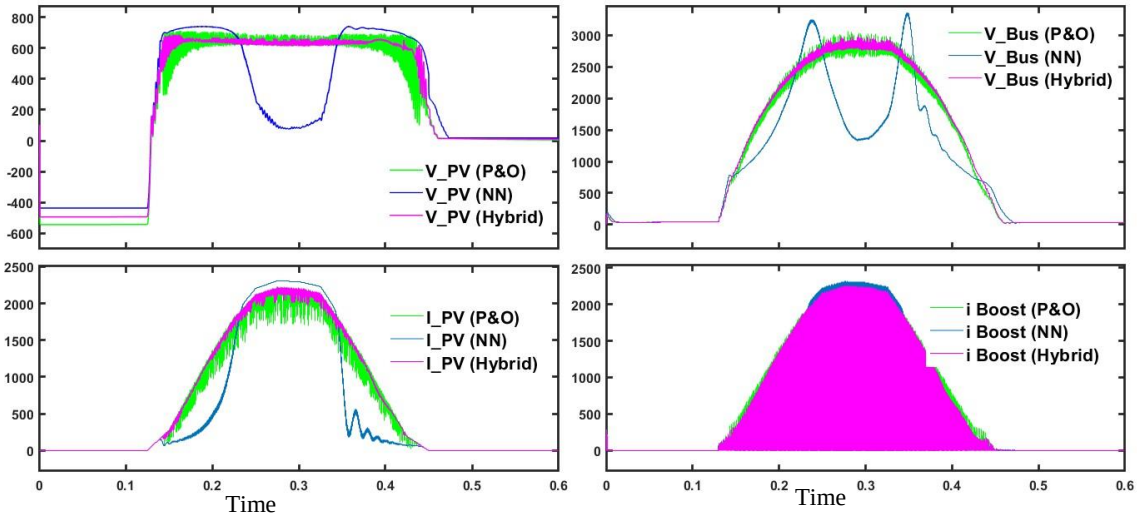


Figure 4.13 Observing whole-day results of PV Voltage, Current, and Bus Voltage and iboost curve of PV array.

The voltage levels are measured with a peak value of 0.150 seconds and a standstill of 0.233. It then drops and overshoots the PV of the neural network by 0.450 seconds due to load demand. At 1850-amp PV current, the hybrid performance varies, which is less than NN performance but still superior to the P&O algorithm, as shown in Figure 4.13. Selecting a suitable MPPT algorithm for PV systems requires that we evaluate the surrounding conditions, quick boost

responses, keep an eye on the stability of the algorithm and maximize energy production. Consider economic and implementation factors, remain up-to-date on industry standards, and investigate breakthroughs in MPPT algorithms to make an informed choice that matches unique system needs. Because of the perception of Figure 4.14, the converter operates at greatest power based on voltage and current values from the P&O, neural network and hybrid (P&O+ neural network) methods. The graphical visualization presents that the battery performance of the NN system is better than the P&O and Hybrid systems. The P&O and hybrid performance of voltage and current look similar to the result, though there is fluctuation as a tiny response, where the NN function system has are slow response due to the effect of temperature at the peak point area.

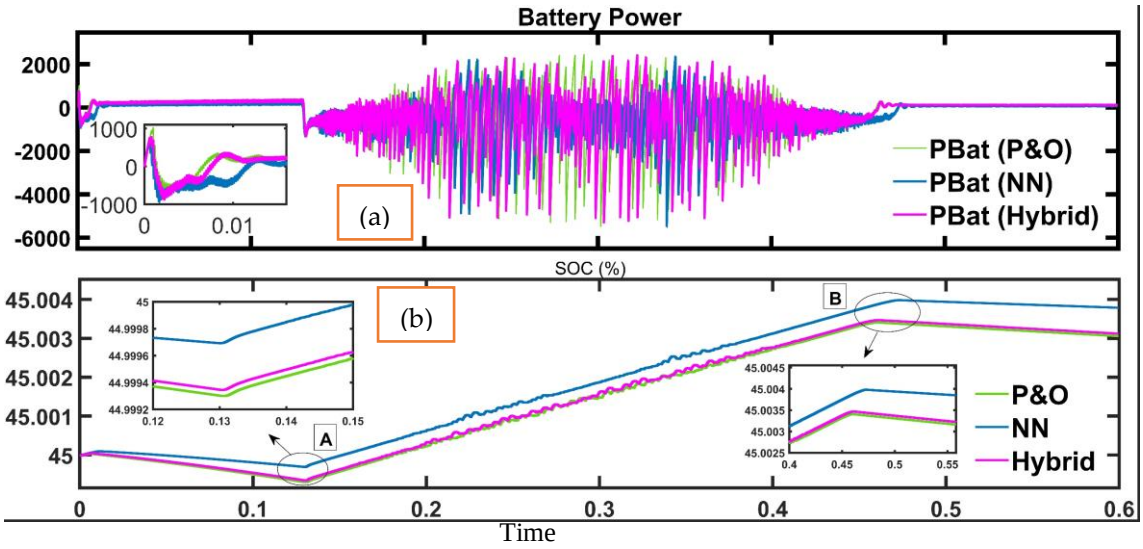


Figure 4.14 Observing whole-day results of PV power, Bus voltage, and SOC, Voltage, Current in Battery Stage.

In Figure 4.14 (a) the starting point of irradiance level, the battery power is empty. when the system starts, a big value fluctuates because the capacitor voltage wants to charge from the DC bus After that the battery power is stable. With the Change of irradiance, the battery condition will charge and discharge along with the DC bus bi-directional DC-to-DC converter from PV. The SOC conditions of Battery charging point A and discharging point B are shown in Figure 4.14 (b). SOC regulates the battery's bus voltage and reference bus voltage.

The reference bus voltage is 48 V, as configured. At roughly a 5 amp drop, the battery SOC indicates that the charging condition is increasing with rising irradiance. Discharge happens when the battery current reaches a maximum of 18 amps, at which point it turns positive with the SOC level lowers.

Furthermore, maximum power is changed based on environmental circumstances. This technique reduces system cost by lowering the number of sensors, while still achieving high efficiency and stability compared to other hybrid MPP tracking methods. The NN-founded MPPT performance is superior to other MPPT performance scenarios, while the stable performance is shown by a hybrid method.

Table 4.5 Comparison of MPPT methods with various Parameters.

Parameters/Items	**P&O**	**NN**	**Hybrid**
Transient behaviours	bad	good	fast
Dynamic behaviours	poor	good	fast
Parameters tuning	no	yes	yes
Tracking	slow	fast	faster
Requirements	P&O algorithm	ML training data	ML & P&O combined
System complexity	simple power calculation	medium	medium

- **Observation of Neural Network Simulation Results:**

Direct Measurement Accuracy:

Input voltage (V) and current (I) provide real-time data for direct maximum power point (MPP) tracking, while irradiance (G) and temperature (T) rely on indirect data, which may introduce delays in MPPT inputs.

Dynamic Response:

VI inputs enable faster neural network MPPT response to load, while GT inputs react more slowly to environmental shifts.

Reduced Complexity:

VI inputs simplify neural network training by directly linking parameters to power output, while GT requires extra modelling and reduced performance.

4.6 PERFORMANCE ANALYSIS OF NPC CONVERTER

The performance study of the NPC converter provides significant details about the solar energy system's reliability and efficiency. By considering critical parameters like power output, generating bus in power quality load, voltage stability, and harmonic distortion, system operators may make informed decisions to improve performance and energy production.

4.6.1 Operation Strategy of Voltage

The suggested hybrid MPPT algorithm, the maximum voltage measured at the PV side of generation is Vpv, while the ultimate output DC bus voltage, Vdc. The maximum range of DC bus voltage is 1000 V. This voltage is converted to approximately 500 V AC by the three-level NPC converter. A DC voltage regulator, which is the controller of this converter, must keep the DC link voltage at 1000V regardless of the amount of active power delivered by the PV array.

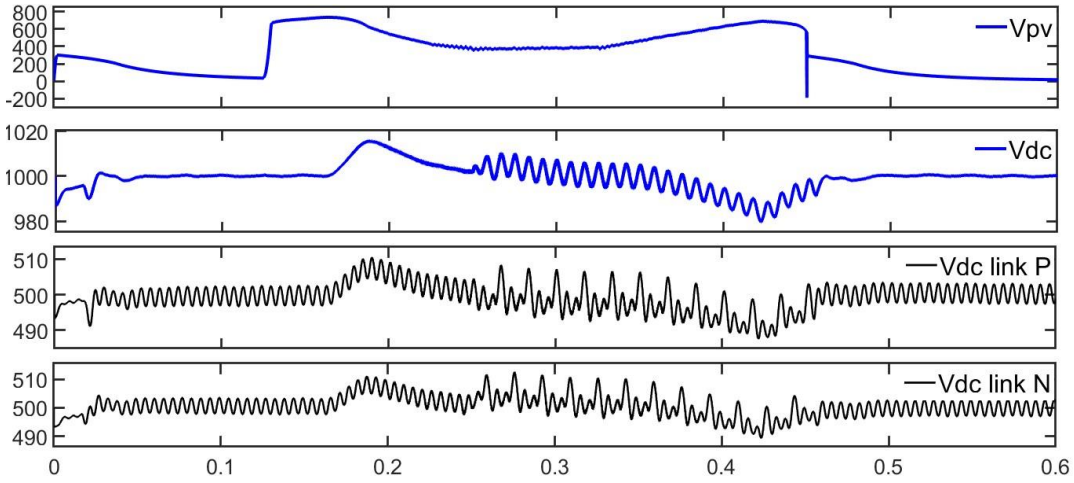


Figure 4.15 Generating Voltage, Vpv; DC Bus Voltage, Vdc and DC link voltage +Vdc/2, -Vdc/2.

Figure 4.15 illustrates the generation of Vpv. The output voltage of the PV boost converter is Vdc, which serves as the DC bus voltage and is split between the positive and negative sides of the Vdc link voltage.

4.6.2 NPC Operation

The NPC converter operation of DC voltage regulator current control is shown in Figure 4.16, where the reference current of both reactive and active current is graphically present according to the reactive and active current of the PLL & Measurements current regulator.

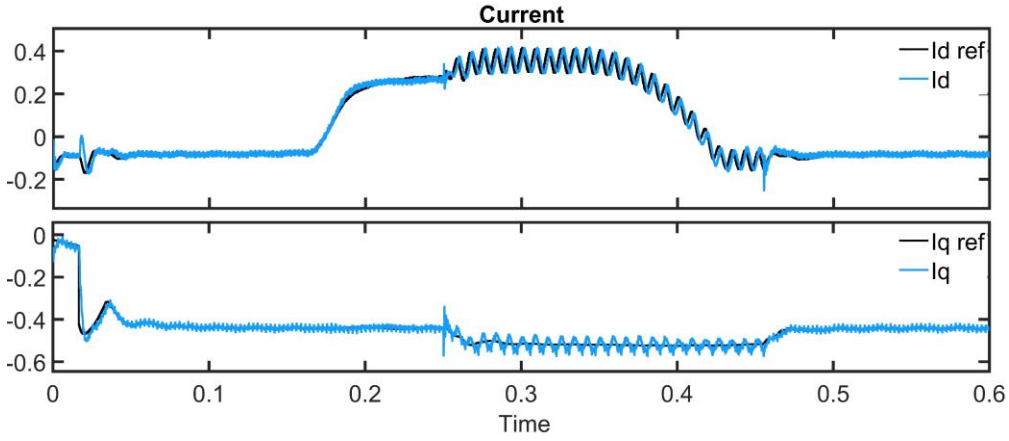


Figure 4.16 Id and Iq curve of the inverter current regulator.

The output of the 3-level NPC converter depends on the value of the modulation index, x. Based on the switching function of the SVPWM technique the range of its ratio x is varied from $0 \leq X \leq 1$ as shown in Figure 4.17 (a) and the 3-level inverter output voltage is displayed in Figure 4.17 (b) which has five voltage output levels (Vdc, Vdc/2, 0, -Vdc/2 and -Vdc) based on switching frequency. According to the duty cycle of the switches at 5 KHz frequency shown in Figure 4.18, regarding the sawtooth waveform.

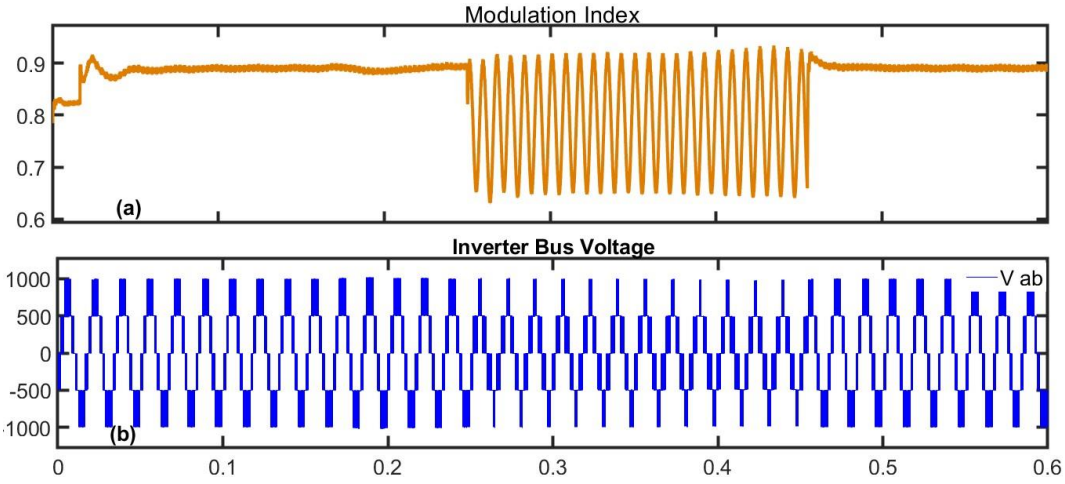


Figure 4.17 (a) Modulation Index; (b) 3-level PWM inverter line-to-line output voltage.

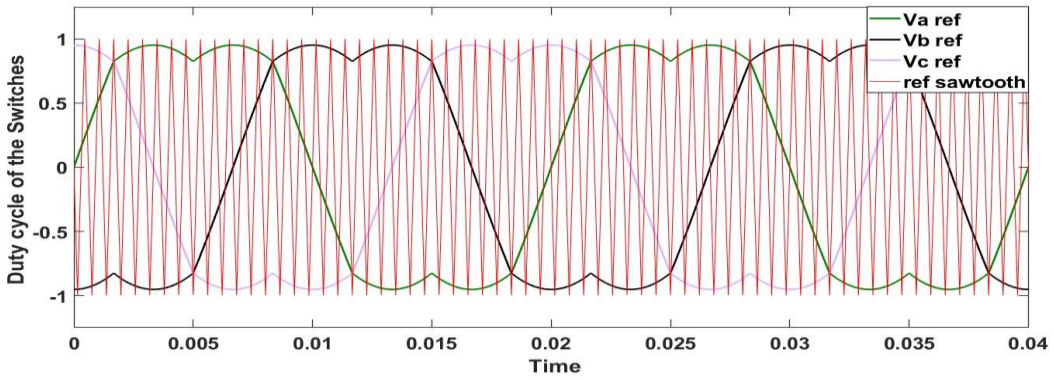


Figure 4.18 Duty cycle of the Switches with reference sawtooth waveform of frequency 5 kHz (SVPWM)

4.7 SYSTEM-LEVEL ANALYSIS: GRID CONNECTED PERFORMANCE

4.7.1 THD Evaluation

The experimental grid waveforms for the rated inverter output currents, $I\ (I_a, I_b, I_c)$ and output voltage, $V\ (V_a, V_b, V_c)$ are shown in Figure 4.19. The inverter system with the LC filter operates effectively with the current controller as it is currently specified. For this proposed model, the regulator of active and reactive power is the controller to allow the converter to generate or absorb up to 1 MW. Figure 4.20 shows the overall experimental grid-connected PV system output power waveforms.

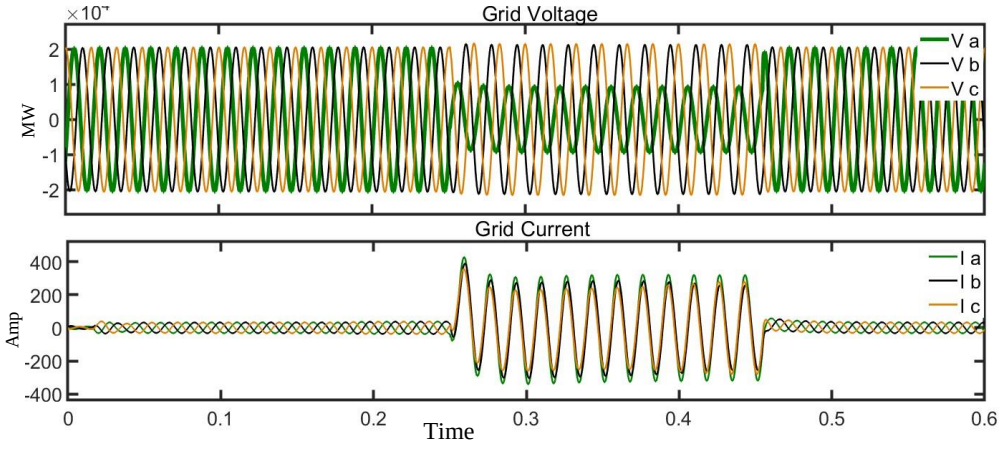


Figure 4.19 Experimental waveforms of 3-phase grid Voltage (Vabc) and Current (Iabc) a, b, c at rated output.

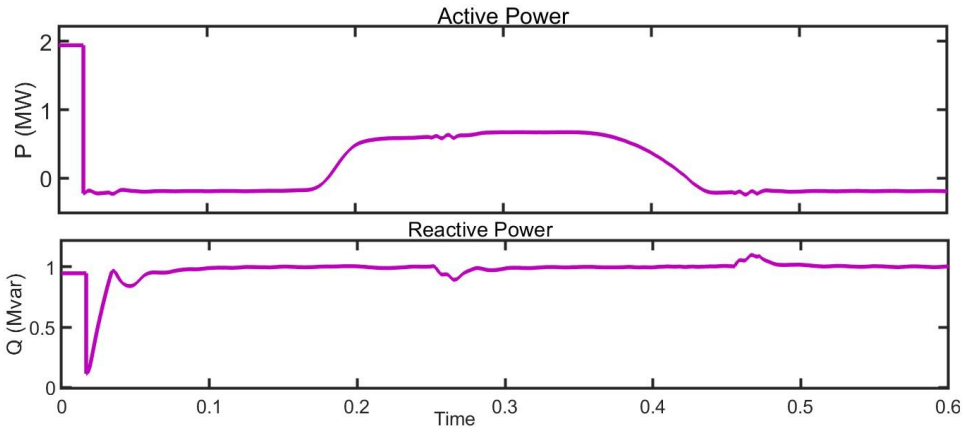


Figure 4.20 Output active and reactive power of the grid, P MW & Q MW.

The reduction of the harmonic content of the spectrum-modulated waveshape depends on the switching frequency. The frequency must be six times greater than the fundamental frequency. For the normalized amplitude of harmonic components based on 60Hz fundamental frequency, the Fast-Fourier-Transformation (FFT) is calculated until the maximum frequency 1k Hz for the waveform signal THD from Figure 4.19, grid current and voltage separately. The whole waveform of the selective FFT window is the phase-to-neutral inverter output current and voltage. In addition, the corresponding FFT analysis of the output total harmonic distortion current and voltage of the inverter grid is presented in Table 4.6.

Table 4.6 FFT Analysis of THD (SVM)

Time		***Number of Cycles***	***Current THD (%)***			***Voltage THD (%)***		
start	end		Ia	Ib	Ic	Va	Vb	Vc
0.1	0.24	15	20.59	20.39	21.77	0.60	0.61	0.62
0.25	0.44	12	11.33	10.08	8.15	2.75	0.86	0.89
0.45	0.6	9	55.47	51.11	66.26	7.18	1.19	1.24
0.1	0.6	36	72.33	61.73	227.4	22.65	2.82	2.41

The SVPWM technique mitigates the THD level eloquently. After simulating the SVPWM approach, the THD level is reduced, as shown in Table 4.7.

Table 4.7 FFT Analysis of THD (SVPWM)

Time		*Number of Cycles*	*Current THD (%)*			*Voltage THD (%)*		
start	end		Ia	Ib	Ic	Va	Vb	Vc
0.1	0.24	15	41.86	38.60	39.35	0.57	0.57	0.57
0.25	0.44	12	6.47	8.70	11.93	2.53	0.72	0.70
0.45	0.6	9	8.37	6.53	6.83	7.17	1.18	1.21
0.1	0.6	36	67.71	113.86	103.03	22.93	2.27	2.57

Considering the number of cycle values, the percentage of THD is the standard level of IEC & IEEE permissible in each phase [127]. After a whole day of observation, it significantly limits the reliability of our research THD level unacceptably exceeds IEEE 519–1992 limits. THD levels exceeded the IEEE 519–1992 limit of 5% during extended operation, primarily due to inadequate neutral-point management in the modulation system, unbalanced DC-link voltages, and improper vector placement. Together with nonlinear load effects and switching device thermal drift, these problems significantly distorted the waveform. As a result, harmonic content exceeded permitted levels, jeopardizing system dependability and power quality compliance.

4.7.2 Power Quality Assessment

The power quality evaluation ensures the solar energy system operates at its best and lasts a long time by assessing the system's capacity to provide clean and reliable electricity. Operators can see any problems and take remedial action to maintain high power quality standards by keeping an eye on variables such as generation, Bus, PQ load, voltage fluctuations, and frequency changes.

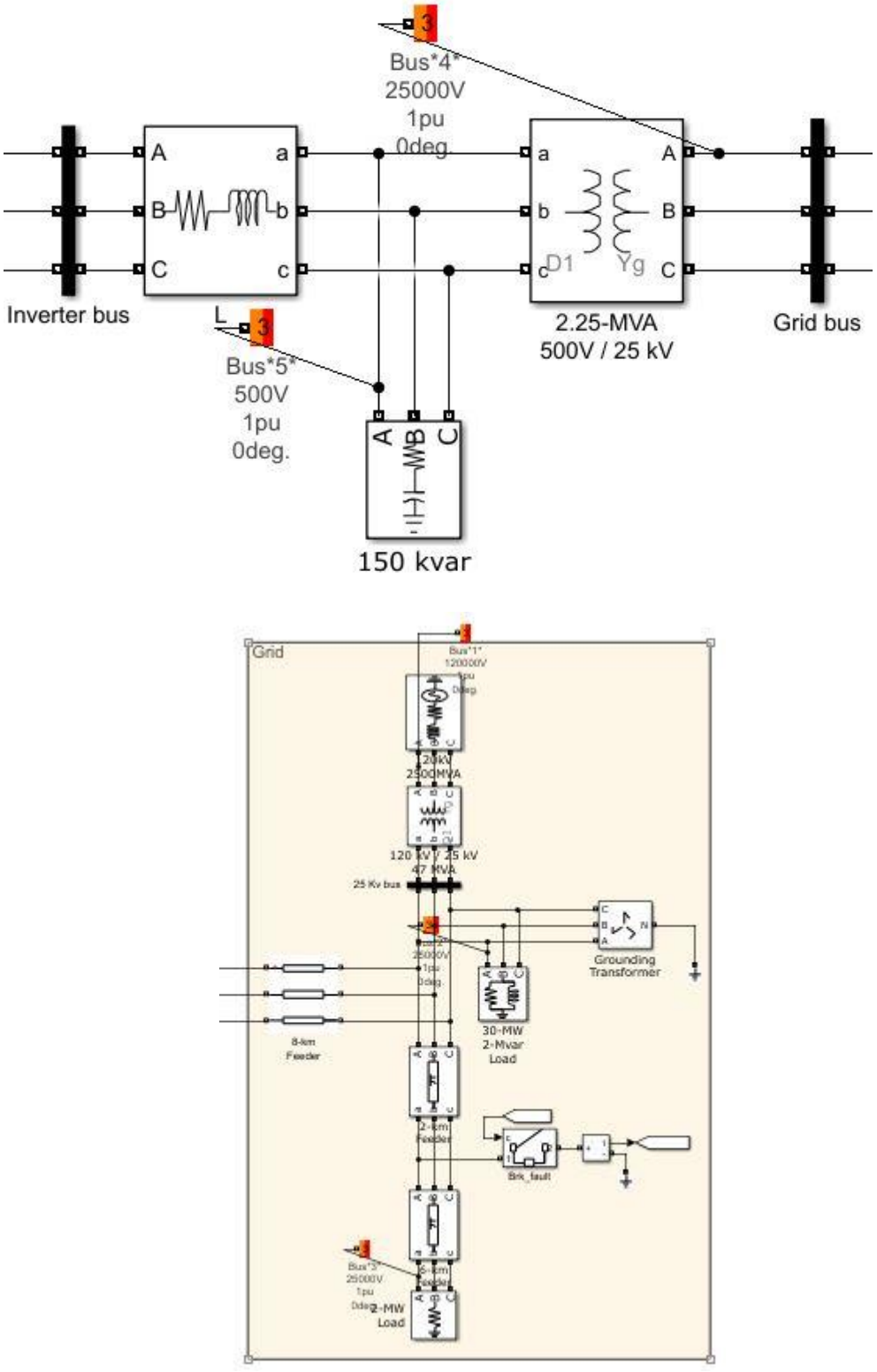


Figure 4.21 Load Flow Analysis Experimental on Proposed PV Model.

The subnetwork of this profile model is iterated in 15 times. The output result of the converged is calculated in Table 4.8.

Table 4.8 Load flow converged in 15 iterations

Summary	P (MW)	Q (Mvar)
Total Generation	17590.70866	548.6935902
Total PQ load	-2.26886E-05	-0.009294638
Total Z shunt	17556.40926	1097.405044
Total losses	34.29941917	-548.7021594
1: Bus*1* V= 1.000 pu/120kV 0.00 deg; Swing bus		
Generation	17590.70866	548.6935902
PQ Load	0	0
Z shunt	17556.40919	1097.363345
Bus*2*	34.29947096	-548.6697546
2: Bus*2* V= 0.000 pu/25kV 146.31 deg		
Generation	0	0
PQ Load	-1.76754E-05	-0.009294511
Z shunt	6.97497E-05	0.041699104
1	9.41709E-06	-3.88775E-12
Bus*1*	-6.24757E-05	-0.032404629
Bus*4*	9.84344E-07	3.54881E-08
3: Bus*3* V= 0.000 pu/25kV 146.31 deg		
Generation	0	0
PQ Load	-8.43241E-07	-4.81432E-13
Z shunt	1.86261E-09	7.45859E-12
1	8.41379E-07	-6.97715E-12
4: Bus*4* V= 0.000 pu/25kV 147.80 deg		
Generation	0	0
PQ Load	-2.1489E-06	-6.02249E-08
Z shunt	2.63715E-06	1.75836E-07
Bus*2*	-5.72248E-07	-3.55378E-08
Bus*5*	8.39936E-08	-8.00732E-08
5: Bus*5* V= 0.000 pu/0.5kV -154.11 deg		
Generation	0	0
PQ Load	-2.02118E-06	-6.72334E-08
Z shunt	2.095E-06	1.39677E-07
Bus*4*	-7.38242E-08	-7.2444E-08
6: *1* V= 0.000 pu/25kV 146.31 deg		
Generation	0	0
PQ Load	1.16619E-10	7.07308E-17
Z shunt	8.07473E-23	4.13843E-21
Bus*2*	-9.94558E-11	-6.08892E-17
Bus*3*	-1.71636E-11	-9.84574E-18

4.7.3 Reliability

The system reliability operators must do routine maintenance checks, monitor performance data, and execute any necessary updates or repairs. Solar energy systems may function at their highest efficiency levels and optimize energy output in the long run by giving priority to these factors.

4.8 SUMMARY

The chapter is organized based on the performance and outcome analysis of the integrated grid-connected PV system. The simulation experiment of different case studies on MPPT algorithms, Battery performance, NPC converter operation, and key findings is discussed. The Hybrid MPPT performance is superior to other approaches. The different parameter measurements of an integrated PV grid system on various environmental conditions were calculated and graphically represented. The setup optimization parameters of the NPC converter with the integrated grid and system-level performance were briefly investigated and discussed. The comparison of the MPPT algorithm with battery storage approaches was analyzed. Therefore, the performance comparison of the P&O, NN, and Hybrid MPPT was graphically illustrated. THD mitigation analysis in two different SVM and SVPWM approaches, where the system-level analysis of the THD performance exceeds IEEE 519–1992 limits. The assessment of the load flow converged with six Buses. Therefore, this chapter proposes a neural network-based hybrid MPPT algorithm with an NPC converter integrated grid system.

5 Conclusions and Future Study

Thus far, we have provided the study and simulation findings chapter by chapter. This chapter summarizes the previous chapter's introduction, methodology, results, and discussion. It briefly summarizes the results of the thesis study. It includes general key findings, conclusions, limitations, implications, and suggestions for future recommendations. Section 5.1 presents a summary of this research without detailed interpretation. The important results are connected, and Sections 5.2 and 5.3, respectively, address some potential implications. Section 5.4 also covers ethical issues. Section 5.5 discusses the limitations of the study, followed by future research directions and recommendations for a machine learning based MPPT PV system on the developed grid connected theoretical NPC converter framework.

5.1 SUMMARY

Battery-based, grid-connected photovoltaic systems are increasingly popular for boosting renewable energy sources alongside traditional electrical power to meet the world's growing energy demand while minimizing environmental impact. However, the main challenge in generating a consistent energy flow from solar power is the sun's intermittent nature. To address this issue, an ANN-based MPPT approach in machine learning has been proposed in this study. It provides the capability to ensure the photovoltaic system continuously adjusts its operating point based on real-time data from environmental sensors such as temperature and solar radiation.

Initially, we explore perturb and observe MPPT, an innovative method for integrating renewable energy sources into the utility of a battery-based grid-

connected solar PV system. The primary goal of this thesis is to reduce energy waste from the proposed solar PV system. A battery-based, grid-connected solar PV system with a 1,500 KW capacity has been proposed for this purpose. Additionally, we compared different MPPT algorithms, including P&O, neural network, and a hybrid approach combining both. Our results showed that hybrid algorithms yield better outcomes. The machine learning-based MPPT responded faster than individual approaches because the ANN-based MPPT quickly adjusts the system's operating point.

Furthermore, we analyze the performance of a solar PV system having an NPC converter integrated with a grid-scale battery system, which helps to convert the energy from solar PV to the utility grid. The converter adjusts the duty cycle of the SV-PWM technique by converting the voltage (power) as a reference point smoothly. Additionally, the total harmonic distortion of current and voltage (%THD i, v) are considered with FFT analysis.

The conclusion of this comparison between the three different algorithm performances the storage system of NN was outperformed than others. The simulation results revealed that the hybrid MPPT was much more effective compared to others.

5.2 KEY INSIGHTS

The insights of the proposed PV model are listed as follows:

- Discussion on MPPT Technology in Energy Harvesting.
  - ✓ Perturb & Observe (P&O)
  - ✓ Neural Network (Artificial Neural Network)
  - ✓ Hybrid (P&O + $NN_{GT)}$
- The recommended Hybrid MPPT PV model was more affordable than any other case studied during analysis.

- NNs can conform swiftly to shifts in solar irradiance and temperature.
- The LM algorithm train NN outperforms, where BFGS comes close in gradient and all performance. Besides, BR also performs well across metrics, but SCG and GDM are less effective in resolving this momentum parameter and lengthy prediction processing time issue.
- The PV system operates at its maximum efficiency on a hybrid MPPT system.
- The NN-based MPPT system's energy storage battery operation performance is better than that of the P&O and Hybrid systems.
- The tiny scale of SOC change (0.001%) indicates a particularly resilient or enormous battery system, with control mechanisms fine-tuning minute SOC variations rather than managing large-scale energy storage. The differences between the methods are subtle but numerically discernible.
- Maintain a stable DC-link voltage, which is crucial for efficient energy conversion with an NPC converter.
- Voltage as a reference point is adjusting the duty cycle of SV-PWM, which performs successfully with the NPC converter.
- Simulation result shows that the THD level performs under IEC and IEEE 519–1992 limits.

5.3 CONTRIBUTION

The advanced battery-based grid system and end-users (prosumers and consumers) are introduced. It is still facing impossible to implication new machine learning MPPT ideas in the practical field due to the lack of good management tools for power systems. Previous work often concentrates on energy-related issues rather than providing an effective and workable battery-based grid operation. This thesis presents a comprehensive design for a grid-

connected solar PV model that utilizes machine learning for MPPT and features a neutral point clamped converter. The proposed battery-based grid-connected model is designed to perform effectively across various sectors, including residential, commercial, and industrial applications.

5.4 ETHICAL CONCERNS

The whole writing process followed the Chittagong University of Engineering and Technology's writing format for the thesis. The author conducted all thesis-related computations and collected historical data for analysis from the following sources: (1) http://www.sreda.gov.bd/; (2) https://www.idcol.org/; and (3) http://power.larc.nasa.gov/data-access-csv. The set of data mentioned in the procedure was obtained for this detection process by myself.

5.5 LIMITATIONS OF THE STUDY

The prime importance of this thesis study is to harvest more energy from the operating solar MPPT technique. However, there are some limitations of the study of the proposed PV model are listed as follows:

- Variation in solar irradiance and temperature affects MPPT efficiency.
- Neural Network MPPT requires extensive training in fine-tuning operations on all conditions.
- The proposed system functions effectively in small to medium-scale solar and battery-based PV grid systems.
- During energy harvesting using the grid energy (purchase) system, battery charging is not a feasible option.

5.6 RECOMMENDATION FOR FURTHER STUDY

This will encourage new scholars to explore this field, as no relevant studies have been conducted in Bangladesh. This research might be carried to a whole new level in the future, as described below:

- NN train MPPT system, the future integration with advanced technologies, like Levenberg-Marquardt (LM) with Reinforcement Learning (RL) and metaheuristic optimization for Adaptive MPPT and Quantum Neural Networks (QNNs) to enhance LM-based training by leveraging quantum parallelism for faster weight updates.
- Practical validation dataset for considering real plant simulation results.
- Implement supercapacitor integration to handle transient power demands and improve battery longevity.
- Improving 3-level NPC converter with grid operation, where battery-based net metering is available to address the distribution utilities.

Bibliography

[1] C. R. Sarin, G. Mani, A. A. Stonier, G. Peter, P. Kumaresan, and V. Ganji, "An extensive critique on expert system control in solar photovoltaic dominated microgrids," *IET Renewable Power Generation*, no. July, pp. 1–16, 2023, doi: 10.1049/rpg2.12875.

[2] Kamavisdar, P., Saluja, S. and Agrawal, S., "A survey on image classification approaches and techniques.," *International Journal of Advanced Research in Computer and Communication Engineering*, vol. 2.1, pp. 1005–1009, 2013.

[3] N. Housseini, … A. O.-I. T. on, and undefined 2017, "Robust nonlinear controller design for on-grid/off-grid wind energy battery-storage system," *ieeexplore.ieee.orgB Housseini, AF Okou, R BeguenaneIEEE Transactions on Smart Grid, 2017•ieeexplore.ieee.org*.

[4] N. Al-Masri, M. E.-I. T. on Industry, and undefined 2015, "Feasibility investigation of a hybrid on-grid wind photovoltaic retrofitting system," *ieeexplore.ieee.orgHM Al-Masri, M EhsaniIEEE Transactions on Industry applications, 2015•ieeexplore.ieee.org*.

[5] "2012 Index IEEE Transactions on Smart Grid Vol. 3," *IEEE Trans Smart Grid*, vol. 3, no. 4, pp. 2297–2330, Jan. 2013, doi: 10.1109/TSG.2013.2239371.

[6] F. Fazelpour, M. Vafaeipour, O. Rahbari, and M. A. Rosen, "Intelligent optimization to integrate a plug-in hybrid electric vehicle smart parking lot with renewable energy resources and enhance grid characteristics," *Energy Convers Manag*, vol. 77, pp. 250–261, Jan. 2014, doi: 10.1016/J.ENCONMAN.2013.09.006.

[7] T. Urmee and A. Md, "Social, cultural and political dimensions of off-grid renewable energy programs in developing countries," *Renew Energy*, vol. 93, pp. 159–167, Aug. 2016, doi: 10.1016/J.RENENE.2016.02.040.

[8] A. El Hammoumi, S. Chtita, S. Motahhir, and A. El Ghzizal, "Solar PV energy: From material to use, and the most commonly used techniques to maximize the power output of PV systems: A focus on solar trackers and floating solar panels," *Energy Reports*, vol. 8, pp. 11992–12010, Nov. 2022, doi: 10.1016/J.EGYR.2022.09.054.

[9] M. A. Koondhar, I. A. Laghari, B. M. Asfaw, R. Reji Kumar, and A. H. Lenin, "Experimental and simulation-based comparative analysis of different parameters of PV module," *Sci Afr*, vol. 16, p. e01197, Jul. 2022, doi: 10.1016/J.SCIAF.2022.E01197.

[10] “https://www.alternative-energy-tutorials.com/solar-power/grid-connected-pv-system.html#google_vignette”.

[11] “Classification of grid connected photovoltaic systems - Grid Connected Solar PV Electric Power.” Accessed: Jan. 12, 2025. [Online]. Available: https://solarenergyandpowersystems.com/classification-of-grid-connected-photovoltaic-systems/

[12] “Energy Storage Systems.” Accessed: Jan. 12, 2025. [Online]. Available: https://www.monolithicpower.com/en/learning/mpscholar/ac-power/the-power-grid/energy-storage-systems

[13] A. E. Gürel, Ü. Ağbulut, H. Bakır, A. Ergün, and G. Yıldız, “A state of art review on estimation of solar radiation with various models,” *Heliyon*, vol. 9, no. 2, 2023, doi: 10.1016/j.heliyon.2023.e13167.

[14] P. Madasamy *et al.*, “Neutral Point Clamped Transformer-Less Multilevel Converter for Grid-Connected Photovoltaic System,” *Electronics 2021, Vol. 10, Page 977*, vol. 10, no. 8, p. 977, Apr. 2021, doi: 10.3390/ELECTRONICS10080977.

[15] S. Alepuz *et al.*, “A Survey on Capacitor Voltage Control in Neutral-Point-Clamped Multilevel Converters,” *Electronics 2022, Vol. 11, Page 527*, vol. 11, no. 4, p. 527, Feb. 2022, doi: 10.3390/ELECTRONICS11040527.

[16] M. Hafeez, M. Hariri, M. Khairunaz, M. Desa, and S. Masri, “Grid-connected PV generation.,” *Energies (Basel)*, vol. 13, no. 17, p. 4279, 2020.

[17] D. W. Kim *et al.*, “Characteristic analysis of HTS magnet charging system combined with PV system using MPPT control,” *Journal of the Korea Institute of Applied Superconductivity and Cryogenics*, vol. 14, no. 1, pp. 8–13, 2012, doi: 10.9714/PSAC.2012.14.1.008.

[18] H. Dallagi, “Study, analysis and simulation of three phase three-level, five-level and seven-level neutral-point-clamped inverters by PSIM,” *STA 2014 - 15th International Conference on Sciences and Techniques of Automatic Control and Computer Engineering*, pp. 654–660, Apr. 2014, doi: 10.1109/STA.2014.7086707.

[19] A. N. Deshmukh and V. K. Chandrakar, “Analysis and Mitigation of Power Quality (Pq) Issues in 0.3Mw Solar Photovoltaic System (Spv) Connected To Grid With Mppt Tracker and Controlled Load Using Pscad Software,” *Engineering Review*, vol. 44, no. 1, pp. 99–115, 2024, doi: 10.30765/er.2397.

[20] A. H. Fathima and K. Palanisamy, “Optimization in microgrids with hybrid energy systems – A review,” *Renewable and Sustainable Energy Reviews*, vol. 45, pp. 431–446, 2015, doi: https://doi.org/10.1016/j.rser.2015.01.059.

[21] R. Falkner, "The Paris Agreement and the new logic of international climate politics," *Int Aff*, vol. 92, no. 5, p. 1107-1125, Sep. 2016, doi: 10.1111/1468-2346.12708.

[22] "Goal 7 | Department of Economic and Social Affairs." Accessed: Jan. 13, 2025. [Online]. Available: https://sdgs.un.org/goals/goal7

[23] "COP29 Azerbaijan - United Nations Climate Change Conference." Accessed: Jan. 13, 2025. [Online]. Available: https://cop29.az/en/home

[24] "https://www.statista.com/statistics/222066/projected-global-energy-consumption-by-source/#statisticContainer."

[25] P. D. board Bangladesh, "Annual Report 2023-24," 2023.

[26] "Final Report Ministry of Power, Energy and Mineral Resources Government of the People's Republic of Bangladesh Integrated Energy and Power Master Plan (IEPMP) 2023," 2023.

[27] A. García-Olivares and J. Ballabrera-Poy, "Energy and mineral peaks, and a future steady state economy," *Technol Forecast Soc Change*, vol. 90, no. PB, pp. 587–598, Jan. 2015, doi: 10.1016/J.TECHFORE.2014.02.013.

[28] "Bangladesh Power Development Board-Government of the People\'s Republic of Bangladesh."

[29] "Power-System-Master-Plan-2016 - Power Division-Government of the People\'s Republic of Bangladesh."

[30] "Sustainable and Renewable Energy Development Authority (SREDA)-Power Division, Ministry of Power, Energy & Mineral Resources."

[31] "Access to electricity (% of population) - Bangladesh | Data."

[32] "Bangladesh Power Development Board-Government of the People\'s Republic of Bangladesh."

[33] "Bangladesh Renewable Energy Sector Opportunities." Accessed: Jan. 14, 2025. [Online]. Available: https://trade.gov/market-intelligence/bangladesh-renewable-energy-sector-opportunities

[34] "Infrastructure Development Company Limited (IDCOL)."

[35] N. Manoj Kumar, S. S. Chopra, A. A. Chand, R. M. Elavarasan, and G. M. Shafiullah, "Hybrid Renewable Energy Microgrid for a Residential Community: A Techno-Economic and Environmental Perspective in the Context of the SDG7," *Sustainability*, vol. 12, no. 10, p. 3944, May 2020, doi: 10.3390/SU12103944.

[36] "SREDA | Renewable Energy Statistics." Accessed: Jan. 15, 2025. [Online]. Available: https://ndre.sreda.gov.bd/index.php?id=8

[37] "RE Generation Mix | National Database of Renewable Energy."

[38] "Solar resource maps and GIS data for 200+ countries | Solargis."

[39] "List of States in Bangladesh with Latitude and Longitude - States in Bangladesh with Latitude Longitude, Popular Places in Bangladesh with Lat Long, List of States in Bangladesh with Latitude and Longitude, Latitude and Longitude of State Capitals of Bang."

[40] "Solar resource maps and GIS data for 200+ countries | Solargis."

[41] M. Abu Saim and I. Khan, "Problematizing solar energy in Bangladesh: Benefits, burdens, and electricity access through solar home systems in remote islands," *Energy Res Soc Sci*, vol. 74, no. February, p. 101969, 2021, doi: 10.1016/j.erss.2021.101969.

[42] M. Abu Saim and I. Khan, "Problematizing solar energy in Bangladesh: Benefits, burdens, and electricity access through solar home systems in remote islands," *Energy Res Soc Sci*, vol. 74, no. February, p. 101969, 2021, doi: 10.1016/j.erss.2021.101969.

[43] "Sustainable and Renewable Energy Development Authority (SREDA)-Power Division, Ministry of Power, Energy & Mineral Resources."

[44] "Solar Home System | National Database of Renewable Energy, SREDA."

[45] S. Bin Amin, M. I. Chowdhury, S. M. Asif Ehsan, and S. M. Zahid Iqbal, "Solar energy and natural disasters: Exploring household coping mechanisms, capacity, and resilience in Bangladesh," *Energy Res Soc Sci*, vol. 79, no. January, p. 102190, 2021, doi: 10.1016/j.erss.2021.102190.

[46] S. Bin Amin, M. I. Chowdhury, S. M. Asif Ehsan, and S. M. Zahid Iqbal, "Solar energy and natural disasters: Exploring household coping mechanisms, capacity, and resilience in Bangladesh," *Energy Res Soc Sci*, vol. 79, no. January, p. 102190, 2021, doi: 10.1016/j.erss.2021.102190.

[47] A. Cuevas, A. Luque, J. Eguren, and J. del Alamo, "50 Per cent more output power from an albedo-collecting flat panel using bifacial solar cells," *Solar Energy*, vol. 29, no. 5, pp. 419–420, Jan. 1982, doi: 10.1016/0038-092X(82)90078-0.

[48] M. R. Islam, M. T. Alam, and A. Al Mamun, "Feasibility study on solar Bi-facial technology and plant shoot configuration in perspective of Bangladesh," *2019 International Conference on Sustainable Technologies for Industry 4.0, STI 2019*, Dec. 2019, doi: 10.1109/STI47673.2019.9068010.

[49] Sarah Lozanova, "What Is MPPT? The Key to Optimizing Solar Output," 2024.

[50] "IET Renewable Power Gen - 2022 - Priyadarshi - High-power DC-DC converter with proposed HSFNA MPPT for photovoltaic based.pdf."

[51] H. Liu, M. Y. A. Khan, and X. Yuan, "Hybrid Maximum Power Extraction Methods for Photovoltaic Systems: A Comprehensive Review," *Energies (Basel)*, vol. 16, no. 15, 2023, doi: 10.3390/en16155665.

[52] R. Alik and A. Jusoh, "An enhanced P&O checking algorithm MPPT for high tracking efficiency of partially shaded PV module," *Solar Energy*, vol. 163, pp. 570–580, Mar. 2018, doi: 10.1016/J.SOLENER.2017.12.050.

[53] W. Xiao and W. G. Dunford, "A modified adaptive hill climbing MPPT method for photovoltaic power systems," *PESC Record - IEEE Annual Power Electronics Specialists Conference*, vol. 3, pp. 1957–1963, 2004, doi: 10.1109/PESC.2004.1355417.

[54] F. Belhachat and C. Larbes, "Global maximum power point tracking based on ANFIS approach for PV array configurations under partial shading conditions," *Renewable and Sustainable Energy Reviews*, vol. 77, pp. 875–889, Sep. 2017, doi: 10.1016/J.RSER.2017.02.056.

[55] M. Y. A. Khan, H. Liu, S. M. Hashemzadeh, and X. Yuan, "A Novel High Step-Up DC–DC Converter with Improved P&O MPPT for Photovoltaic Applications," *Electric Power Components and Systems*, vol. 49, no. 9–10, pp. 884–900, 2021, doi: 10.1080/15325008.2022.2049649.

[56] Y. Wang and B. Nan, "Research of MPPT control method based on PSO algorithm," *Proceedings of 2015 4th International Conference on Computer Science and Network Technology, ICCSNT 2015*, pp. 698–701, Jun. 2016, doi: 10.1109/ICCSNT.2015.7490840.

[57] I. Pervez, A. Sarwar, M. Tayyab, and M. Sarfraz, "Gravitational Search Algorithm (GSA) based Maximum Power Point Tracking in a Solar PV based Generation System," *2019 Innovations in Power and Advanced Computing Technologies, i-PACT 2019*, Mar. 2019, doi: 10.1109/I-PACT44901.2019.8960130.

[58] N. Kumar, I. Hussain, B. Singh, and B. K. Panigrahi, "MPPT in Dynamic Condition of Partially Shaded PV System by Using WODE Technique," *IEEE Trans Sustain Energy*, vol. 8, no. 3, pp. 1204–1214, Jul. 2017, doi: 10.1109/TSTE.2017.2669525.

[59] D. Pilakkat and S. Kanthalakshmi, "An improved P&O algorithm integrated with artificial bee colony for photovoltaic systems under partial shading conditions," *Solar Energy*, vol. 178, pp. 37–47, Jan. 2019, doi: 10.1016/J.SOLENER.2018.12.008.

[60] F. Fitriyah, M. Z. Efendi, and F. Dwi Murdianto, "Modeling and Simulation of MPPT ZETA Converter Using Human Psychology Optimization Algorithm under Partial Shading Condition," *IES 2020 - International Electronics Symposium: The Role of Autonomous*

and Intelligent Systems for Human Life and Comfort, pp. 14–20, Sep. 2020, doi: 10.1109/IES50839.2020.9231890.

[61] X. Li, H. Wen, Y. Hu, L. Jiang, and W. Xiao, "Modified Beta Algorithm for GMPPT and Partial Shading Detection in Photovoltaic Systems," *IEEE Trans Power Electron*, vol. 33, no. 3, pp. 2172–2186, Mar. 2018, doi: 10.1109/TPEL.2017.2697459.

[62] D. Baimel, S. Tapuchi, S. Bronshtein, Y. Horen, and N. Baimel, "Novel Segmentation Algorithm for Maximum Power Point Tracking in PV Systems under Partial Shading Conditions," *Proceedings - 2018 IEEE 18th International Conference on Power Electronics and Motion Control, PEMC 2018*, pp. 406–410, Nov. 2018, doi: 10.1109/EPEPEMC.2018.8521880.

[63] R. Venkata Rao, "Jaya: A simple and new optimization algorithm for solving constrained and unconstrained optimization problems," *International Journal of Industrial Engineering Computations*, vol. 7, no. 1, pp. 19–34, Dec. 2016, doi: 10.5267/J.IJIEC.2015.8.004.

[64] L. M. Elobaid, A. K. Abdelsalam, and E. E. Zakzouk, "Artificial neural network-based photovoltaic maximum power point tracking techniques: A survey," *IET Renewable Power Generation*, vol. 9, no. 8, pp. 1043–1063, 2015, doi: 10.1049/iet-rpg.2014.0359.

[65] H. A. Sher, A. F. Murtaza, and K. Al-Haddad, "A hybrid maximum power point tracking method for photovoltaic applications with reduced offline measurements," in *Proceedings of the IEEE International Conference on Industrial Technology*, Institute of Electrical and Electronics Engineers Inc., Apr. 2017, pp. 1482–1485. doi: 10.1109/ICIT.2017.7915585.

[66] M. R. Al-Soeidat, A. Cembrano, and D. D. C. Lu, "Comparing effectiveness of hybrid mppt algorithms under partial shading conditions," in *2016 IEEE International Conference on Power System Technology, POWERCON 2016*, Institute of Electrical and Electronics Engineers Inc., Nov. 2016. doi: 10.1109/POWERCON.2016.7754024.

[67] Gökhan Yüksek; A. Naci Mete, "A hybrid variable step size MPPT method based on P&O and INC methods | IEEE Conference Publication | IEEE Xplore," in *A hybrid variable step size MPPT method based on P&O and INC methods*, IEEE, 2017.

[68] A. M. Farayola, A. N. Hasan, and A. Ali, "Optimization of PV Systems Using Data Mining and Regression Learner MPPT Techniques," *Indonesian Journal of Electrical Engineering and Computer Science*, vol. 10, no. 3, pp. 1080–1089, 2018, doi: 10.11591/ijeecs.v10.i3.pp1080-1089.

[69] S. Alkhalaf, Z. M. Ali, and H. Oikawa, "A novel hybrid gravitational and pattern search algorithm based MPPT controller with ANN and perturb and observe for photovoltaic system," *Soft comput*, vol. 26, no. 15, pp. 7293–7315, Aug. 2022, doi: 10.1007/S00500-022-07139-Z/FIGURES/18.

[70] S. Nikolovski, H. R. Baghaee, and D. Mlakic, "ANFIS-Based Peak Power Shaving/Curtailment in Microgrids Including PV Units and BESSs," *Energies 2018, Vol. 11, Page 2953*, vol. 11, no. 11, p. 2953, Oct. 2018, doi: 10.3390/EN11112953.

[71] L. B. Prasad, S. Sahu, M. Gupta, R. Srivastava, L. Mozhui, and D. N. Asthana, "An improved method for MPPT using ANN and GA with maximum power comparison through Perturb & Observe technique," in *2016 IEEE Uttar Pradesh Section International Conference on Electrical, Computer and Electronics Engineering, UPCON 2016*, Institute of Electrical and Electronics Engineers Inc., Apr. 2017, pp. 206–211. doi: 10.1109/UPCON.2016.7894653.

[72] L. Bouselham, M. Hajji, B. Hajji, and H. Bouali, "A New MPPT-based ANN for Photovoltaic System under Partial Shading Conditions," *Energy Procedia*, vol. 111, pp. 924–933, Mar. 2017, doi: 10.1016/J.EGYPRO.2017.03.255.

[73] B. Babes, A. Boutaghane, and N. Hamouda, "A novel nature-inspired maximum power point tracking (MPPT) controller based on ACO-ANN algorithm for photovoltaic (PV) system fed arc welding machines," *Neural Comput Appl*, vol. 34, no. 1, pp. 299–317, Jan. 2022, doi: 10.1007/S00521-021-06393-W/FIGURES/27.

[74] L. Chen and X. Wang, "Enhanced MPPT method based on ANN-assisted sequential Monte–Carlo and quickest change detection," *IET Smart Grid*, vol. 2, no. 4, pp. 635–644, Dec. 2019, doi: 10.1049/IET-STG.2019.0012.

[75] A. D. Martin, J. R. Vazquez, and J. M. Cano, "MPPT in PV systems under partial shading conditions using artificial vision," *Electric Power Systems Research*, vol. 162, pp. 89–98, Sep. 2018, doi: 10.1016/J.EPSR.2018.05.005.

[76] C. Manickam, G. R. Raman, G. P. Raman, S. I. Ganesan, and C. Nagamani, "A Hybrid Algorithm for Tracking of GMPP Based on P&O and PSO with Reduced Power Oscillation in String Inverters," in *IEEE Transactions on Industrial Electronics*, Institute of Electrical and Electronics Engineers Inc., Oct. 2016, pp. 6097–6106. doi: 10.1109/TIE.2016.2590382.

[77] Z. Yang, Q. Duan, J. Zhong, M. Mao, and Z. Xun, "Analysis of improved PSO and perturb & observe global MPPT algorithm for PV array under partial shading condition," in *Proceedings of the 29th Chinese Control and Decision Conference, CCDC 2017*, Institute of Electrical and Electronics Engineers Inc., Jul. 2017, pp. 549–553. doi: 10.1109/CCDC.2017.7978154.

[78] K. Bataineh and N. Eid, "A Hybrid Maximum Power Point Tracking Method for Photovoltaic Systems for Dynamic Weather Conditions," *Resources 2018, Vol. 7, Page 68*, vol. 7, no. 4, p. 68, Nov. 2018, doi: 10.3390/RESOURCES7040068.

[79] M. Premkumar, C. Kumar, R. Sowmya, and J. Pradeep, "A novel salp swarm assisted hybrid maximum power point tracking algorithm for the solar photovoltaic power generation systems," *Automatika : časopis za automatiku, mjerenje, elektroniku, računarstvo i komunikacije*, vol. 62, no. 1, pp. 1–20, Mar. 2021, doi: 10.1080/00051144.2020.1834062.

[80] S. Mohanty, B. Subudhi, and P. K. Ray, "A Grey Wolf-Assisted Perturb & Observe MPPT Algorithm for a PV System," *IEEE Transactions on Energy Conversion*, vol. 32, no. 1, pp. 340–347, Mar. 2017, doi: 10.1109/TEC.2016.2633722.

[81] A. Kihal, F. Krim, A. Laib, B. Talbi, and H. Afghoul, "An improved MPPT scheme employing adaptive integral derivative sliding mode control for photovoltaic systems under fast irradiation changes," *ISA Trans*, vol. 87, pp. 297–306, Apr. 2019, doi: 10.1016/J.ISATRA.2018.11.020.

[82] C. Manickam, G. P. Raman, G. R. Raman, S. I. Ganesan, and N. Chilakapati, "Fireworks enriched P&O algorithm for GMPPT and detection of partial shading in PV systems," in *IEEE Transactions on Power Electronics*, IEEE, Jun. 2017, pp. 4432–4443. doi: 10.1109/TPEL.2016.2604279.

[83] K. Sundareswaran, V. Vigneshkumar, P. Sankar, S. P. Simon, P. Srinivasa Rao Nayak, and S. Palani, "Development of an Improved P&O Algorithm Assisted Through a Colony of Foraging Ants for MPPT in PV System," *IEEE Trans Industr Inform*, vol. 12, no. 1, pp. 187–200, Feb. 2016, doi: 10.1109/TII.2015.2502428.

[84] K. Sundareswaran, V. Vigneshkumar, and S. Palani, "Development of a hybrid genetic algorithm/perturb and observe algorithm for maximum power point tracking in photovoltaic systems under non-uniform insolation," *IET Renewable Power Generation*, vol. 9, no. 7, pp. 757–765, Sep. 2015, doi: 10.1049/IET-RPG.2014.0333.

[85] Q. D. Phan, D. K. Le, H. L. Hong, M. P. Le, and N. T. D. Vu, "The new MPPT algorithm using ANN-based PV," in *2010 International Forum on Strategic Technology, IFOST 2010*, 2010, pp. 402–407. doi: 10.1109/IFOST.2010.5668004.

[86] L. Jiang and D. L. Maskell, "A simple hybrid MPPT technique for photovoltaic systems under rapidly changing partial shading conditions," *2014 IEEE 40th Photovoltaic Specialist Conference, PVSC 2014*, pp. 782–787, Oct. 2014, doi: 10.1109/PVSC.2014.6925034.

[87] M. E. Haque and N. Mohammad, "Design and Performance Analysis of Neural Network-Based MPPT in PV System with Energy Storage Management," in *Proceedings - 6th International Conference on Electrical Engineering and Information and Communication Technology, ICEEICT 2024*, IEEE, 2024, pp. 1378–1383. doi: 10.1109/ICEEICT62016.2024.10534419.

[88] A. Kwasinski, P. T. Krein, and P. L. Chapman, "Time domain comparison of pulse-width modulation schemes," *IEEE Power Electronics Letters*, vol. 1, no. 3, pp. 64–68, 2003, doi: 10.1109/LPEL.2003.822370.

[89] Z. Shu, J. Tang, Y. Guo, and J. Lian, "An efficient SVPWM algorithm with low computational overhead for three-phase inverters," *IEEE Trans Power Electron*, vol. 22, no. 5, pp. 1797–1805, Sep. 2007, doi: 10.1109/TPEL.2007.904228.

[90] K. Zhou and D. Wang, "Relationship between space-vector modulation and three-phase carrier-based PWM: A comprehensive analysis," *IEEE Transactions on Industrial Electronics*, vol. 49, no. 1, pp. 186–196, Feb. 2002, doi: 10.1109/41.982262.

[91] A. Reza Reisi, M. Hassan Moradi, and S. Jamasb, "Classification and comparison of maximum power point tracking techniques for photovoltaic system: A review," *Renewable and Sustainable Energy Reviews*, vol. 19, pp. 433–443, 2013, doi: 10.1016/j.rser.2012.11.052.

[92] D. R. Kishore *et al.*, "Grid-Connected Solar PV System with Maximum Power Point Tracking and Battery Energy Storage Integrated with Sophisticated Three-Level NPC Inverter," *International Transactions on Electrical Energy Systems*, vol. 2023, no. 1, p. 3209485, Jan. 2023, doi: 10.1155/2023/3209485.

[93] C. Bharatiraja, S. Jeevananthan, R. Latha, and V. Mohan, "Vector selection approach-based hexagonal hysteresis space vector current controller for a three phase diode clamped MLI with capacitor voltage balancing," *IET Power Electronics*, vol. 9, no. 7, pp. 1350–1361, Jun. 2016, doi: 10.1049/IET-PEL.2015.0184.

[94] I. Harbi *et al.*, "Common DC-Link Multilevel Converters: Topologies, Control and Industrial Applications," *IEEE Open Journal of Power Electronics*, vol. 4, pp. 512–538, 2023, doi: 10.1109/OJPEL.2023.3291662.

[95] A. Taghvaie, M. E. Haque, S. Saha, and M. A. Mahmud, "A new step-up switched-capacitor voltage balancing converter for NPC multilevel inverter-based solar PV system," *IEEE Access*, vol. 8, pp. 83940–83952, 2020, doi: 10.1109/ACCESS.2020.2992093.

[96] R. Zhu, X. Wu, and Y. Tang, "Duty cycle-based three-level space-vector pulse-width modulation with overmodulation and neutral-point balancing capabilities for three-phase neutral-point clamped inverters," *IET Power Electronics*, vol. 8, no. 10, pp. 1931–1940, Oct. 2015, doi: 10.1049/IET-PEL.2014.0721.

[97] K. J. Pratheesh, G. Jagadanand, and R. Ramchand, "A Generalized-Switch-Matrix-Based Space Vector Modulation Technique Using the Nearest Level Modulation Concept for Neutral-Point-Clamped Multilevel Inverters," *IEEE Transactions on Industrial Electronics*, vol. 65, no. 6, pp. 4542–4552, Jun. 2018, doi: 10.1109/TIE.2017.2772172.

[98] N. Beniwal, H. D. Tafti, G. G. Farivar, S. Ceballos, J. Pou, and F. Blaabjerg, "A Control Strategy for Dual-Input Neutral-Point-Clamped Inverter-Based Grid-Connected Photovoltaic System," *IEEE Trans Power Electron*, vol. 36, no. 9, pp. 9743–9757, 2021, doi: 10.1109/TPEL.2021.3063745.

[99] E. Mamarelis, G. Petrone, and G. Spagnuolo, "A two-steps algorithm improving the P&O steady state MPPT efficiency," *Appl Energy*, vol. 113, pp. 414–421, Jan. 2014, doi: 10.1016/J.APENERGY.2013.07.022.

[100] M. Valan Rajkumar and P. S. Manoharan, "FPGA based multilevel cascaded inverters with SVPWM algorithm for photovoltaic system," *Solar Energy*, vol. 87, no. 1, pp. 229–245, Jan. 2013, doi: 10.1016/J.SOLENER.2012.11.003.

[101] A. Calle-Prado, S. Alepuz, J. Bordonau, P. Cortes, and J. Rodriguez, "Predictive Control of a Back-to-Back NPC Converter-Based Wind Power System," *IEEE Transactions on Industrial Electronics*, vol. 63, no. 7, pp. 4615–4627, Jul. 2016, doi: 10.1109/TIE.2016.2529564.

[102] C. K. Das, A. Kirubakaran, and V. T. Somasekhar, "A Five-Level Quasi Z-Source Based NPC Inverter for PV Applications," *Proceedings - 2019 IEEE International Conference on Environment and Electrical Engineering and 2019 IEEE Industrial and Commercial Power Systems Europe, EEEIC/I and CPS Europe 2019*, Jun. 2019, doi: 10.1109/EEEIC.2019.8783928.

[103] U. Abronzini, C. Attaianese, M. D'arpino, M. Di Monaco, and G. Tomasso, "Induction Motor Drives Fed by an NPC Inverter with Unbalanced DC-Link," *Electronics 2019, Vol. 8, Page 1379*, vol. 8, no. 12, p. 1379, Nov. 2019, doi: 10.3390/ELECTRONICS8121379.

[104] T. Sathiyanarayanan and S. Mishra, "Synchronous Reference Frame Theory based Model Predictive Control for Grid Connected Photovoltaic Systems," *IFAC-PapersOnLine*, vol. 49, no. 1, pp. 766–771, Jan. 2016, doi: 10.1016/J.IFACOL.2016.03.149.

[105] H. Özbay, S. Öncü, and M. Kesler, "SMC-DPC based active and reactive power control of grid-tied three phase inverter for PV systems," *Int J Hydrogen Energy*, vol. 42, no. 28, pp. 17713–17722, Jul. 2017, doi: 10.1016/J.IJHYDENE.2017.04.020.

[106] F. J. Lin, K. C. Lu, and T. H. Ke, "Probabilistic Wavelet Fuzzy Neural Network based reactive power control for grid-connected three-phase PV system during grid faults," *Renew Energy*, vol. 92, pp. 437–449, Jul. 2016, doi: 10.1016/J.RENENE.2016.02.036.

[107] J. W. Jung, N. T. T. Vu, D. Q. Dang, T. D. Do, Y. S. Choi, and H. H. Choi, "A three-phase inverter for a standalone distributed generation system: Adaptive voltage control design and stability analysis," *IEEE Transactions on Energy Conversion*, vol. 29, no. 1, pp. 46–56, Mar. 2014, doi: 10.1109/TEC.2013.2288774.

[108] X. Yan *et al.*, "Adaptive-MPPT-Based Control of Improved Photovoltaic Virtual Synchronous Generators," *Energies 2018, Vol. 11, Page 1834*, vol. 11, no. 7, p. 1834, Jul. 2018, doi: 10.3390/EN11071834.

[109] G. G. Koch, H. Pinheiro, R. C. L. F. Oliveira, and V. F. Montagner, "Experimental evaluation of robust and nonrobust H∞ controllers for three-phase grid-connected converters," *14th Brazilian Power Electronics Conference, COBEP 2017*, vol. 2018-January, pp. 1–6, Jul. 2017, doi: 10.1109/COBEP.2017.8257233.

[110] B. Salma, J. Tarik, B. Mohamed Khalifa, N. Elmehdi, and L. Roa, "Improving Photovoltaic System Performance with Artificial Neural Network Control," *Data and Metadata*, vol. 2, pp. 144–144, Dec. 2023, doi: 10.56294/DM2023144.

[111] A. Dawahdeh, H. Sharadga, and S. Kumar, "Novel MPPT Controller Augmented with Neural Network for Use with Photovoltaic Systems Experiencing Rapid Solar Radiation Changes," *Sustainability 2024, Vol. 16, Page 1021*, vol. 16, no. 3, p. 1021, Jan. 2024, doi: 10.3390/SU16031021.

[112] F. G. Bishaw, M. K. Ishak, and T. H. Atyia, "Review Artificial Intelligence Applications in Renewable Energy Systems Integration," *Journal of Electrical Systems*, vol. 20, no. 3, pp. 566–582, Apr. 2024, doi: 10.52783/JES.2983.

[113] "https://power.larc.nasa.gov/data-access-csv (Access on 04 August 2023)."

[114] B. Shiva Kumar and K. Sudhakar, "Performance evaluation of 10 MW grid connected solar photovoltaic power plant in India," *Energy Reports*, vol. 1, pp. 184–192, 2015, doi: 10.1016/j.egyr.2015.10.001.

[115] X. Gong, F. Dong, M. A. Mohamed, E. M. Awwad, H. M. Abdullah, and Z. M. Ali, "Towards distributed based energy transaction in a clean smart island," *J Clean Prod*, vol. 273, p. 122768, 2020, doi: 10.1016/j.jclepro.2020.122768.

[116] C. Li, X. Jia, Y. Zhou, and X. Li, "A microgrids energy management model based on multi-agent system using adaptive weight and chaotic search particle swarm optimization considering demand response," *J Clean Prod*, vol. 262, no. xxxx, p. 121247, 2020, doi: 10.1016/j.jclepro.2020.121247.

[117] S. Tang, M. Jiang, R. Abbassi, H. Jerbi, and M. latifi, "A cost-oriented resource scheduling of a solar-powered microgrid by using the hybrid crow and pattern search algorithm," *J Clean Prod*, vol. 313, no. May, p. 127853, 2021, doi: 10.1016/j.jclepro.2021.127853.

[118] C. Xie, D. Wang, C. S. Lai, R. Wu, X. Wu, and L. L. Lai, "Optimal sizing of battery energy storage system in smart microgrid considering virtual energy storage system and high

photovoltaic penetration," *J Clean Prod*, vol. 281, p. 125308, 2021, doi: 10.1016/j.jclepro.2020.125308.

[119] A. R. Jordehi, M. S. Javadi, and J. P. S. Catalão, "Energy management in microgrids with battery swap stations and var compensators," *J Clean Prod*, vol. 272, p. 122943, 2020, doi: 10.1016/j.jclepro.2020.122943.

[120] Y. Cao, B. Zhou, S. W. Or, K. W. Chan, N. Liu, and K. Zhang, "An interactive tri-level multi-energy management strategy for heterogeneous multi-microgrids," *J Clean Prod*, vol. 319, no. May, p. 128716, 2021, doi: 10.1016/j.jclepro.2021.128716.

[121] H. S. Lee and J. J. Yun, "Advanced MPPT Algorithm for Distributed Photovoltaic Systems," *Energies 2019, Vol. 12, Page 3576*, vol. 12, no. 18, p. 3576, Sep. 2019, doi: 10.3390/EN12183576.

[122] F. Zhang, K. Thanapalan, A. Procter, S. Carr, and J. Maddy, "Adaptive hybrid maximum power point tracking method for a photovoltaic system," *IEEE Transactions on Energy Conversion*, vol. 28, no. 2, pp. 353–360, 2013, doi: 10.1109/TEC.2013.2255292.

[123] I. Ahmed, V. B. Borghate, A. Matsa, P. M. Meshram, H. M. Suryawanshi, and M. A. Chaudhari, "Simplified Space Vector Modulation Techniques for Multilevel Inverters," *IEEE Trans Power Electron*, vol. 31, no. 12, pp. 8483–8499, Dec. 2016, doi: 10.1109/TPEL.2016.2520078.

[124] Q. M. Attique, "A Survey on Space-Vector Pulse Width Modulation for Multilevel Inverters," *CPSS Transactions on Power Electronics and Applications*, vol. 2, no. 3, pp. 226–236, Sep. 2017, doi: 10.24295/CPSSTPEA.2017.00021.

[125] M. T. Hussain, A. Sarwar, M. Tariq, S. Urooj, A. BaQais, and M. A. Hossain, "An Evaluation of ANN Algorithm Performance for MPPT Energy Harvesting in Solar PV Systems," *Sustainability 2023, Vol. 15, Page 11144*, vol. 15, no. 14, p. 11144, Jul. 2023, doi: 10.3390/SU151411144.

[126] M. Rokonuzzaman *et al.*, "Levenberg-Marquardt algorithm-based solar PV energy integrated internet of home energy management system," *Appl Energy*, vol. 378, p. 124407, Jan. 2025, doi: 10.1016/J.APENERGY.2024.124407.

[127] A. Kalair, N. Abas, A. R. Kalair, Z. Saleem, and N. Khan, "Review of harmonic analysis, modeling and mitigation techniques," *Renewable and Sustainable Energy Reviews*, vol. 78, pp. 1152–1187, Oct. 2017, doi: 10.1016/J.RSER.2017.04.121.

Appendices

Appendix A: Specification of System Parameters

Solar PV System Specification:

Table A.5.1. Specifications of the solar PV modules.

Parameters	*Values*
MPP Voltage, V_{mpp}	43.4 V
MPP Current, I_{mpp}	8.18 A
Maximum Power, P_{max}	355.012 W
Open Circuit Voltage, V_{oc}	51.9 V
Short Circuit Current, I_{sc}	8.68 A
No. of Cell in Series, N_s	15
No of Cell in Parallel, N_p	282
Cells per module, N_{cell}	83
Diode ideality factor	0.92618
Shunt resistance, R_{sh}	389.4331
Series resistance, R_S	0.29289
Temperature coefficient of V_{oc}	-0.304 % ℃
Temperature coefficient of I_{sc}	0.017 % ℃

Appendix B: Pseudocode of this thesis Algorithm

Perturb and Observe Approach:

The pseudocode briefly describes the implementation of the P&O MPPT algorithm, which is used in this research. The algorithm rapidly samples the string voltage and current and then calculates the power by multiplying the voltage and current. The algorithm compares the values of the current power and

voltage with the previous power and voltage and then adjusts the reference voltage based on the conditions present in pseudocode.

Algorithm A1: Perturb and Observe MPPT Algorithm

```
1:  procedure P&OMPPT (Vst, Ist, Vref)
2:      Vst,n← Vst
3:      Ist,n← Ist
4:      Pst,n← Vst,n×Ist,n          { Sample the string voltage and current
                                      Calculate the string power
5:      If finit→ False then
6:          Vref←Vst,n−Smin         { Check if the initialization has been performed
7:          finit←True                or not, If not, reduce the string voltage reference
                                      then set the initialization flag to True
8:      else
9:          If Pst,n > Pst,n−1 then
10:             If Vst,n > Vst,n−1 then
11:                 Vref ← Vref + Smin   Check if the panel power and voltage is increased or not,
12:             else                     if Vst/dPst> 0, increase Vref by the step size Smin
13:                 Vref←Vref−Smin       if Vstd/Pst< 0, decrease Vref by the step size Smin
14:             end if
15:         else
16:             If Vst,n > Vst,n−1 then
17:                 Vref ← Vref − Smin
18:             else                     Check if the panel power and voltage is decreased or not,
18:                 Vref←Vref+Smin       if Vst/dPst< 0, decrease Vref by the step size Smin
19:             end if                   if Vst/dPst> 0, increase Vref by the step size Smin
20:         end if
21:     end if
22:     Vst,n−1 ← Vst,n             { Update the previous voltage sample
23:     Pst,n−1 ←Pst,n                by the present voltage sample
                                      Update the previous power value
                                      by the present power value.
24:     return Vref
25: end procedure
```

Neural Network Approach:

The pseudocode for the ANN-based MPPT algorithm.

Algorithm A2: Proposed ANN Algorithm

```
//Neural Network Constants//
Define: Ts=Timestep, X=Input over Ts, Y=Output over
Ts, Q=Sample/series
1.  Star
2.  Input: X [Xoffset, Gain, Ymin]
3.  Hidden Layer
    Layer 1: b1, W1; Layer 2: b2, W
4.  Output: Y [Ymin, Gain, Xoffset]
//Simulation//
5.  Input Argument
    if X={X}
  end
6.  Dimensions: TS= size (X,2)
    if Q=size (X{1}, 1)
   else Q=0
  end
7.  Allocate Outputs: Y= cell (1, TS)
8.  Time Loop: For ts=1:Ts
    Input 1; Layer 1; Layer 2; Output
  end
9.  Final Delay States:
    Xf=cell (1,0), Af=cell (2,0)
10. Format Output Agreements: if Y=cell2mat (Y)
  end
//Module Functions//
11. Min. and Max. Input Processing Function (PF)
12. Sigmoid Symmetric Transfer Function:
    function a=tansig_apply (n,~)
    a=2. / (1 + exp(-2*n)) -1
   end
13. Min. & Max. Output Reverse PF
14. Stop
```

Appendix C: Architecture of Grid Connected Model on MATLAB Simulink

The proposed neural network-based interface MATLAB Simulink MPPT grid-connected solar PV model.

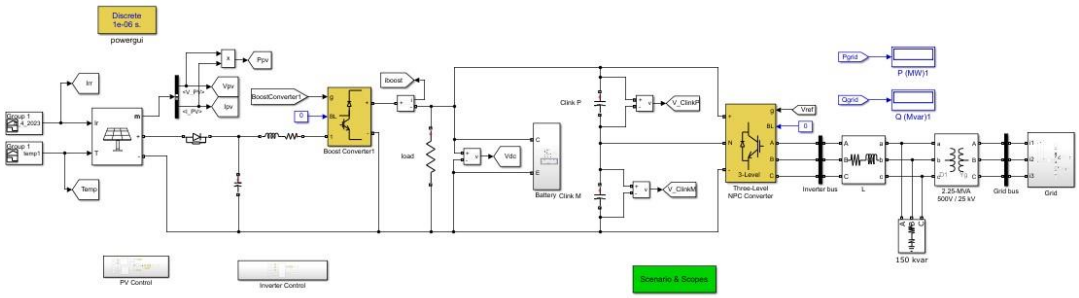


Fig. B.01 The proposed MATLAB Simulink model.